FUNDAMENTAL STUDIES ON SOLAR-ACTIVATED ZEOLITE-SUPPORTED PHOTOCATALYSTS FOR WATER SPLITTING APPLICATION

by

AMIN TAHERI NAJAFABADI

B.SC., SHARIF UNIVERSITY OF TECHNOLOGY, 2009

A THESIS SUBMITTED IN PARTIAL FULFILLMENT OF

THE REQUIREMENTS FOR THE DEGREE OF

MASTER OF APPLIED SCIENCE

in

THE FACULTY OF GRADUATE STUDIES

(CHEMICAL AND BIOLOGICAL ENGINEERING)

THE UNIVERSITY OF BRITISH COLUMBIA

(VANCOUVER)

JUNE 2012

Abstract

Robust calculations show that the incidence of solar energy on the earth's surface by far exceeds all human energy needs. Undoubtedly, the most trusted way of utilizing solar energy is to convert and store it in the form of an energy carrier such as hydrogen. Semiconductors capable of absorbing light energy so-called photocatalysts can potentially drive water splitting reaction for hydrogen generation.

In this research, fundamental studies on a new class of solar-activated supported photocatalysts for water splitting application are presented. This resulted in significantly higher rates of H_2 production in comparison to the existing supported TiO_2 series under visible light. The composition comprises silico-aluminates (zeolite) as the support, titanium dioxides (TiO_2) as the semiconductor, cobalt compounds as hydrogen evolution sites and heteropolyacids (HPAs) as multifunctional solid acids with excitability under visible light. Using this composition, I ended up with at least 2.6 times higher hydrogen evolution rates under visible light in comparison to Degussa P25, the best commercially available titania product. The chemical point of view of this successful combination was investigated, attributing the higher photocatalytic activity of the synthesized chemical compositions to the basicity of the matrix. The more basicity properties besides HPA presence can overcome the negative impacts of titania interactions with the zeolite which are band gap widening and anodic shift of the TiO_2 band edges.

Furthermore, the effect of cobalt precursors (nitrates and chlorides) on the photocatalytic activity of the prepared photocatalysts was also investigated. Although nitrate-based photocatalysts exhibited an improvement in the UV-VIS absorbance spectra toward visible light, they caused an almost 30% lower H_2 production rate in comparison to the

chloride salts. Overshadowing the poisoning and parasitic effects of Cl^- anions on the photo-oxidation sites in the zeolite-supported composition was another notable outcome of this study. This suggests emulation of the core-shell photocatalysis concept insofar with providing a reasonable distance between redox sites. The results indicate the importance of zeolite's structural and chemical properties as the photocatalyst support. This can be addressed through the selection of suitable zeolite types, taking an important step in the development of visible-light-activated photocatalysts based on earth-abundant materials.

Preface

All manuscript based chapters of this thesis were co-authored with my research supervisor, Dr. Fariborz Taghipour. My contribution was the conduction of the preparation and characterization of the synthesized photocatalysts, collection and the analysis of experimental data obtained from my designed experimental setup, and the writing of the manuscripts. Dr. Fariborz Taghipour largely contributed to the discussion of results and the revision of the manuscript drafts.

Table of Contents

List of Tables

List of Figures

Nomenclature

2,4-DCP	2,4-Dichlorophenol
2,4-D	2,4-Dichlorophenoxyacetic acid
AM	air mass
AQY	apparent quantum yield
AFM	atomic force microscopy
E_g	band-gap energy
bipy	bipyridine
BET	Brunauer-Emmett-Teller
CBC	calcium binding capacity
CSA	Canadian safety association
CBD	chemical bath deposition
CVD	chemical vapor deposition
CST	concentrating solar thermal
CB	conduction band
DR	diffuse reflectance
eV	electron volt
EDX	energy-dispersive X-ray spectroscopy
FCC	fluid catalytic cracking
GC	gas chromatography
HPA	heteropoly acid
HPB	heteropolyblue
HPLC	high-performance liquid chromatography

IC	ion chromatography
MPA	mercaptopropionic acid
MLCT	metal-to-ligand charge transfer
MCM	Mobil composition of matter
M	molar concentration
PMA	phosphomolybdic acid
PWA	phosphotungstic acid
J_{ph}	photo-current surface density
PEC	photo-electrochemical
PV	photovoltaic
QD	quantum dot
R_{H2}	rate of hydrogen production
A/R	redox couple
SEM	scanning electron microscope
SBU	secondary building unit
P_{Solar}	solar irradiation power
STC	solar thermochemical
STH	solar to hydrogen
ΔG^0	standard Gibbs free energy change
SHE	standard hydrogen electrode
SMR	steam methane reforming
SILAR	successive ionic layer adsorption
TiO_2	titania, titanium dioxide

DOE	U.S. department of energy
UV	ultraviolet
VB	valence band
VLS	vapor-liquid-solid
VIS	visible
XPS	X-ray photoelectron spectroscopy

Acknowledgements

I would like to express my appreciation to my supervisor, Dr. Fariborz Taghipour, who provided me with this opportunity to come to UBC and be a part of his research group. His support, patience, and constant guidance helped me to overcome many of the challenges that I faced during my studies.

I would like to acknowledge Dr. Kevin Smith and Dr. Majid Mohseni for reviewing my thesis and being a part of my research committee. Dr. Naoko Ellis went beyond the call of duty by establishing connections with the USHIO Company, Japanese branch, purchasing one of the key elements of my research.

I also want to thank Dr. Kevin Smith, Dr. Madjid Mohseni and Dr. Naoko Ellis from Department of Chemical and Biological Engineering for letting me use their laboratories and equipment as well as great technical supports received from them and their graduate students (Shahin, Ali, Hooman, and Ross from Dr. Smith group, Ramin, Clara, Gustavo, and Mahdi from Dr. Mohseni group, and Amir and Joy from Dr. Ellis group). My special thanks also go to Dr. Michael Wolf from Chemistry Department for his support in UV-VIS DR analysis, and his graduate student, Lyndsey Earl for her help in performing this analysis. I would like to appreciate Dr. Mark Johnson from Mining Department and his graduate student Ashlee Jollymore for their favor of doing ion chromatography analysis.

I am also very grateful to my family, particularly my parents and my brother, who have always been supportive and encouraging in every aspect of my life, especially regarding continuing my education.

My thanks are also extended to my dear friends, Sayyed Soroush Nasseri, Mohammad Mahdi Bazri, Mohammad Sadegh Masnadi, Sayyed Alireza Bagherzadeh, Amir

Mehdi Dehkhoda, Omid Vahidi, Ali H. Alzaid and Siamak Elyasi who always encouraged and helped me whenever I was in need.

Last but not least, I would like to thank the Almighty for all the failures and successes of my life as I have learnt a lot from failures and gained a lot out of my successes!

TO MY BELOVED PARENTS AND BROTHER

Chapter 1: Introduction

Robust calculations show that the incidence of solar energy on the earth's surface by far exceeds all human energy needs [1]. Considering the incredible energy bombardment of earth by the sun with about 180,000,000,000,000,000 W (or 180,000 TW) of radiant power, solar irradiation would be potentially the ultimate energy source for all the species on earth. This energy is high enough to power 3 quadrillion of 60 W light bulbs! Of this massive amount of energy, about 36,000 TW is absorbed at the earth's land masses where the installation of the terrestrial solar conversion plants is practical [2]. To bring more sense to the numbers, it should be noted that world energy consumption is 13-15 TW expecting to be doubled by midcentury considering current consumption rate. Although this amount is overwhelming by itself, it's still a small percentage of the solar energy incidence, potentially satisfying all the limitless hunger of humankind for energy [3]. Approximately 1% of the earth's land coverage with 10% efficient solar conversion plants would deliver 20 TW of power, nearly twice the world's consumption rate of fossil energy [4]. Therefore, the power level of 1,000 $W.m^{-2}$, which is the average radiated energy from the sun, would contribute significantly to our electrical and chemical needs. Sunlight in the near-infrared, visible, and ultraviolet regions releases this amount of energy [5].

Undoubtedly, the most trusted way of utilizing solar energy is to convert and store it in the form of an energy carrier such as hydrogen. In the perspective of hydrogen economy, hydrogen is envisioned being the ideal energy carrier as to store and distribute renewable energy resources such as solar, wind, geothermal, hydroelectric, etc. This determining chemical compound can be converted to power or heat with zero carbon emission via fuel cell or combustion engine technologies, introducing water as the primary by-product.

Nowadays, electricity is a key energy carrier and will still keep its remarkable role through the long term future. However, the complementary role of the hydrogen should not be overlooked emerging promisingly in large scale storage and long distance distribution. Figure 1-1 demonstrates the roadmap proposed by U.S. department of energy (DOE) for the transition to the hydrogen-based economy.

Simultaneously, hydrogen, the world's most abundant element is a key chemical commodity currently. In the modern industry market, hydrogen has a significant portion with more than 5,000,000 kg consumption per year [4]. Major applications include the chemical production, semiconductor processing, generator cooling, fertilizer production, etc. The main reason of utilizing H_2 for aforementioned purposes is its low density, high thermal conductivity and strong chemical reducing properties.

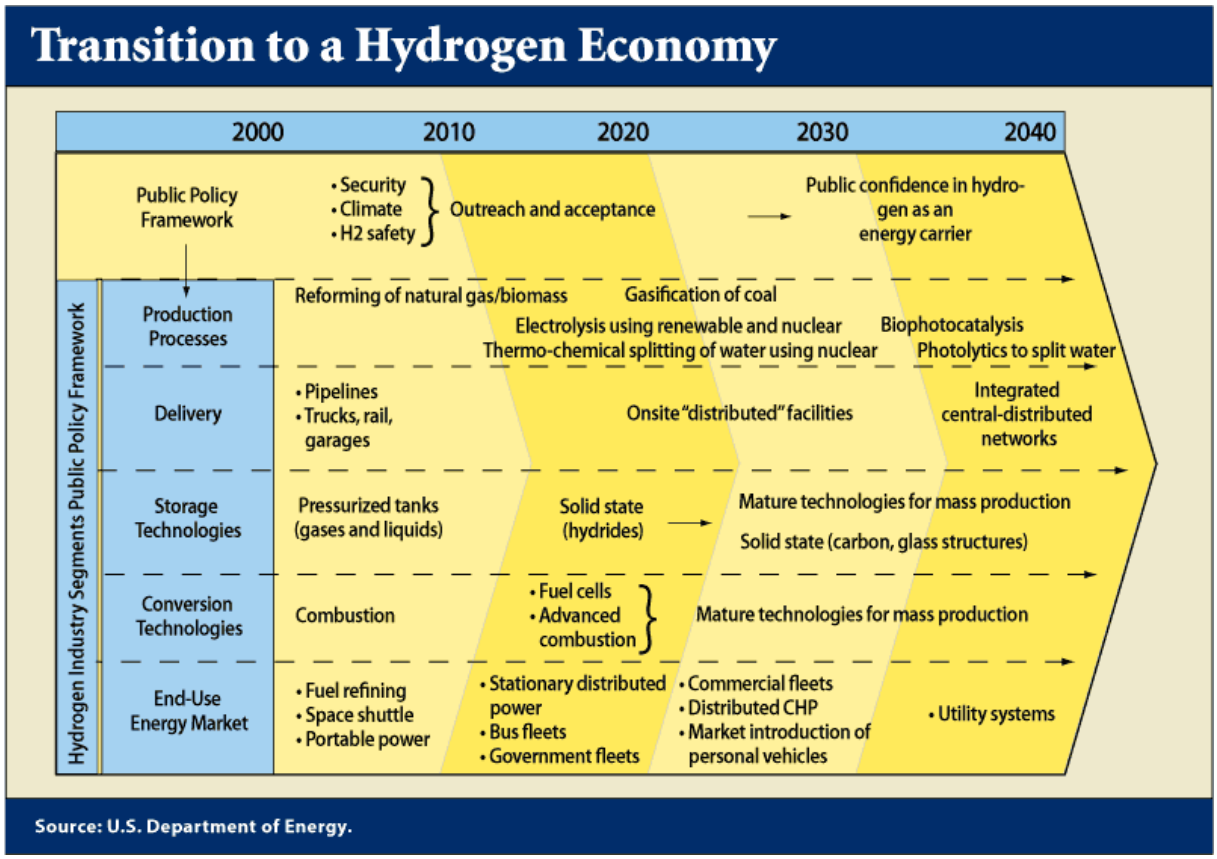

Figure 1-1: Transition to the hydrogen-based economy.

The bottom line is that without exaggeration, hydrogen has a significant role in the current world energy cycles and surely its importance is increasingly strengthened considering its application as an energy carrier for the development of the renewable energy infrastructures.

To meet the supply requirements, current H_2 production technologies are mainly based on fossil fuel conversions. More than 95% of the worldwide produced hydrogen comes from natural gas, oil or coal conversion [4]. US has focused more on steam methane reforming (SMR) in this regard—steam reaction with methane in high temperature producing hydrogen and carbon monoxide [3]. However, the notable decline in the fossil fuel sources and subsequent cost increase beside CO_2 emission and air pollution concerns are the main disadvantages. Consequently, all the downstream industries consuming hydrogen undergo similar aforementioned drawbacks and risks. Hence, H_2 production with almost zero greenhouse gas emissions is the ideal state for hydrogen supply issue. One way is to combine SMR with sequestration of carbon dioxide which is unfortunately yet an unproven technology [6]. Another option is biomass gasification—heating operation on organic compounds like wood and crop wastes in order to make them release hydrogen and carbon monoxide. This method is carbon neutral considering the primary CO_2 adsorption by the plants during photosynthesis process. The third choice is water electrolysis using renewable power sources such as wind, solar cells and wind turbines.

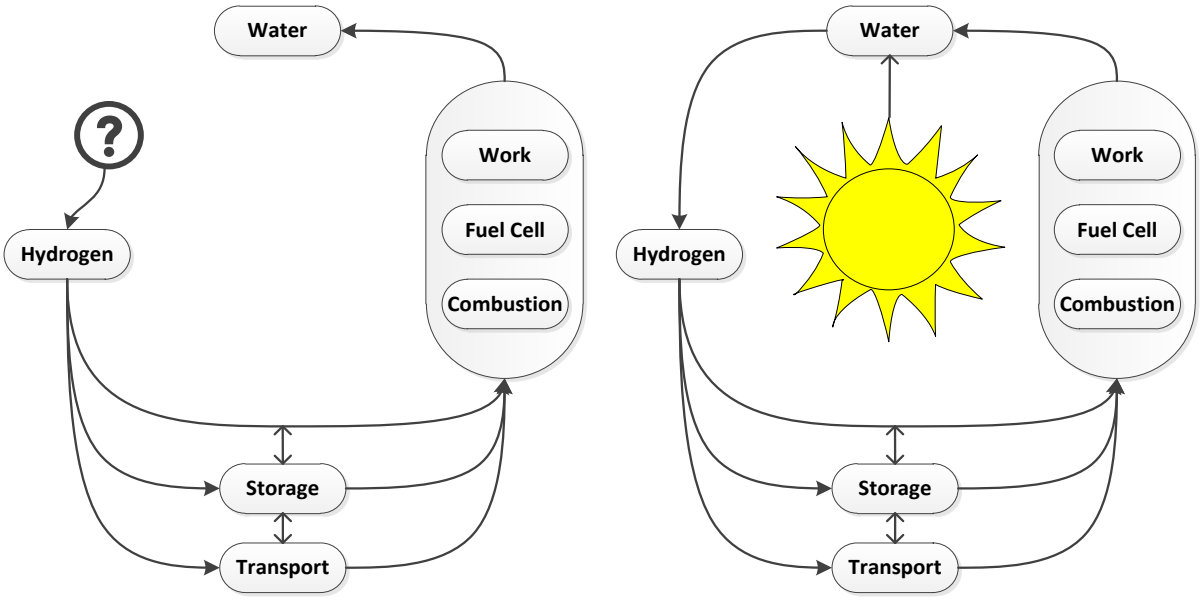

Figure 1-2: The water splitting/hydrogen fuel cycle without (left) or with (right) considering solar energy.

Considering the third option and the advantages of solar energy as the most abundant renewable energy source, solar-to-hydrogen conversion is one of the hottest scientific challenges in the twenty-first century [7]. Figure 1-2 depicts the role of the sun in the water splitting to hydrogen fuel's green cycle. Water splitting via sunlight to produce hydrogen can be achieved through several conversion routes [4, 8, 9]. As shown in Figure 1-3, the solar thermal path basically begins with a photon-to-thermal conversion step followed by a thermal-to-chemical process, overall so-called solar thermochemical (STC) approach. Another two-step route triggers by a photon-to-electric i.e. photovoltaic (PV) process which is then followed by an electric-to-chemical phenomenon. CST-electrolysis pathway, which stands for concentrating solar thermal, comprises three steps of photon-to-heat, heat-to-electricity, and finally electric-to-chemical conversion process. The last route presented in Figure 1-3 exhibiting a one-shot process which is direct photon-to-chemical conversion so-called photo-electrochemical (PEC) pathway. Other solar-to-hydrogen options are doable

including photo-biological methods [10] and ultra-high temperature thermolysis technique [11]. All the counted techniques can contribute to the hydrogen supply for the green economies, but economics rules over the prevailing method.

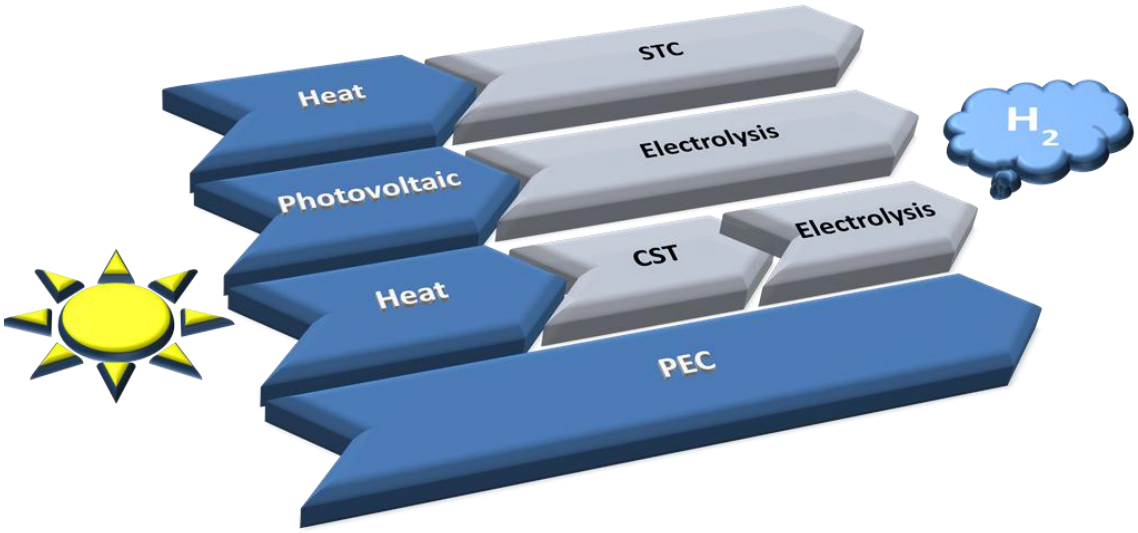

Figure 1-3: Solar-to-hydrogen conversion pathways (STC accounts for solar thermochemical, CST for concentrating solar thermal, and PEC for photo-electrochemical).

From the economical point of view, it is worth noting that hydrogen and electricity together will play an important role as the renewable-energy carriers in the future. Thus, pathways capable of generating both like PV-electrolysis and CST-electrolysis could be more beneficial. In fact, based on recent progresses of these techniques, it is viable to produce inexpensive electricity and hydrogen using mass produced components in near future. Simultaneously, it is necessary to devote more time and energy on some other alternatives which might seem premature currently. One of the key incentives has to do with the higher energy losses associated with the multistep conversion pathways of the aforementioned techniques [12]. From this point of view, the direct one-shot conversion processes like PEC could be advantageous in terms of maximum reachable performance. Afterwards, this single-stage technique for hydrogen production demonstrates one of the most promising and front-

running alternatives. This process mimics photosynthesis by converting water into H_2 and O_2 using inorganic semiconductors that induce the water-splitting reaction (Figure 1-4) [13].

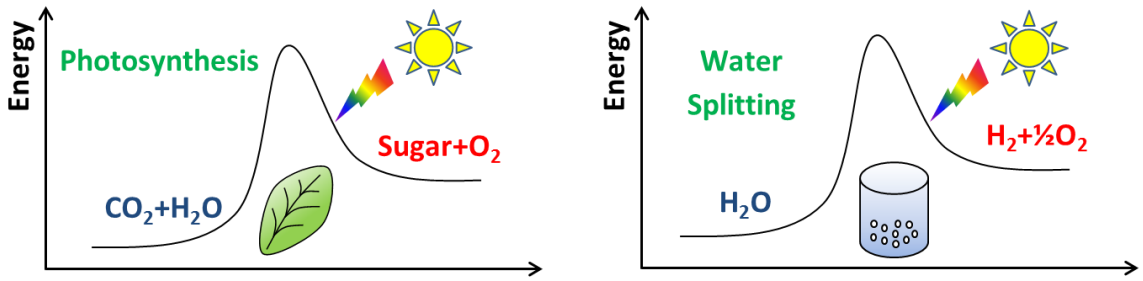

Figure 1-4: Analogy of the photocatalytic water splitting (artificial photosynthesis) (right) with photosynthesis of the green plants (left).

The revolutionary experiments of Fujishima and Honda [14] in 1972 on the semiconductors capable of absorbing light energy proved that this class of materials can drive water splitting reaction for hydrogen generation. Since this inspiring research, numerous studies performed on the various types of semiconductors to enhance their performance for photocatalytic water dissociation under visible light employing a greater portion of solar spectrum more efficiently [8, 13, 15, 16].

1.1 Photoelectrochemistry of water splitting

Like any other photocatalytic processes, photo-electrochemical water splitting is initiated with the absorption of light photons by a semiconductor with energies greater than its band-gap energy (E_g). This absorption causes the generation of excited photoelectrons in the conduction band (CB) and holes in the valence band (VB) of the semiconductor, depicted in Figure 1-5a. As indicated in Figure 1-5b, once the photoexcited electron-hole pairs are created in the bulk of the material, they must migrate separately to the surface (paths i and ii in Figure 1-5b) and compete strongly with the electron-hole recombination process (path iii in Figure 1-5b) that consumes the pairs, generating heat. Finally, at the surface of the

semiconductor, absorbed water molecules are reduced and oxidized by photo-induced electrons and holes to produce gaseous hydrogen and oxygen, respectively by the following reactions:

$$Oxidation: H_2O + 2h^+ \rightarrow 2H^+ + \frac{1}{2}O_2$$

$$Reduction: 2H^+ + 2e^- \rightarrow H_2$$

$$Overall\ Reaction: H_2O \rightarrow H_2 + \frac{1}{2}O_2$$

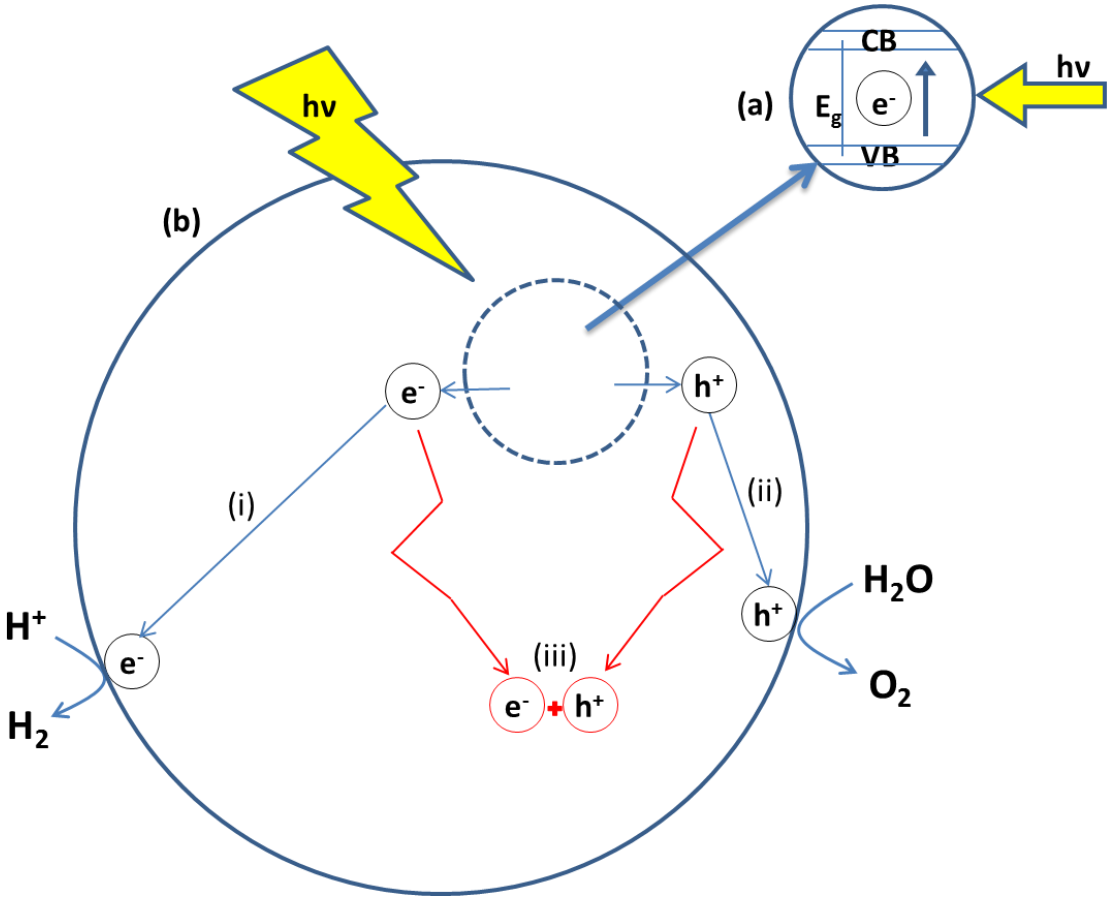

Figure 1-5: The basics of photocatalytic water splitting: (a) Photo-excitation in the photocatalyst generating electron-hole pairs. (b) Processes happening on photocatalyst particle following photo-excitation.

The decomposition of water into H_2 and O_2 is classified as an "up-hill" photocatalytic reaction due to its occurrence upon a large positive change in the Gibbs free energy (ΔG^0=237 kJ.mol^{-1}, 2.46 eV per molecule) (Figure 1-6a).

For reduction of the water, the flat band potential of the photocatalytic semiconductor must exceed the proton reduction potential (0.00 V against the standard hydrogen electrode, SHE, at pH=0, Figure 1-6b). On the other side, to drive water oxidation, the VB edge must exceed the oxidation potential of water (1.23 V against NHE, at pH=0, Figure 1-6b). Hence, based on the mentioned requirements, the theoretical semiconductor band-gap energy of 1.23 eV is needed to trigger the water dissociation reaction.

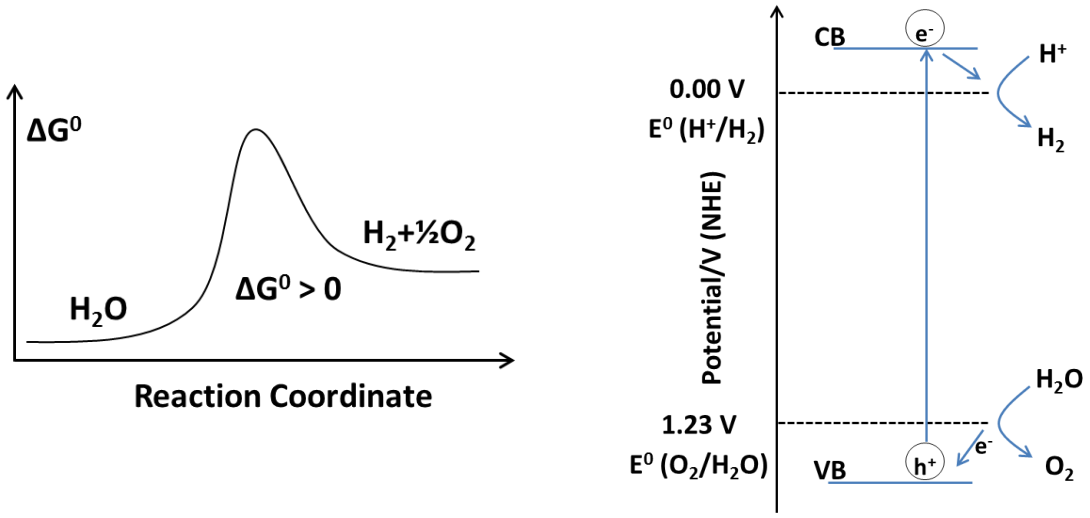

(a) **(b)**

Figure 1-6: (a) Large positive Gibbs free energy change associated with water splitting (uphill reaction). (b) Band requirements energy diagram for photocatalytic water splitting using a single semiconductor system.

1.2 Configurations for artificial photosynthesis

Two major configurations can be employed for photo-electrochemical technique of water cleavage: (i) electrode-based, and (ii) particle-based. The first method utilizes two electrodes immersing in an aqueous electrolyte, one is the semiconductor (i.e. photocatalyst)

exposed to the irradiation and the other play the role of counter-electrode to complete the electron cycle (Figure 1-7a). The second system involves photocatalysts in the form of particles or powders suspended in the electrolyte or reaction solution (Figure 1-7b). In this way, each particle should behave as micro-photo-electrode configuration providing redox active sites to split water on its surface. Certainly this configuration has its own disadvantages in comparison to the electrode-based systems, including lower efficiency in electron-hole separation and reverse reaction of the products on the surface of the photocatalyst, decreasing gas evolution rates.

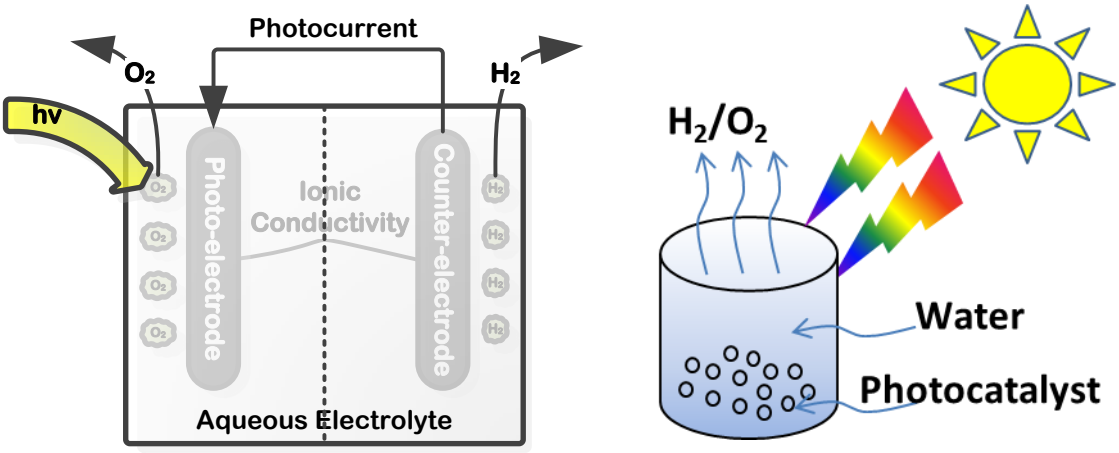

(a) (b)

Figure 1-7: Two major configurations for photocatalytic water splitting: (a) electrode-based, and (b) powder-based.

However, working with photocatalysts as particles has the merits of being much simpler and less expensive for development in comparison to the photo-electrochemical cells. More information about the electrode-based systems is available in a number of references about this concept [17-19].

1.3 Solar spectrum and water-splitting efficiency

The average incident of solar irradiation before entering the earth's atmosphere is 1353W.m^{-2} [1]. This amount is then modified by the aerosol scattering, ozone (in UV region), water and CO_2 absorption (in IR region). The extent of these phenomena's impact basically depends on the air mass (AM) ratio, which is the ratio of the optical path length of the sunlight through the atmosphere to the equivalent distance when the sun is at the zenith. Thus, AM0 means the extraterrestrial sunlight while AM1 means the sun in the zenith, and AM25 refers to the condition of sunrise. Figure 1-8 presents the solar irradiance spectrum under the global AM condition 1.5 (AM1.5), equivalent to the sun's position at the zenith angle of 48.19˚, being the representative of the temperate latitudes of northern hemisphere.

The conversion efficiency of the solar to hydrogen energy (STH) is the main determining factor and of course the bottleneck for the hydrogen production using photocatalytic water splitting. This parameter is defined as

$$STH(\%) = \frac{\Delta G_{H_2} * R_{H_2}}{P_{Solar} * Area} * 100$$

where ΔG is the Gibbs free energy change associated with hydrogen production from water, R_{H2} is the rate of hydrogen production, P_{Solar} is the solar irradiation power and Area is the active photo-electrode area exposed to the irradiation. In the electrode-based systems under the AM1.5 condition, this quantity can be simplified as

$$STH(\%) \approx 1.23 * J_{ph}[mA.cm^{-2}]$$

where J_{ph} is the photo-current surface density on the exposed electrode.

As mentioned in previous section, the theoretical potential for this process in the minimum amount of 1.23 eV per photon which comes from the thermodynamics energy calculations. This energy corresponds to the wavelength of 1,010 nm, introducing about 70%

of the solar irradiated photons capable of deriving water cleavage reaction [20]. However, considering the intrinsic energy losses during the water cleavage process on the surface of the photocatalyst, the amount of the energy per photon should be higher than the theoretical value of 1.23 eV in order to proceed the redox reactions [21]. This is explained more in the next section.

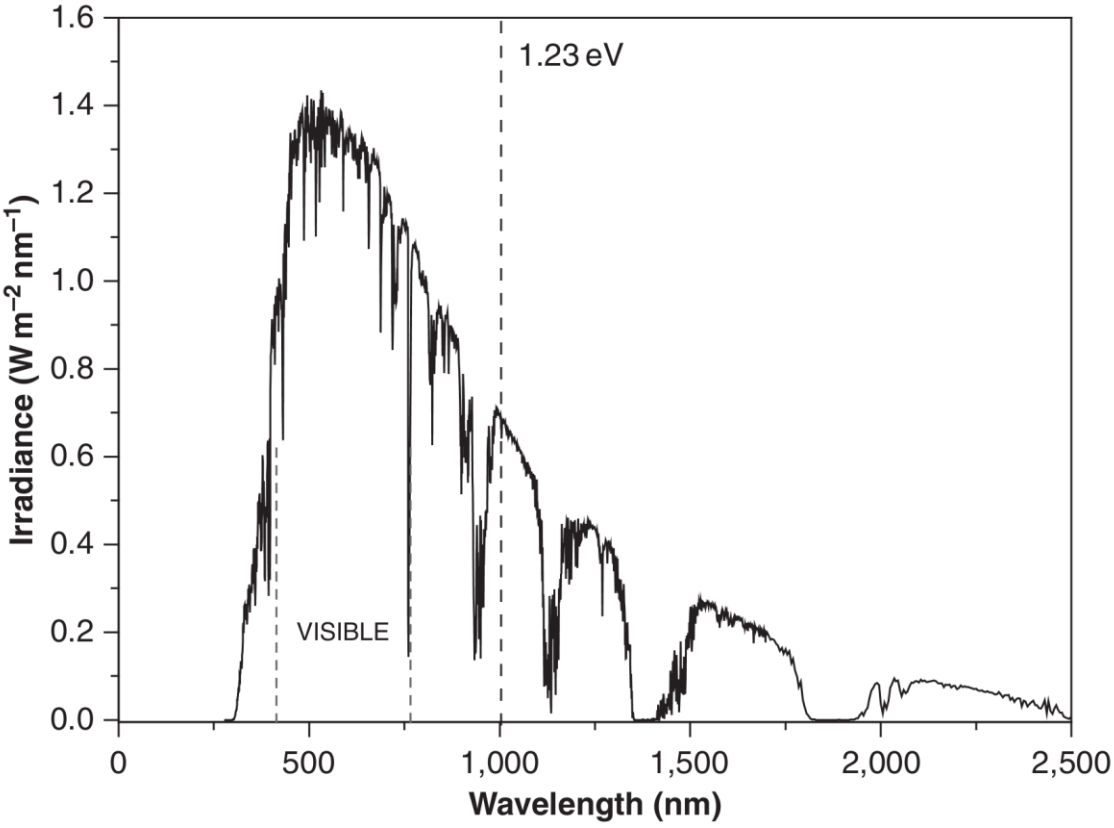

Figure 1-8: Solar irradiation spectrum (AM 1.5) versus photon wavelength (reprinted with permission of [22]).

1.4 Material characteristics

Figure 1-9 demonstrates the band gap positions of various semiconductors with respect to the redox requirements versus standard hydrogen electrode (SHE) in pH=7. As it is inferable form Figure 1-9, $KTaO_3$, $SrTiO_3$, TiO_2, ZnS, CdS and SiC can fulfill the band requirements for the water splitting process. It should be noted that this is just the thermodynamic point of

view and considering energy losses associated with the solar-to-hydrogen conversion, the optimum band gap value for the high-performance photocatalysis under visible light is set to lie between 2-2.2 eV in comparison to the theoretical condition which is 1.23 eV [5, 13].

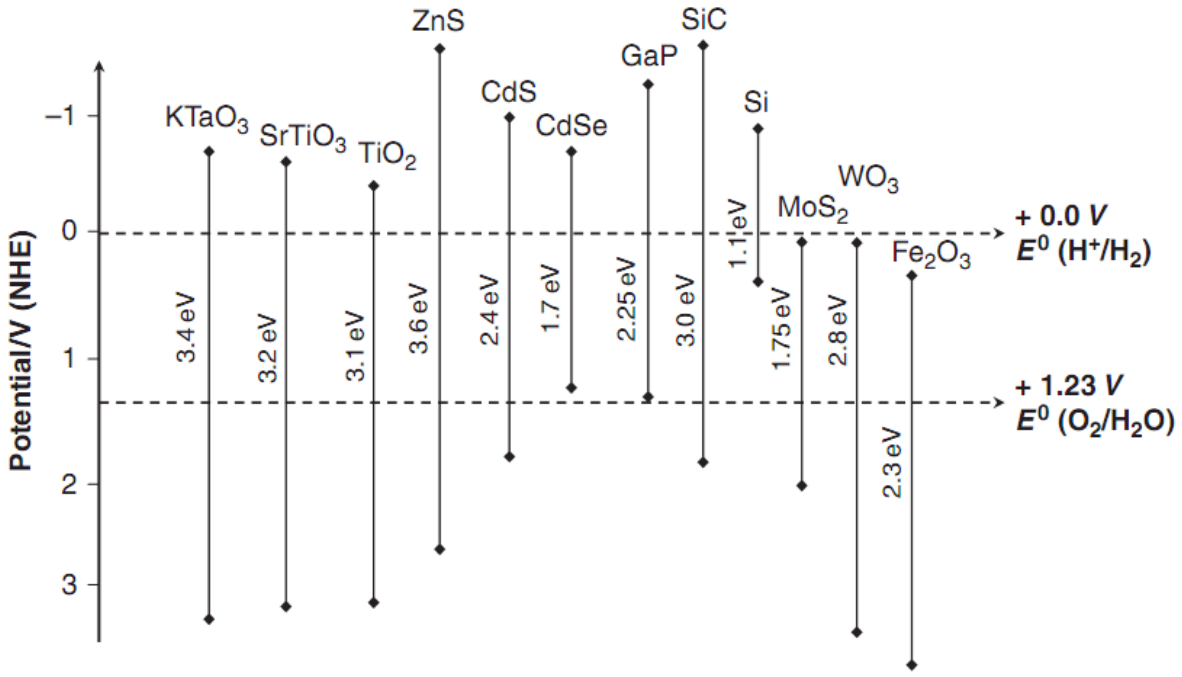

Figure 1-9: Band-gap energy and relative band position of various semiconductors with respect to the standard hydrogen electrode (SHE) for water redox reactions (reprinted with permission of [5]).

The photo-generated electron-hole charge transfer basically depends on the both microstructural and surface properties of the photocatalyst. Generally, the higher crystallinity brings the higher photoactivity where the density of the lattice defects decreases, lowering the recombination centers of the electrons and holes [23].

Another necessity for the water splitting process is the photocatalyst resistivity to the reaction occurring on the solid/liquid interface, including electrochemical corrosion, photo-corrosion and dissolution. In this way, a significant group of the materials with suitable semiconducting properties for the solar conversions (CdS, GaP, etc.) does not emerge as stable compounds in the water oxidation process. The anions of these semiconductors are

more prone to the oxidation than water, causing their degradation in the course of reaction [24, 25].

Surface reactivity from surface area to the active reaction sites is also determining. The photocatalyst particle size plays an important role in this regard, affecting the charge transport efficiency as well. Keeping in record that the diffusion length of the charge carriers must be long in comparison with the size of the photocatalyst in order to reach the surface, otherwise recombination occurs rapidly. As the result, the charge recombination possibility lowers with the decrease of the particle size. Nonetheless, the efficiency obtained from the higher crystallinity is prevailing over the enhancement associated with the particle-size decrease [13].

Considering the aforementioned criteria for the photocatalytic water decomposition, the photocatalysts used for this process must meet several expectations with respect to semiconducting and electrochemical properties [8, 13, 15, 16]: (i) band gap of around 2.0-2.2 eV and band edge potentials suitable for overall water splitting to be activated under visible light, (ii) successive separation of photo-excited electrons from reactive holes, (iii) minimum energy losses associated with charge transport and recombination of photo-excited charges, (iv) corrosion and photo-corrosion resistivity in aqueous mediums, (v) facilitated electron transfer properties from photocatalyst surface to water, and (iv) low production cost.

The following section aims to wrap major efforts toward obtaining more efficient photocatalysts, achieving higher rates of water splitting under visible light.

1.5 Visible light activated photocatalyst development

In this section, it is worthy to begin with the definition of the apparent quantum yield (AQY) as a touchstone for the photocatalytic water splitting under visible light. This parameter is defined as

$$AQY(\%) = \frac{2H}{I} * 100$$

where H and I represent the number of produced hydrogen molecules and incident photons, respectively.

The AQY is still the bottleneck of the utilizing photocatalytic energy conversion systems. As mentioned earlier, the efficiency of the photocatalytic processes mainly depends on the successful photo-excited charges separation and their delivery to the surface deriving photocatalytic reactions. For instance, femtosecond studies of the intensity dependence of electron-hole dynamics for titania shows about 90% electron-hole recombination right after excitation via irradiation [26]. This is the major concern about relatively low AQY of the most semiconductor-based photocatalytic systems. The obtained AQY values are still far from 10% which is the initial feasibility point for practical usage [5]. Hence, the development of the new materials for the photocatalytic water cleavage is a major issue and due to the insufficient progress in this concept, it is still counted as a premature technique. Extensive research has been performed in order to decrease the rate of the electron-hole recombination enhancing the quantum yield of the synthesized photocatalysts under visible light [8, 13, 15, 16, 27-35]. This involves considering the delicate control over the interrelated connections between the electronic, microstructural and surface properties of the particles, achieved by the careful design of the both bulk and surface characteristics. Various approaches are employed to introduce more efficient materials for water splitting purposes which can be

counted as follows: (i) search for the new single-phase semiconductors, (ii) band-gap modification of the UV-activated photocatalysts, (iii) cocatalyst deposition on the surface to catalyze surface redox reactions reducing activation energies, (iv) using sensitization effect, and (v) utilizing nanofabrication techniques controlling size and morphology of the synthesized semiconductors.

The following sections aim to expand some of the important above-mentioned strategies to develop various classes of the semiconductors for the water cleavage application under solar irradiation.

1.5.1 Band gap engineering

It is vital to rule over the energy structure (i.e. band gap) of the semiconductor in order to develop active photocatalysts under visible light. There are typically four strategies employed which can be classified as following: (i) ion doping, (ii) use of semiconductor composites, (iii) semiconductor alloy approach, and (iv) multi-photon transfer technique so-called z-scheme.

1.5.1.1 Cation or anion doping

There have been many efforts around semiconductor doping in order to enhance the response of those wide-band-gap photocatalyst (i.e. UV-active) to the visible light. One of the approaches is doping via transition metals to develop the visible-light-responsive semiconductor based on appropriate dopant selection. For instance, Sb- or Ta- and Cr-doped TiO_2 and $SrTiO_3$ [36, 37], doping ZnS with Cu or Ni [38, 39], or TiO_2 doping with C [40].

Cation doping effectiveness is due to the replacement of the transition metals in the crystal lattice of the wide-band-gap semiconductor, creating impurity energy levels within

the band-gap of the photocatalyst and enhancing the absorption in the visible region (see Figure 1-10).

Despite the positive effect of cation-doping on the absorption in the visible-light, most of the cation-doped photocatalyst have not emerged as promising candidates for water splitting application. This is mainly due to the significant lattice defect formation as the result of the dopant incorporation inside the structure of the semiconductor, generating noticeable photo-generated electron-hole recombination sites [41]. In addition, the impurity phases are commonly discrete or agglomerated which exacerbates the low efficiency of the photo-generated holes' migration [42]. Hence, it is crucial to delicately control the content and the depth of cation structural substitution in the parent photocatalyst to drive the redox photo-electrochemical reactions efficiently. There are various techniques employed for this purpose: (i) chemical methods such as impregnation and precipitation, or (ii) advanced ion implantation technique which involves incorporation of the high-energy accelerated ions via high voltage (50-200 keV) in the material structure. Although the second method exhibits higher level of accuracy and finesse, containing inevitable operational costs makes it almost infeasible for the mass production purposes [13].

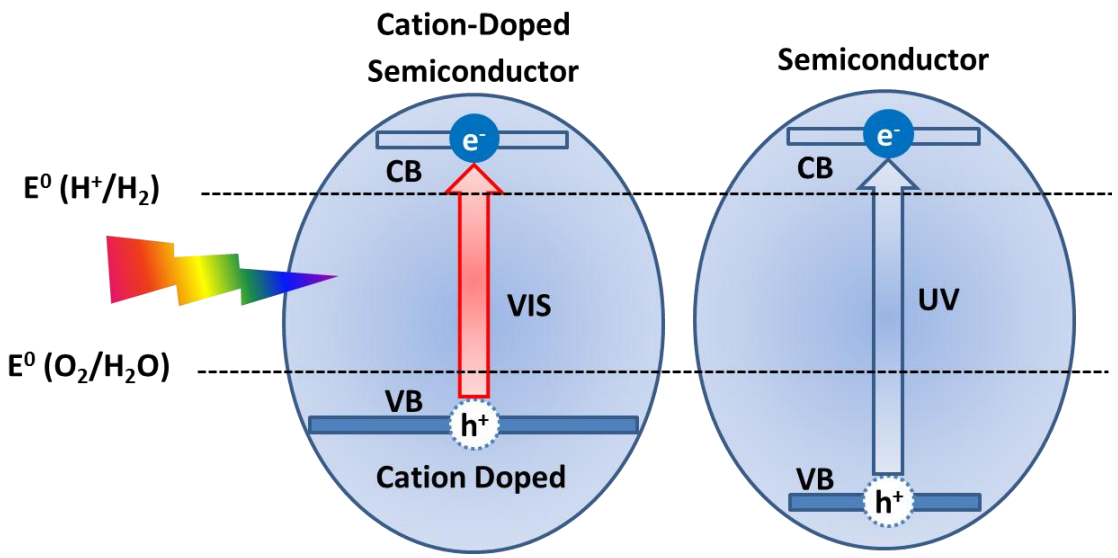

Figure 1-10: Cation doping effect on the wide-band-gap semiconductor photocatalyst with a visible light activity enhancement.

Another approach would be anion-doping to improve the visible-light response of UV-activated semiconductors. Recently, numbers of inspiring papers are published about this concept evaluating various semiconductors' performance under anion-dopings. For instance, in the oxide semiconductors, anions such as N [40, 43-45] are examined for oxygen substitution in the oxide lattice. The rationale behind this technique is to mix the p orbital states of the doped anion (N,S, or C) with the O 2p orbitals of the parent matrix, shifting the valence band edge upward and narrowing the photocatalyst band-gap as the result (see Figure 1-11).

In contrast with cation-doping method, anionic incorporation usually causes lesser recombination centers, being more suitable to improve the photocatalytic activity. However, it is essential to fine-tune the number of oxygen defects in the anion-doped semiconductors using controlled doping conditions. This is because of different formal oxidation numbers of the O and the dopant anions which can behave as the recombination centers.

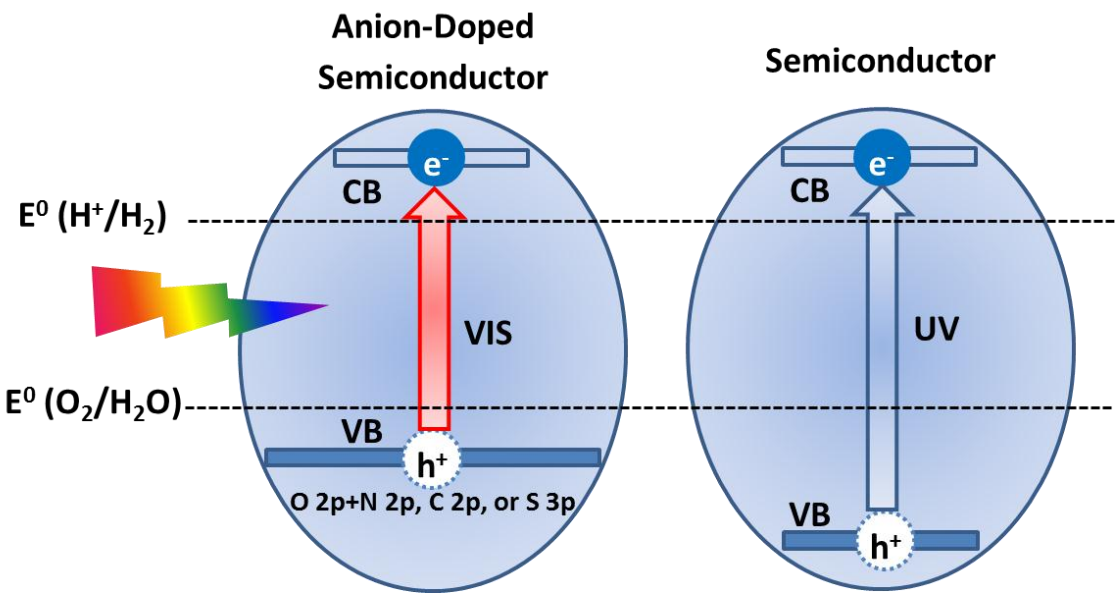

Figure 1-11: Anion-doping impact on the wide-band-gap semiconductor with a visible-light activity.

1.5.1.2 Composite semiconductors

Mixing of the semiconductors (i.e. semiconductor composites) is another major strategy in order to develop the visible-light responsive photocatalysts from their UV-active companions. The logic of this approach mainly relies on coupling a wide-band-gap semiconductor with a narrow-band one owning more negative conduction band level. In this way, it is likely that the conduction band electrons of the narrow-band semiconductor are injected via excitation into the UV-activated material, increasing the absorption capability of the formed composite (see Figure 1-12). Further motivation toward implementing this technique is reducing the rate of recombination via inter-particle electron transfer, inhibiting back electron transfer.

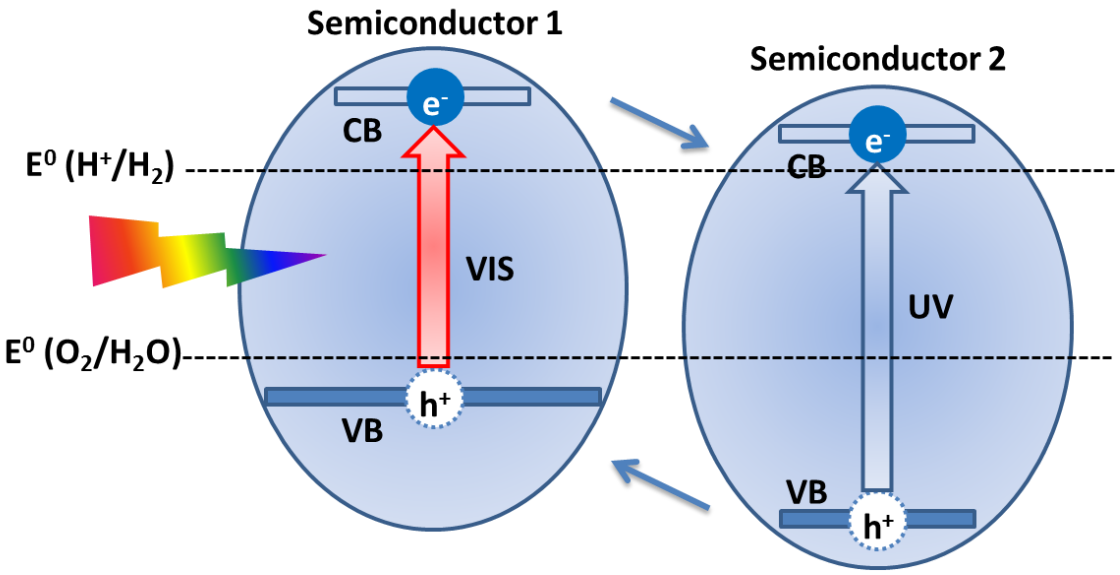

Figure 1-12: Composite photocatalyst concept with enhanced visible-light absorption, using a mixture of wide- and narrow-band-gap semiconductors.

It should be noted that as there is no mixing in the molecular level of the two coupled semiconductors and establishing an electronic connection between them is necessary, several criteria should be met: (i) the conduction band level of the narrow-band semiconductor should be more negative than the equivalent band in the other one, (ii) the conduction-level of the wide-band semiconductor should be more negative than the water reduction potential, and (iii) electron injection should be performed quickly and efficiently. The CdS-TiO_2 composites are the most salient examples of implementing this technique for water dissociation reaction [46-48]. CdS-$K_4Nb_6O_{17}$ [48] and $Ca_2Fe_2O_4$-$PbBi_2Nb_{1.9}W_{0.1}O_9$ [47] are among other evaluated compositions for water splitting under visible light.

1.5.1.3 Semiconductor alloys

The third approach to make the UV-active photocatalysts responsive to visible-light is to form solid solutions of the wide- and narrow-band-gap semiconductors with quite similar lattice structure, as illustrated in Figure 1-13. Inter-dispersion of the lattice sites of the solid

solution of two or more semiconductors brings the customization of the band in comparison to the parent matrices by changing the solution composition. Well-known examples of this approach are GaN-ZnO [34], ZnS-CdS [49], ZnS-$AgInS_2$ [50], and CdS-CdSe [51].

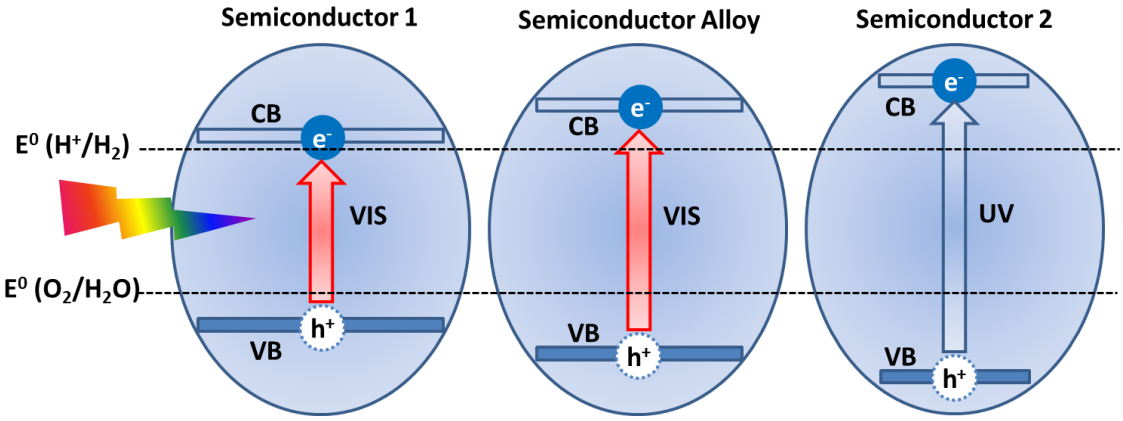

Figure 1-13: Band structure modification via solid solutions of wide- and narrow-band-gap photocatalysts.

1.5.1.4 Multi-photon water splitting (z-scheme)

Small band gap semiconductors can be also mixed to meet the requirements for the water splitting reaction through multi-photon processes so-called z-scheme. As it is depicted in Figure 1-14, the two step water cleavage using a reversible redox couple chemical (A/R) is achieved via two narrow-band semiconductors with different band-gaps and band positions [52-55]. One is well-suited for O_2 evolution (semiconductor 1 in Figure 1-14) while the other one meets the H_2 production criteria (semiconductor 2 in Figure 1-14).

Water is reduced to H_2 over the hydrogen evolution photocatalyst via photoexcited electrons while the electron donor (R in Figure 1-14) is oxidized through the holes to its electron-acceptor format (A in Figure 1-14). On the oxygen evolution semiconductor, the photo-excited electrons reduce the electron-acceptor (A) back to the electron-donor form (R) and the holes oxidize water to O_2. However, the simultaneous hydrogen and oxygen

evolution efficiency using this two-step water-splitting arrangement is strongly determined by the backward reactions proceed on the surface of each photocatalyst [56, 57].

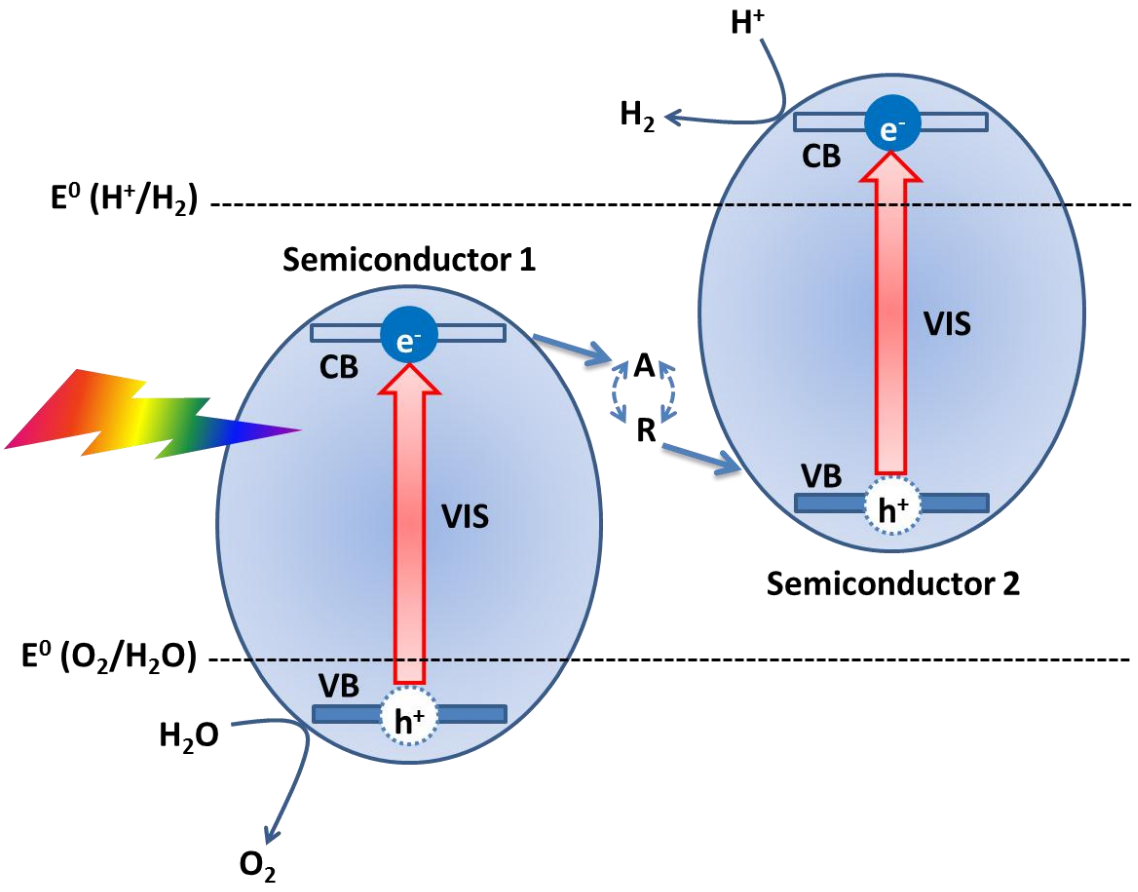

Figure 1-14: Multi-photon water splitting using a redox shuttle (A/R).

1.5.2 Surface modification using cocatalyst

As mentioned earlier, the photocatalytic water dissociation comprises surface gas evolution reactions. The photogenerated electrons and holes which can successfully reach to the surface of the photocatalyst overcoming recombination are able to reduce and oxidize surface absorbed water molecules, respectively. Both surface absorption and gas evolution reactions can be catalyzed employing noble metals or metal oxides so-called cocatalyst (Pt, Rh, NiO, RuO_2, etc.) on the surface of photocatalyst. These metallic compounds as depicted in Figure 1-15 increase the gas evolution efficiency based on the following impacts: (i)

capturing the electrons of conduction-band or the holes of valence-band for the excitation sites (sink role) [58], and (ii) transferring charge carriers to the surface absorbed waters, reducing the activation energy of the redox reactions.

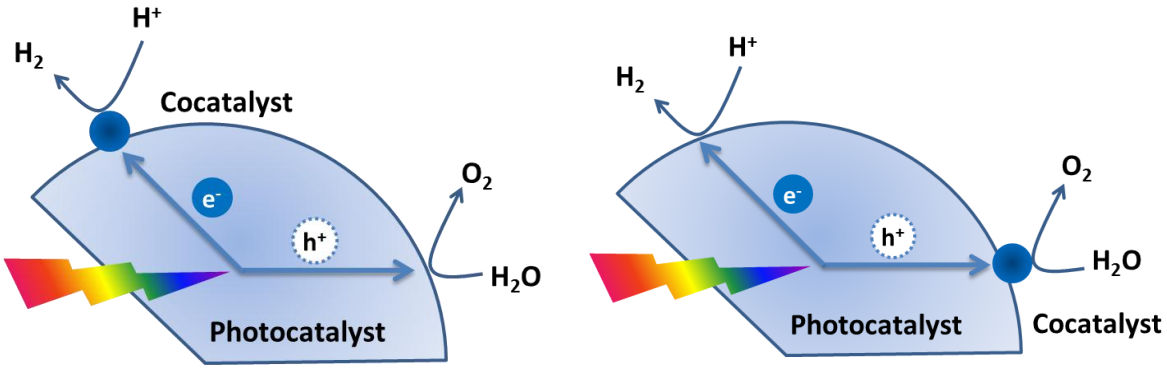

(a) (b)

Figure 1-15: Schematic of photocatalyst surface modification via cocatalyst addition facilitating the (a) hydrogen or (b) oxygen evolution in water cleavage.

1.5.3 Sensitization

In order to increase the number of electrons in the conduction band of the wide-band-gap semiconductors under visible light it is doable to take the advantage of a chromophore excitation such as an organic dye. Figure 1-16 shows the schematic of sensitizing approach for photocatalytic water splitting under visible light using titania as the base semiconductor.

The photo-sensitization approach of the UV-activated photocatalysts such as TiO_2 by dye junctions has been investigated sine late 1960s [59, 60]. The earlier studies performed on the flat electrode-based configurations, facing an intrinsic problem: only the top exposed monolayer of the dye was capable of efficient electron injection into the semiconductor, taking into account the small efficiency of the single dye layer solely. Concurrently, the dye-sensitized solar cells' development using single-crystal semiconductor electrodes has been

hindered considering the poor light-harnessing efficiencies and low photo-current densities [61].

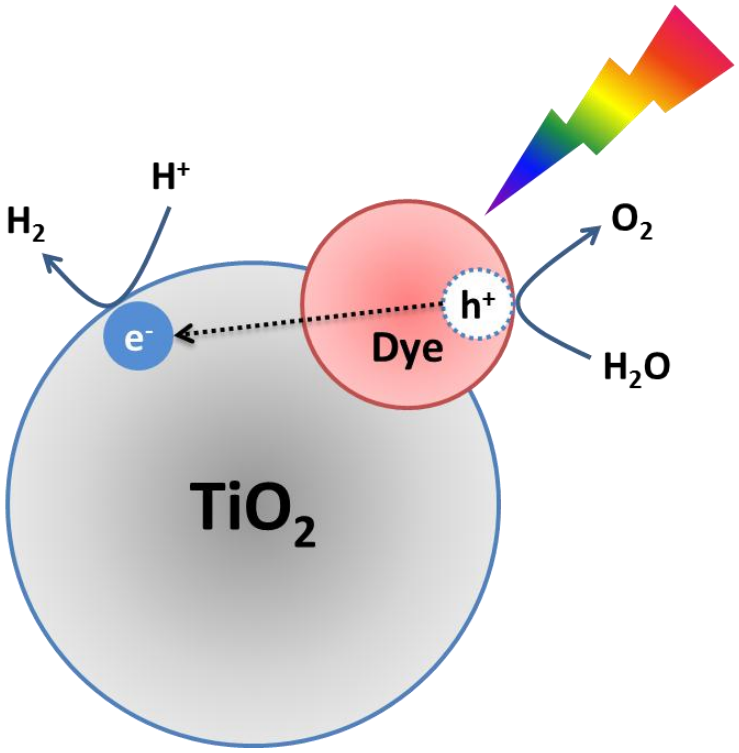

Figure 1-16: Schematic of dye sensitizing approach in photocatalytic water splitting under visible light.

In the porous film of TiO_2 nanoparticles where the surface area can be enhanced 1000-fold, making more efficient light absorption even with a single dye layer on each particle can be facilitated. In fact, nature utilizes similar technique of absorption improvement piling chlorophyll-containing thyalkoid membranes of the chloroplast to form granular configurations [59, 60]. It is worthy to note that the fascinating characteristic of the mentioned TiO_2 porous films is their highly efficient charge carrier transport through the particle, bulk and the grain boundaries with the quantum yield being practically equal to unity [62].

Although there is a massive amount of experimental data gathered on the dye-sensitized semiconductors over the decades, obtaining more detailed information with respect

to the unknown electron injection and recapturing mechanisms is vital to make more fundamental progress in this field. The intrinsically fast occurrence of these processes brings the importance of employing fast kinetic analysis techniques, which in the case of solid semiconductor powders is challenging. The recognized examples of various sensitizers are porphyrins and $Ru(bipy)_3^{2+}$ ("bipy" stands for bipyridine anions) derivatives or $Fe(CN)_6^{4-}$ surface-derivatized TiO_2 particles [63, 64]. Figure 1-17 depicts a water splitting dye-sensitized solar cell, employing a sensitizer-capped $IrO_2.nH_2O$ catalyst particle in the mesopores of the TiO_2 electrode film [61].

In all the presented instances the rate of the back-electron transfer from the semiconductor to the oxidized sensitizer occurred slower than that of forward injection with several orders of magnitude difference. Therefore, colloidal semiconductor particle combined with the sensitizer brings more capability for photo-induced charge separation [63]. This dramatic difference in lowering the back-electron transfer rates should be more discussed. One hypothesis has to do with the large driving force associated with recapturing the conduction-band electrons, putting this phenomenon in the inverted region where the rate decreases with heat release increase. Furthermore, investigation of this reaction from entropic point of view would be more telling. If a single sensitizer cation considered at the surface, the back reaction cannot easily afford the notable entropy drop of 67 $JK^{-1}mol^{-1}$ to proceed [63].

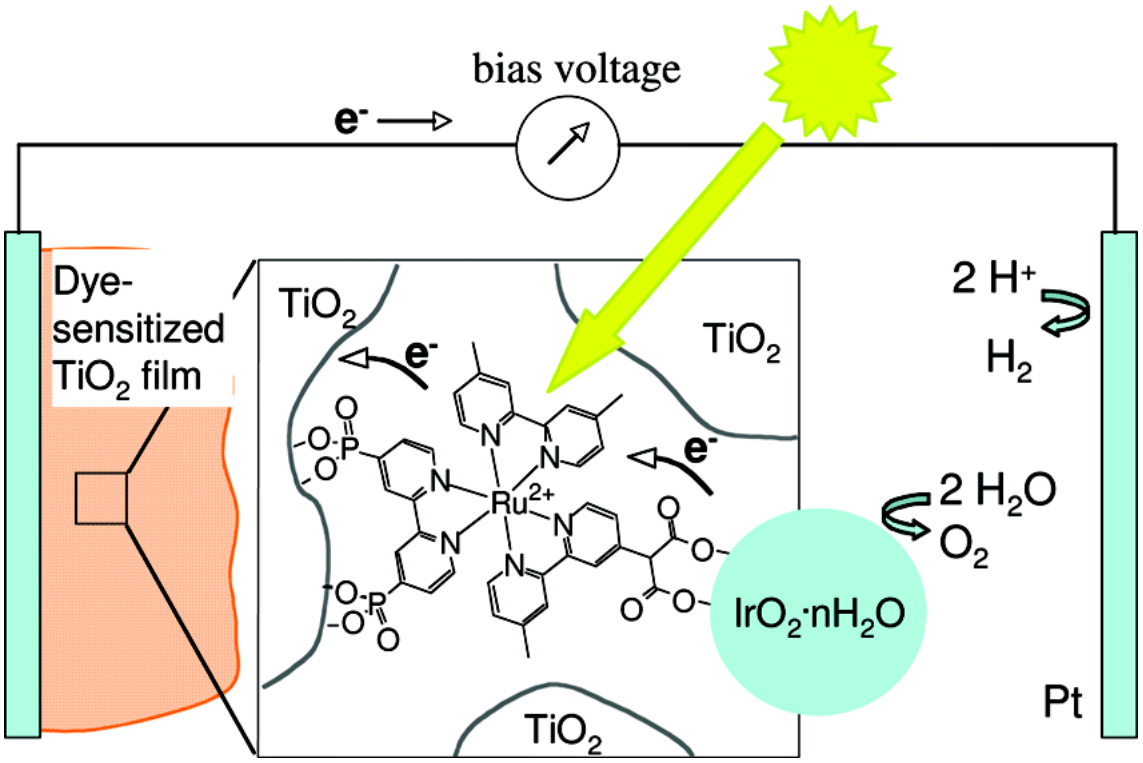

Figure 1-17: Schematic diagram of a water-splitting dye-sensitized solar cell, employing a sensitizer-capped $IrO_2.nH_2O$ catalyst particle in the mesopores of the TiO_2 electrode film [61].

Incorporation of a multicomponent system consisting of a number of chromophoric molecular components can also enhance the solar irradiation harvesting capability. This so-called antenna system absorbs incident light, channeling the energy through a common acceptor i.e. reaction center. Obviously, porphyrins, the main chromophores of natural photosynthesis have been examined for designing synthetic antenna systems [64-66]. Other intriguing assembly of polynuclear species of large nuclearity, so-called "dendrimers" or "arborols" because of their shape, has been synthesized using Ru^{II} and/or Os^{II} as metal centers, bisbipyridine type ligands as bridging groups, and bipyridine-type terminal ligands [67, 68]. In order to tune the nature and the position of the metal centers, bridging ligands and terminal ligands, an integrated synthesis strategy known as "complexes-as-metals/complexes-as-ligands" can be employed [65]. Using a well-recognized and

foreseeable method based on the information about the metals and ligands, it is possible to estimate the metal-to-ligand charge transfer energy (MLCT) in the excited state. As the result, more control over preparation leads to more control over the internal energy flow direction through these compounds [65, 66].

For the sake of practicality, one-dimensional antenna configurations might be more preferred due to the concern of interface binding having decent surface coverage associated with highly branched antenna systems. In the one-dimensional antennas, energy transfer should be stepwise along a chain of molecular components, and the number of components (i.e. maximum pathway distance of the system) heavily depends on the extent of driving force introduced by each energy-transfer step. Probability of achieving efficient energy propagation alongside the antenna systems has been verified using cyano-bridged pentanuclear compounds [69]. The findings led to the inference of efficient energy migration occurrence between isoenergetic adjacent molecular components. In order to afford the directionality, having higher-energy “stopper“ on one end and a lower-energy “trap“ at the other side is necessary [65, 66].

1.5.4 Advances in nanoscale engineering

The photocatalytic water splitting only happens when the photo-generated charge carriers can successfully overcome the recombination, reaching the surface of the semiconductor during their life time and find their suitable active sites and partners: protons for electrons and water molecules for the holes. Consequently, generation and separation of the photo-excited electron-hole pairs having low recombination rate is vital to meet the aforementioned criteria. The photo-generated charges’ transport is a function of crystal size and structure, nature and number of lattice defects, and the surface characteristics of photocatalysts. Having efficient

photo-induced charge transfer dynamics requires longer diffusion path length in comparison to the particle size. Thus, the probability of reaching the charge carriers to the surface increases with a decrease in particle size [70]. During this charge transportation phenomenon structural defects deteriorate the efficiency adversely acting as trapping or recombination point of the photo-induced electron-hole pairs, depending on the nature and location of the defects. It is worth noting that the presence of defects on the surface may enhance the reaction occurrence by trapping the photo-generated charges while having them in the bulk and grain boundaries is totally counter-productive as trapping and recombination centers. The higher crystallinity affords more fluent charge dynamics especially with the decrease of the structural defects in the bulk and grain boundaries [71, 72]. Setting aside the mentioned effect, the crystalline size has a noticeable impact on the electronic properties of the semiconductor. It is addressed by several researchers that the band gap of the crystalline semiconductor depends on its particle size [73-75]. When the particle size of the semiconductor drops from its bulk to that of the Bohr radius (i.e. the first excitation state), the size quantization (Q-size) impact appears due to the spatial confinement of charge carriers. Accordingly, photo-excited electron-hole pairs confined via a potential well are not affected by the delocalization occurring in the bulk phase. As a result, the band-gap of the semiconductor increases with a decrease of particle size to the nanometer range, lowering the photon absorption rate along with the change in the redox potential of the electron-hole pairs [73, 76, 77]. Furthermore, another impact of the dramatic change in the particle size to the nanometer range has to do with the presence of new electronic states combined with the surface vacancies acting as trapping centers enhancing charge separation process. This quantum size effect has been evaluated for different class of semiconductors, including CdS

[78], HgSe, PbSe, CdSe [79], ZnO [80], and TiO_2 [81, 82]. As a result it would be doable to control the redox characteristics of the photocatalyst nanoparticles by the aid of controlling their size. Although particle size effect may vary for various types of semiconductors due to their nature, the reported size effect along with the semiconductor clusters has been observed in the sizes from 3 to 15 nm. With respect to the effects of nano-sized particles on the absorption capabilities, charge transfer dynamics, and surface area, a great deal of effort has been performed to control the synthesis of the materials optimizing the particle size, morphology, lattice defects and crystallinity of the photocatalysts at the nanometer scale. There are number of contemporary approaches in synthesis employed in order to rule over the photocatalytic activity using nano-structuring of the crystalline semiconductors; for instance, sol–gel [83-85], micelle and inverse micelle [86, 87], hydrothermal [88, 89], chemical vapor deposition (CVD) [90, 91], sonochemical [92], and others.

One common and major phenomenon is that in the nanometer regime, particles usually tend to agglomerate having strong inter-particle affinity toward each other. To overcome this unfavorable happening there have been efforts to incorporate photocatalysts within the framework of the microporous hosts; for instance, Mobil Composition of Matter (MCM) [93, 94], zeolites [95, 96], and activated carbons [97, 98].

Aside from fine-tuning of the individual particles in the nano-structural configuration, the importance of utilizing a three-dimensional network to improve the overall efficiency should not be overlooked. It is observed that the colloidal TiO_2 cluster exhibit superior photocatalytic activity when they tend to form a three-dimensional network along a predefined crystallographic template [99]. Figure 1-18 demonstrates Advances in nano-scale

semiconductor preparation from individual nanoparticles to three-dimensional oriented structures [100].

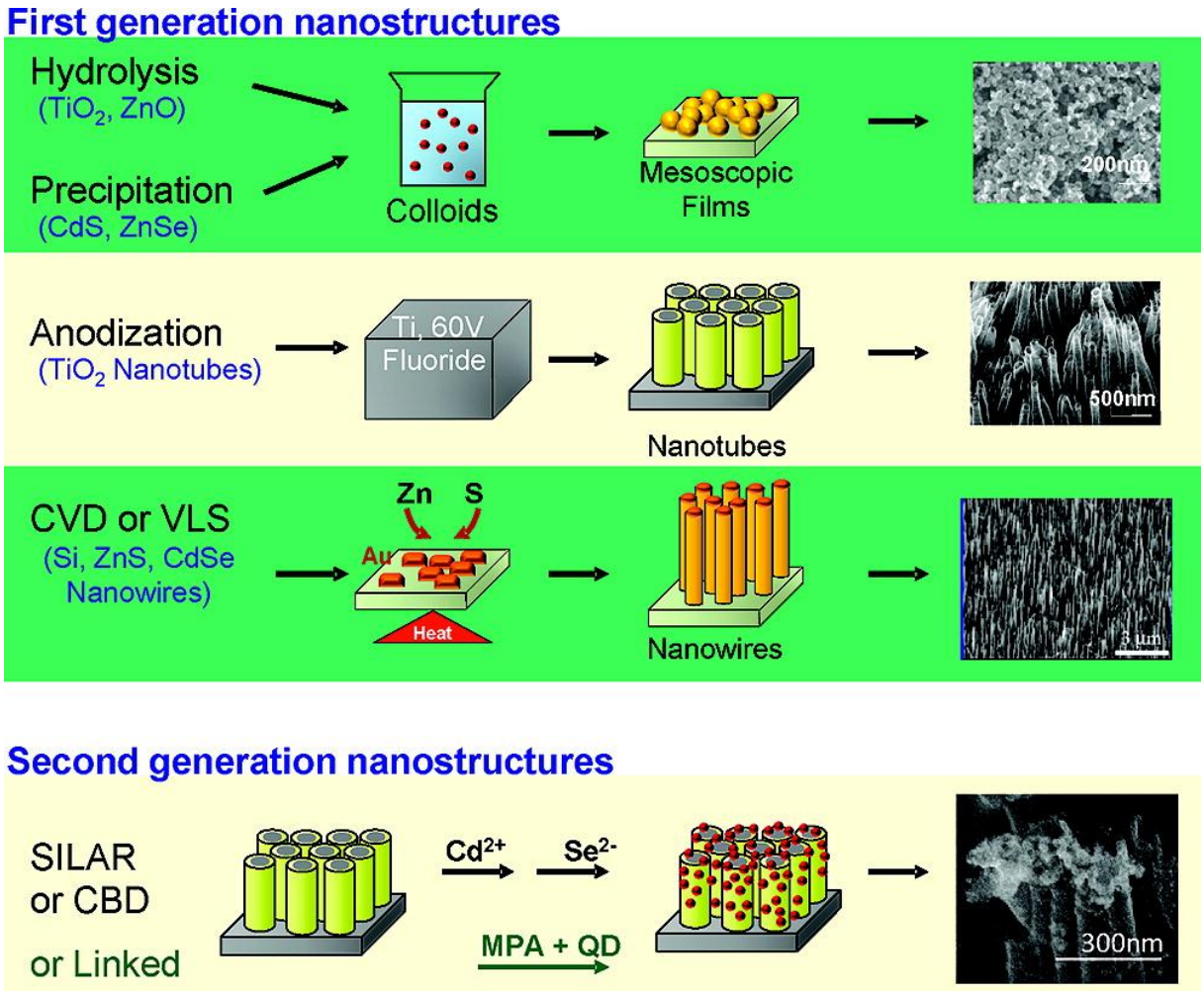

Figure 1-18: Advances in nano-scale semiconductor preparation from individual nanoparticles to three-dimensional oriented structures (VLS stands for vapor-liquid-solid, SILAR for successive ionic layer adsorption and reaction, CBD for chemical bath deposition, MPA for mercaptopropionic acid, and QD for quantum dot) (reprinted with permission of [100]).

Based on the experiments, researchers suggested a relatively new mechanism so-called antenna mechanism. In this process, the three-dimensional architecture obtained via a certain template and orientation behaves as an antenna system, aiming to propagate the photon energy from the original excitation location to the reaction active sites. This

successful antenna configuration can be potentially applied over all types of the photocatalytic systems. Most recently used photocatalyst powders containing primary nanocrystalline particles can be managed to be agglomerated in an oriented manner forming secondary structures with micrometer dimensions. In this way, the whole material as photocatalyst with strong electronically interconnected structure shows more significant photocatalytic activity as the result of intensified antenna effect. Afterwards, it should be doable to employ smarter molecular self-assembly techniques in order to achieve higher photocatalytic activities via more efficient internal electronically coupling of the nanoparticles.

1.6 Zeolite-based TiO_2 with heteropolyacids

As mentioned in previous section, TiO_2 has an intriguing characteristic of being highly efficient in charge carrier transport through the particle, bulk and the grain boundaries with the quantum yield being practically equal to unity [62]. Having a great capability to serve water dissociation reaction under irradiation, titania particles, however, are not well-suited for solar irradiation with their wide-band-gap which is in UV region [16]. Hence, there have been many efforts based on the aforementioned strategies to perform band-gap engineering, obtaining more visible-light response. It is worthy to note that in terms of internal structure, there are two types of the titania used for photocatalytic applications so-called anatase and rutile (Figure 1-19). It is inferred by experimental studies that the anatase phase has more suitable active sites for the photocatalytic water cleavage [101].

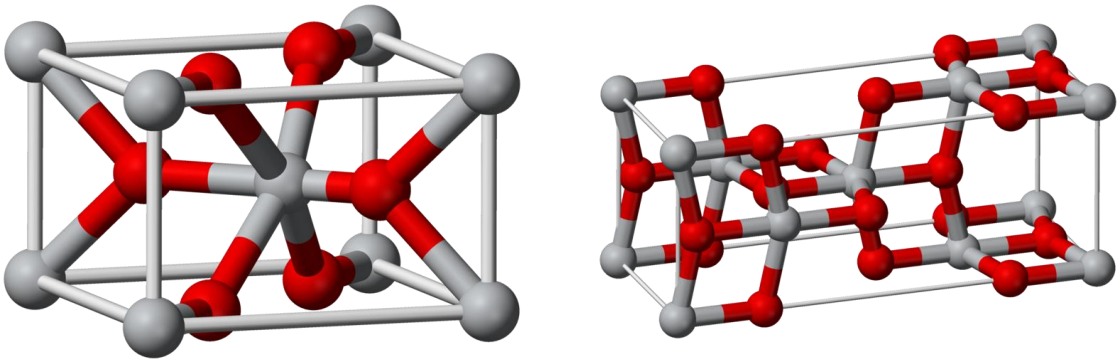

(a) **(b)**

Figure 1-19: Ball-and-stick model of the crystal structure of two commonly used titania structures (oxygen atoms are colored red while titaniums are grey) [102]: (a) rutile, and (b) anatase.

Among the counted approaches, sensitizing strategy has brought considerable attention recently, due to the advances in the various fabrication processes as well as new material developments, hiring the closest mechanism to the photosynthesis process. However, it is addressed several times that most of dye-sensitized compositions are not stable in the aqueous mediums suggesting nonaqueous electrolytes such as iodide solutions to deliver the electro-hole pairs to the water molecules [15]. Besides, the majority of the experiments have employed electrode-based configuration in order to follow sensitizing approach criteria. However, recently, a relatively new class of the combination of TiO_2 and a dye using particle-based approach utilizing zeolites as the support has been examined successfully for water cleavage reaction under visible light [95, 96]. These efforts deserve further investigations in order to conduct more meaningful experiments on this concept in future. The utilized dye–which the phrase of "dye" is just one side of that–is classified in the category of the heteropolyacids (HPA) and cobalt compounds (instead of precious platinum deposits) have been used as cocatalyst in conjunction with the support framework facilitating hydrogen evolution reaction.

In this section, it is worthy to briefly focus on two components of the introduced formula, which have not been covered so far in this chapter. The first chemical is zeolite and the second one is HPA.

Zeolites are available in two types of natural (which is known for almost 250 years as aluminosilicate minerals such as faujasite, mordenite, offretite totally about 40 types) and synthetic (which is more optimized, purified and monolithically structured totally about 191 types) [103]. The synthetic zeolites after their advent by Barrer and Milton from ca. 1948 to 1955 began to play a significant role in catalysis. The most remarkable field of their application was initiated by introducing synthetic faujasites (zeolites X and Y) in industrial fluid catalytic cracking (FCC) of heavy oil distillates in 1962, one of the key chemical processes in worldwide energy and economy [104]. The synthesized zeolites were not only emerged noticeably more active than the previously used amorphous silica-alumina catalysts, but also increased the yield of gasoline drastically, the most valuable product of the FCC plants.

Taking the advantage of their highly crystalline structure, zeolites contain silicon, aluminum and oxygen forming an internal framework with cavities and channels, where cations and/or small molecules may reside. Due to their unique porosity properties, zeolites afford a wide variety of applications from catalysis to the ion exchange and separation processes known as molecular sieves.

As the matter of the linkage of primary tetrahedral units built of SiO_4 and AlO_4 via sharing oxygen atoms, zeolites own open three-dimensional framework structures. The manner of linkage is determining the type of zeolite, introducing a wide variety of fascinating structures. Zeolite structures can be considered to exist of finite or infinite (chains, layers,

etc.) component units. The finite units which are shown in Figure 1-20 are also called as the secondary building units (SBUs). In the Figure 1-20, the Si or Al atoms are located at the corners whereas oxygen atoms are in the mid-points of the lines connecting each Si or Al atom (oxygens are not shown for more clarity).

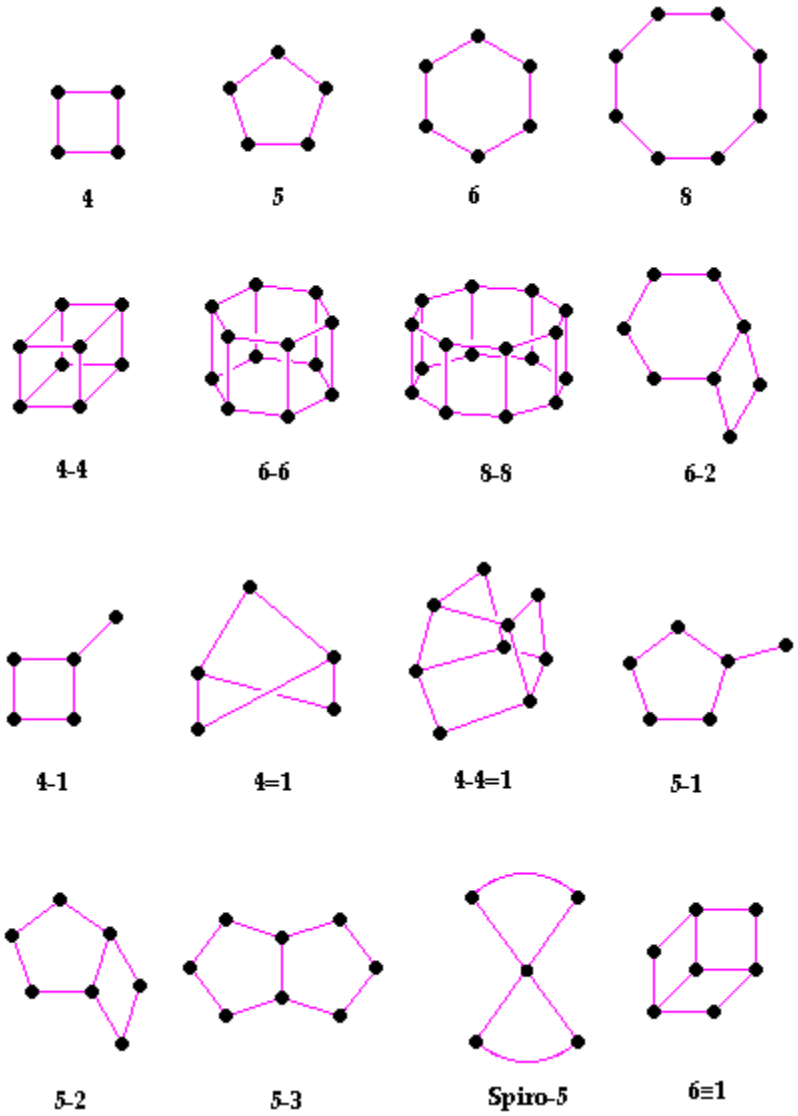

Figure 1-20: Various types of secondary building units (SBUs) in zeolites. The corner of the polyhedral represents tetrahedral atoms [105].

The SBUs can contain up to 16 primary building units which are the tetrahedral structures of SiO_4 and AlO_4. It should be noted that the SBUs are non-chiral (neither left nor

right "handed"), each unit cell containing the same number of them. Although scarce, some frameworks can have various combinations of the SBUs within the structure [105].

The shape of the connections between SBUs may lead to the formation of interconnected cages, cavities or channels spacious sufficiently allowing small molecules to enter. This is inferable from the relatively low density of the zeolites in comparison to the nonporous solids. The framework of the aluminosilicate has a net negative charge absorbing cations to meet the electro-neutrality criterion.

Figure 1-21 depicts the tile style of three selected zeolite types applied in this research for the water splitting application. Zeolites are the only class of structured materials which are now mass produced and available in a very wide range of structure, pore size, and also chemical properties specially acidity at a relatively low price. Thus, potentially, they can be promising feasible structured materials for this application.

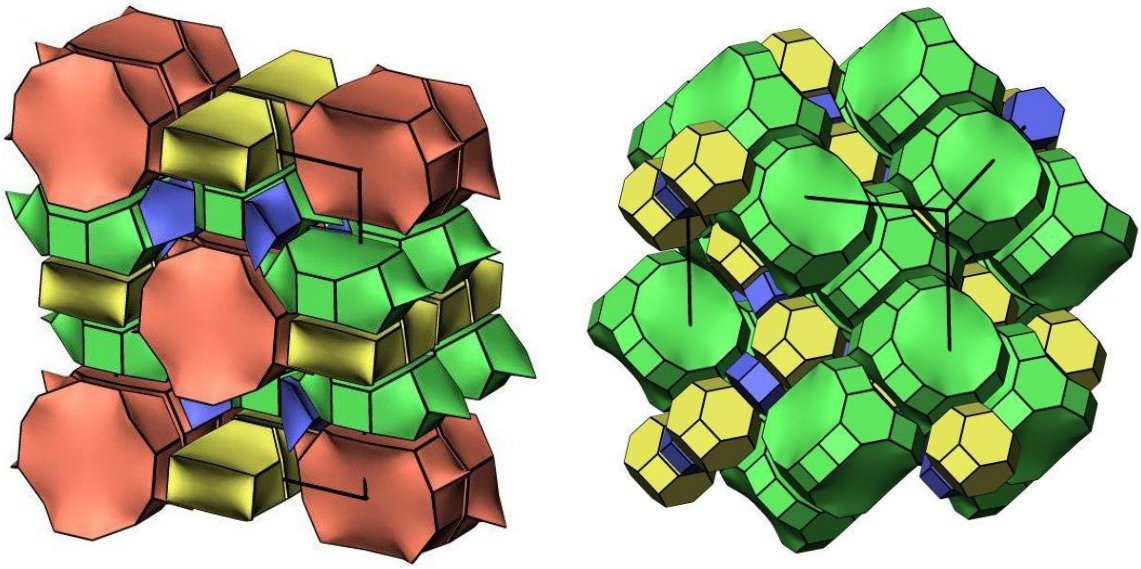

(a) **(b)**

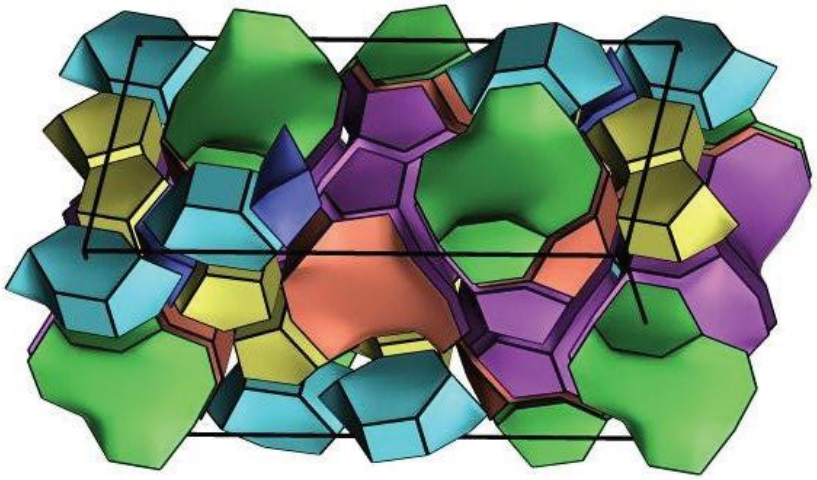

(c)

Figure 1-21: Three selected zeolite types for the water splitting application [103]. (a) Mordenite, (b) Y, and (c) Beta.

A heteropolyacid is a class of acid made up of a certain combination of hydrogen and oxygen with particular metals (mostly tungsten, molybdenum or vanadium), and non-metals (mostly silicon, phosphorus or arsenic) [106]. This type of acid is frequently used as a re-usable acid catalyst in chemical reactions. Application of heteropolyacids (HPAs) and the related polyoxometalate chemicals is increasingly emerging in the field of catalysis. This is basically due to a number of their advantages whether economically or environmentally [107]. On one side, they have very strong Bronsted acidity approaching superacid region; on the other side, they are inspiring oxidants, showing reversible multi-electron redox shuttles under rather mild conditions with a relatively fast conversion rate. Their redox abilities and acid-base characteristics heavily rely on the chemical composition of this class of materials. Having discrete ionic structure including mobile basic heteropolyanions and counter-cations (usually protons), solid HPAs exhibit high proton mobility [106]. They also have high solubility in some specific polar solvents with a fairly high thermal stability. The mentioned properties afford HPA to emerge as a promising acid, redox and bifunctional catalyst in

homogeneous and heterogeneous configurations [106]. During last three decades a wide range of applications for the HPAs is found mostly in the selective transformation of the organic molecules [108].

In terms of structure, the metal addenda atoms connected through oxygen atoms forming a fairly large molecule with the hetero-atom inside bonded via oxygen atoms, also known as polyoxometalate. Due to various combinations of addenda atoms and different types of hetero-atoms there is a wide variety of heteropolyacids. Two of the well-known categories of HPAs are based on the Keggin, $H_nXM_{12}O_{40}$, and Dawson, $H_nX_2M_{18}O_{62}$, structures (Figure 1-22).

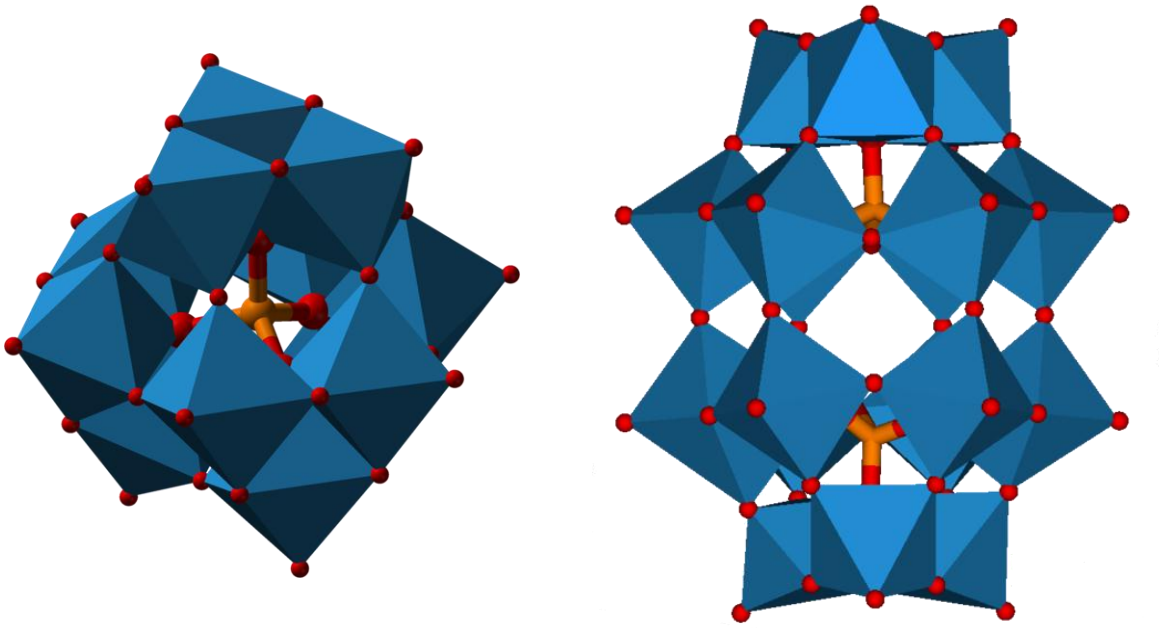

(a) **(b)**

Figure 1-22: Two available structures for heteropolyacids [109]: (a) Keggin structure, $XM_{12}O_{40}^{n-}$, and (b) Dawson structure, $X_2M_{18}O_{62}^{n-}$.

Another intriguing feature of this class of materials is the excitability properties of their anions, making them usable in photocatalytic applications. Besides, in some cases, they convert to another state so-called heteropolyblue (HPB) under irradiation which has a wide

range of response to the visible light [110]. In this way, they are capable of emulating the dye sensitizing concept as well as their remarkable role as cocatalyst and solid electrolyte medium.

Nonetheless, the number of research performed on the inspiring combination of zeolites, titania and HPA using cobalt compounds as cocatalayst is not significant due to the relatively novel and multidisciplinary nature of this concept. The degree of importance of each element, individual roles and probable synergetic impacts are still unclear.

1.7 Thesis scope and objectives

Based on the presented concept in the previous section, a better understanding of the fundamentals of the zeolite-based TiO_2 water dissociation through isolated experiments under visible light using various chemical promoters is the overall objective of this research. This would ultimately lead to the development of a new class of solar-activated zeolite-supported photocatalysts for water splitting application.

To meet the overall goal in a reasonable manner, the following specific objectives are set to be satisfied employing a series of controlled experiments and related analysis:

1. Study the role of zeolite as the support in the water splitting ability of the TiO_2-based photocatalysts.
2. Study the effect of heteropolyacids on the absorption spectra and photocatalytic activity of TiO_2-based samples under visible light.
3. Study the impact of the nanometer-sized titania particles and semiconductor-support interactions specifically in the case of TiO_2-zeolite.
4. Study the application of the synthesized photocatalysts for the oxidation of the organic compounds specifically 2,4-dichlorophenoxyacetic acid (2,4-D).

5. Finding the impact of preparation method specifically cocatalyst impregnation step in the photocatalytic activity of the synthesized photocatalysts.
6. Proposing novel concepts for the development of the next generation of the photocatalytic water cleavage using supported semiconductors under visible light.

1.8 Thesis layout

This dissertation is presented in the form of two manuscripts, each aims to meet some of the aforementioned objectives. Additional information regarding the designed and manufactured experimental setup for photocatalytic activity measurements besides complimentary background experiments' explanations are presented in Appendices A and B, respectively. The following is a detailed description of how each of the above objectives has been met with respect to their presentation in the following chapters and/or appendices.

Chapter 2 covers the related material to meet the Objectives 1 to 4. This manuscript is oriented in such a way as to investigate the chemical point of view of the successful combination of zeolite, titania, HPA, and cobalt for photocatalytic water splitting under visible light. Considering pros and cons, it is tried to provide a realistic insight regarding the role of the support on the hydrogen evolution potential under visible light. In this regard, four classes of zeolites have been evaluated: Na-Y, Na-Mordenite, H-Y and H-Beta with various Si/Al ratios and sodium content. Simultaneously deeper characterization techniques have been employed to make the role of HPA and nanometer-sized titania on the support clearer, evaluating their performance for environmental applications as well.

Chapter 3 contributes to meeting Objective 5 and 6. From the preparation point of view, the synthesis of the objective photocatalyst compound consists of three impregnation steps of TiO_2, Co, and HPA, respectively, followed by a specific thermal treatment for each

stage. The focus of this study is on the cobalt impregnation step. The aim is to investigate the impact of two commercially available cobalt precursors on the photocatalytic activity of the final synthesized photocatalysts, especially hydrogen production rate. The interesting side observations of this study led to the hypothesis of the presence of the core-shell photocatalysis, opening a new window of opportunity in this concept.

Chapter 4 aims to wrap up the conclusions provided in the thesis, generalizing the highlights for the future work; especially in the concept of supported photocatalysts using various types of chemicals as promoters, different semiconductors and supports. This tries to expand an inspiring approach, which because of being outside the scope of the current work, only a limited portion of that have been put to the practice. Hopefully, following the promising results of this research, it grabs more attention in order to cultivate and implement more ideas accomplishing more related projects in near future.

Appendix A contains complimentary information regarding the experimental setup designed and manufactured during this research for photocatalytic activity measurements under visible light. All the steps from conceptual design to the final instrumentation, piping and troubleshooting were taken by the researcher, ending up with a robust apparatus for evaluating the performance of the prepared photocatalysts in the slurry-based photoreactor.

Appendix B aims to explain various background experiments needed for acquiring reliable data which can be directly attributed to the photocatalytic performance of the synthesized photocatalysts under visible light. Although it's explained in the body of the thesis insofar with the related analysis, putting extra information with respect to some of the related highlights would be complementary.

Chapter 2: Characterization and performance evaluation of zeolite-supported TiO_2 photocatalysts[1]

2.1 Introduction

Using solar energy in the form of light is the most efficient solar path to hydrogen due to the absence of the inefficiencies associated with thermal transformation or the conversion of solar energy to electricity followed by electrolysis [5]. Hence, the most promising way to hydrogen toward a renewable energy source is water decomposition using photocatalytic technologies coupled with solar energy. This process mimics photosynthesis by converting water into H_2 and O_2 using inorganic semiconductors that induce the water-splitting reaction [13].

$$H_2O \xrightarrow{h\nu} H_2 + \frac{1}{2}O_2 \qquad \Delta G^0 = 237\ kJ.mol^{-1}$$

The revolutionary experiments of Fujishima and Honda [14] in 1972 on semiconductors capable of absorbing light energy proved that this class of materials can drive the water-splitting reaction for hydrogen generation. Since this inspiring research, numerous studies have been performed on various types of semiconductors in order to enhance their performance for photocatalytic water dissociation processes especially under visible light [27-35]. The common conclusion is that the energy conversion of these materials strongly depends on their intrinsic properties [5, 13, 15, 16, 111].

Regarding the photo-electrochemical phenomena of water decomposition, the photocatalysts used for this process must meet several expectations with respect to

[1] A version of this chapter has been submitted for publication.
Amin Taheri Najafabadi, Fariborz Taghipour, Photocatalytic hydrogen production of zeolite-supported TiO_2 nanoparticles under visible light.

[2] A version of this chapter has been submitted for publication.
Amin Taheri Najafabadi, Fariborz Taghipour, Photocatalytic hydrogen production of zeolite-supported TiO_2 nanoparticles under visible light.

semiconducting and electrochemical properties [5, 13, 15, 16, 111]: (i) band gap of around 2.0-2.2 eV and band edge potentials suitable for overall water splitting to be activated under visible light, (ii) successive separation of photo-excited electrons from reactive holes, (iii) minimum energy losses associated with charge transport and recombination of photo-excited charges , (iv) corrosion and photocorrosion resistivity in aqueous mediums, (v) facilitated electron transfer properties from photocatalyst surface to water, and (iv) low production cost.

During the last two decades, extensive studies have been performed based on the impregnation of various photocatalyts on support materials [112-119] to meet some of the above mentioned expectations. The major incentives for implementing the supported photocatalyst idea are: (i) inhibition of the back electron transfer as limiting parameter in redox systems, (ii) taking advantage of nano-sized semiconductors while using them in easily separable micro-sized level of the support, (iii) utilizing the support to add more solid chemical promoters, and (iv) structural and chemical characteristics of the support by itself.

Glass beads [120-122], fiber glass [123, 124], and silica [125, 126] are among the traditional choices for the support whereas there are more advanced options with relatively high mobility of protons or electrons, whether locally or overall, such as Mobil Composition of Matter (MCM-41) [93, 94], zeolites [95, 96] and activated carbons [97, 98]. The hydrogen evolution rates are encouraging in some cases but it is time to go through further detailed studies of the related works.

In this study, zeolites are selected as the photocatalyst support due to some of their advantages in comparison to the other structured materials. Zeolites are the only class of structured materials that are now mass produced and are available in a very wide range of structure, pore size, and chemical properties especially acidity at a relatively low price.

Hence, this can be a promising and feasible choice for photocatalyst support application. It should be noted that undue emphasis on the advantages of supported photocatalysts can be counterproductive and misleading. Therefore, it is necessary to address the negative points as well.

A combination of the zeolite-supported TiO_2 with cobalt-based co-catalysts has been examined with promising hydrogen evolution rates in the presence of heteropolyacids under visible light [95, 96, 110, 127]. Recently, few of these studies investigated the effect of zeolite structure on the hydrogen production potential [95, 96]. However, no comprehensive explanation has been offered due to the multidisciplinary nature of the involved photocatalytic processes. Hence, more fundamental studies can open a new window of opportunity for research in this field.

In this study, the physical and chemical roles of the zeolite as the support in the photocatalytic processes have been investigated with the emphasis on the latter role. This was achieved by examining four classes of the zeolites namely Na-Y, Na-Mordenite, H-Y and H-Beta. The synthesized photocatalysts were evaluated for both water splitting reaction and photocatalytic degradation of organic compounds, specifically 2,4-Dichlorophenoxyacetic acid (2,4-D) with the related characterizations. In addition to a comprehensive study of the chemical characterization of the support, some important aspects of its physical contribution were also investigated to make the effect of chemical properties clearer.

2.2 Experimental approach

2.2.1 Materials

Synthesis of the photocatalysts was carried out using the following zeolite structures namely Na-Y (SiO_2/Al_2O_3 =5.1, ID: CBV100), H-Y (SiO_2/Al_2O_3 =30, ID: CBV720), H-Beta

(SiO_2/Al_2O_3 =25, ID: CP814E) and Na-Mordenite (SiO_2/Al_2O_3 =13, ID: CBV10A) all from Zeolyst International Company. The other materials used in the preparation of photocatalysts were cobalt chloride hexahydrate 98%, phosphomolybdic acid (PMA) 78% as the utilized HPA, and titanium isopropoxide 97% all from Sigma-Aldrich, and isopropanol plus sulfuric acid 98% from Fisher Scientific. All the chemicals used were of the analytical grade. Double distilled water was applied in all the synthesis procedures.

2.2.2 Photocatalyst preparation

The general method for the synthesis of the four batches of photocatalyst powders is presented as follows. 1.850 g of titanium isopropoxide was dissolved in 50 ml of isopropanol then added to 5.000 g of the zeolite. This is equivalent to 10 wt% loading of TiO_2 on zeolite. The formed slurry was mixed thoroughly to be kept in homogeneous condition which was then dried for 12 h at 80±5°C and then calcinated at 500°C for 3 h. The conditions were chosen in a way to preserve TiO_2 anatase phase based on related literature [128, 129] which is identified to be more active for water splitting application [101]. The supported titania was then added to 100 ml of double distilled water to form the first slurry. The precursor solution was prepared by dissolving a specific amount of cobalt chloride equal to 5% of calcium binding capacity (CBC) of the support in 250 ml double distilled water. The first slurry and cobalt solution were mixed using a magnetic stirrer to facilitate cobalt ion exchange with the ions of zeolite. After 45 minutes, the solution was vacuum filtered and the treated zeolite was washed thoroughly with double distilled water. It was then dried on a hot plate at 80±5°C for 4 h (higher temperature avoided to prevent cobalt oxidation). The heteropolyacid (HPA) solution was incorporated by dissolving 0.500 g of HPA in 10 ml of double distilled water before adding it to the filtered mass obtained in the previous step to form slurry. The slurry

was dried on a hot plate maintained at 65±5°C for 8 h (higher temperature can cause structural changes or decomposition) while it was initially stirred continuously with a glass rod to make it homogeneous. The dried bulk was then finely homogenized using an agate mortar pestle. The framework of the preparation was designed in such a way to be consistent with the related literature for the sake of comparison [95, 96].

Two standard samples were prepared as the basis to compare their photocatalytic activities with those of the four synthesized batches. Degussa P25 has been used in many studies as a touchstone for the comparison of TiO_2 performance; however this basis was considered insufficient as it contains various phases of the titania [130]. Hence, an additional standard of the unsupported TiO_2 was prepared (T_tr500) using titanium isopropoxide as precursor and isopropanol as solvent with the same drying and calcination conditions of the main synthesized batches. For a comprehensive investigation, various percentages of the TiO_2 on the zeolite supports (10%, 25% and 50%) were also impregnated, dried and calcined keeping the predefined framework. Table 2-1 represents the specific amount of ingredients for the preparation of each photocatalyst batch. For the names, the number in front of "CB" is the sample number and the number in front of "P" is the impregnation step.

Table 2-1: Summary of the composition of the four synthesized photocatalysts.

Name	Zeolite *	Si/ Al	Raw Surface Area (m^2/g)	Type	Na_2O wt%	Titanium Ispropoxide*	Cobalt Chloride*	PMA *
CB1P3	5.000	5.1	900	Y	13	1.850	0.127	0.500
CB2P3	5.000	13	425	Mordenite	6.5	1.850	0.064	0.500
CB3P3	5.000	30	780	Y	0.03	1.850	0.029	0.500
CB4P3	5.000	25	680	Beta	0.05	1.850	0.039	0.500

*** Unites are all in grams.**

2.2.3 Characterization

The elemental analysis and surface morphology of the prepared photocatalysts were performed by energy-dispersive X-ray (EDX) spectroscopy and scanning electron microscope (SEM), respectively using Hitachi Model S3000N VPSEM. A Micromeritics surface area analyzer (ASAP2020) was utilized to determine the BET surface area of the synthesized photocatalysts. UV-VIS diffuse reflectance (DR) spectra were obtained using Agilent Cary 5000 spectrophotometer. $BaSO_4$ was used as the white reference material utilizing Praying Mantis™ diffuse reflection accessory for direct powder analysis. X-ray photoelectron spectroscopy (XPS) was done using Leybold Max200 for the surface elemental composition and binding energy analysis of the synthesized powders.

2.2.4 Degradation of organic compounds

The photocatalytic degradation of 2,4-D was performed in a batch slurry reactor equipped with a 100 W high-pressure mercury lamp (UM-102 Ushio Japan) via a quartz tube filled with aqueous $NaNO_2$ solution as a selective filter of UV irradiation (nominally $\lambda > 400$ nm) [131] at room temperature. The quartz lamp was immersed in a temperature-controlled vessel containing 1000 mL reactant solution, 100 ppm (4.5×10^{-4} M) of 2,4-D and 100 mg of catalyst with ethanol addition with ratio of 1:40 with respect to water as the electron donor, facilitating HPA photo-conversion processes [95, 132, 133]. In order to achieve the saturation of dissolved oxygen and assure the adsorption of the 2,4-D molecule on the photocatalyst, the vessel was stirred with magnet at 400 rpm with bubbling for 1 h before turning the light source on. The photocatalytic degradation was monitored with an HPLC (Dionex UltiMate 3000) by following the main 2,4-D absorption band at 229 nm as a function of the irradiation time.

It should be noted that some precise studies have recently been conducted to investigate the accuracy of using dyes for visible-light-activated photocatalysts [130, 134]. The common conclusion was that photosensitive materials are not suitable as model compounds for photocatalytic activity analysis, especially those for investigation of activity under visible light. Hence, it is recommended to utilize chemicals that are more transparent in the visible light region like 2,4-D to avoid further misleading results. Performing background experiments to find other possible roots of degradation including direct photolysis and dark catalytic oxidation, as conducted in our studies, is also necessary in this regard.

In dark absorption analysis, after putting the photocatalyst in the vessel starting the stirring process, sampling was performed every five minutes until reaching the absorption saturation point in the absence of the irradiation. The typical waiting time before starting the main experiment for the samples considering the results obtained from this experiment was 1 h, during which between 15 to 20 ppm of the 2,4-D with the initial concentration of 100 ppm was absorbed (sample data reported in Section 2.3.2). As for the direct photolysis, the organic compound solution was studied in the absence of the photocatalyst and presence of the irradiation. Using continuous sampling analysis, the direct photolysis impact was subtracted from the main kinetic analysis. Its overall impact was approximately 10 ppm 2,4-D photolysis in 15 minutes of running the experiment in the presence of light source. The related data is addressed in Section 2.3.2. Further details are provided in Appendix B.

2.2.5 Evolution of hydrogen

Figure 2-1 shows the schematic of the experimental setup for hydrogen evolution analysis. Reactions were carried out in a borosilicate inner-irradiation type reaction vessel. 100 mg sample of the photocatalyst powder was examined in reactant solutions (1000 mL) containing

1:20 ratio of ethanol to water, enhancing HPA photo-conversion processes [95, 132, 133]. The reactor was immediately closed and then mounted on a magnetic stirrer for keeping the catalyst in suspension during the reaction period. The solution was first evacuated several times to ensure complete air removal, and then irradiated under a 100 W high-pressure mercury lamp (UM-102 Ushio Japan) via a quartz tube filled with aqueous $NaNO_2$ solution as adoptive UV filter (nominally $\lambda > 400$ nm) for four hours. The reactant solution was maintained at room temperature by a flow of cooling water during the reaction. The evolved gases passed through a membrane-based water demister followed by a Nafion dryer for complete moisture removal and then were analyzed using a GC-TCD (Agilent 7890A) with argon as the carrier gas.

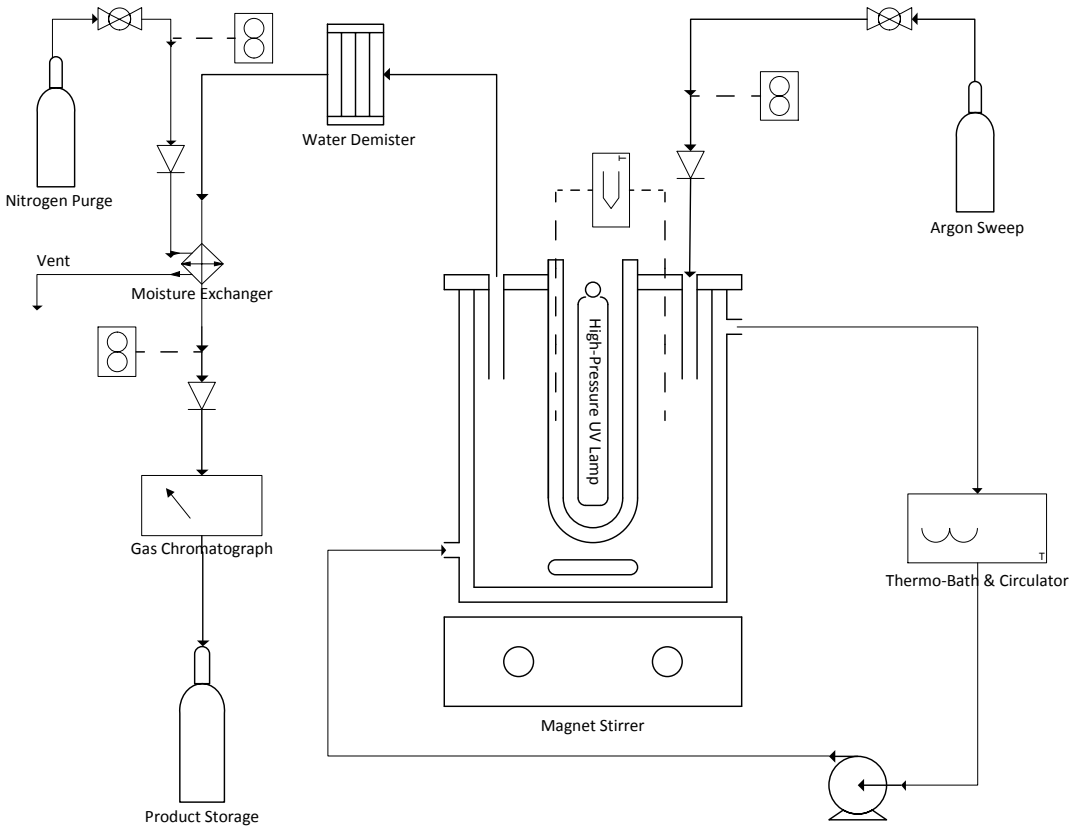

Figure 2-1: Experimental setup used for gas evolution measurements.

2.3 Results and discussion

2.3.1 Characterization

2.3.1.1 EDX

The results of the elemental analysis of the synthesized photocatalysts are given in Table 2-2 while Figure 2-2 shows a sample graph (CB1P3) for the EDX analysis. The peaks related to Au are attributed to the gold coating pre-treatment for SEM imaging. This process should be performed in order to deblur the images with depositing a conductive layer on the samples.

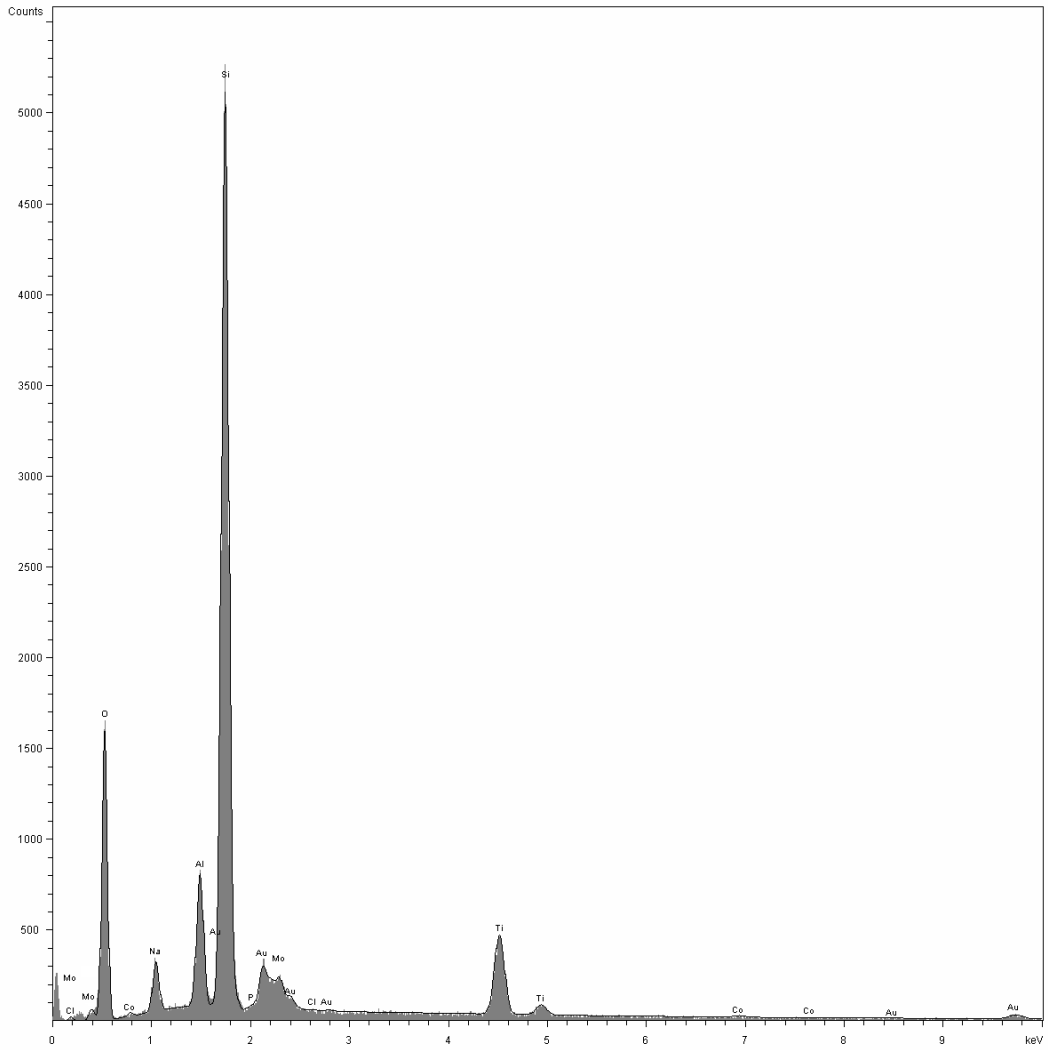

Figure 2-2: Sample EDX analysis for CB1P3.

Overall, the percentages of various elements are approximately consistent with the theoretical values. Based on the comparison of the EDX results (representing the bulk composition) and the XPS results (representing the surface composition–see Section 2.3.1.5), it is possible to identify the whereabouts of the elements whether in the bulk or on the surface. Another way to implicitly double-check this estimation is to monitor the BET results during the impregnation steps, which is explained in the next section. The homogeneity of the prepared batches was confirmed in this study using sampling from various portions of each batch and juxtaposing the results, showing significantly uniform distribution.

Table 2-2: Elemental analysis for photocatalysts (the unit is weight percent).

Sample	Si	Al	Na	Ti	Mo	Co
CB1P3	18.20	6.74	5.38	5.56	2.00	0.30
CB2P3	24.91	3.54	2.72	5.71	2.25	0.28
CB3P3	30.22	1.74	-	5.37	1.80	0.14
CB4P3	24.45	1.76	-	5.11	2.80	0.20

2.3.1.2 BET

The BET surface area of the synthesized photocatalysts is summarized in Table 2-3. CB3P1, CB3P2 and CB3P3 represent the isolated samples after each step of impregnation for the batch number 3, respectively. A decrease in the surface area of the photocatalysts is observed when they are compared with that of the parent zeolite matrix. As demonstrated in Figure 2-3, the major drop in the surface area is attributed to the cobalt ion exchange process (CB2P2), leading to this conclusion that these transition metals are mainly placed inside the pores i.e. the bulk of material whereas the presence of the titania and PMA on the surface causes lesser decrease in the surface area. This justification has been validated using

comparison of EDX and XPS analysis in the following sections. The observed impact of the cobalt ion exchange on the surface area is in good agreement with some recent related studies [95, 96].

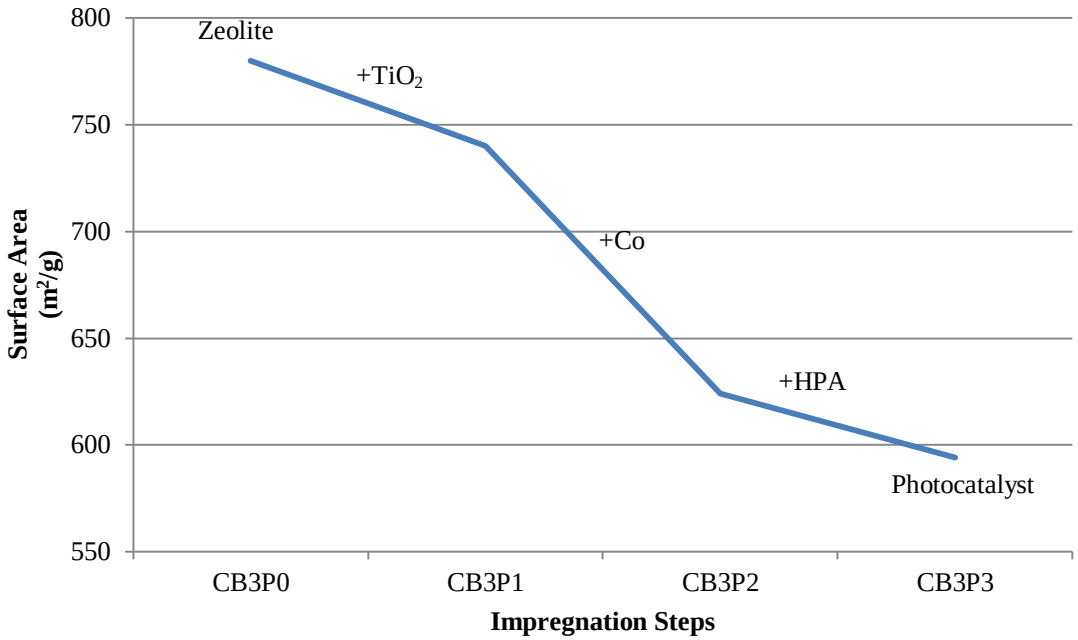

Figure 2-3: BET trend of various impregnation steps for CB3 (the last digit of the sample name indicates the impregnation step).

In a separate study, the average pore diameter for various percentages of TiO_2 on the zeolite was monitored (data presented in Section 3.3.1.2). No considerable variation was observed, validating the inference of titania's position on the surface. On the other hand, a considerable drop in the pore diameter was observed following the cobalt ion exchange step, confirming the presence of cobalt ions inside the pores.

However, pore size measurement of the microporous materials such as zeolites used in this work with conventional BET devices suffers from intrinsic limitations. For instance, the basis of data analysis for BET is the adsorption-desorption isotherms of nitrogen in 77 K; while nitrogen cannot enter to some range of the pores that are smaller than that of N_2

molecular diameter [105]. Nonetheless, observing the same trend over different classes of the zeolites with various pore size ranges make the above-derived conclusions more reliable. There are also numbers of evidences in literature which add more credibility to this technique for the inference of cobalt presence in the pores using BET analysis [95, 132].

Table 2-3: BET surface area results for various photocatalysts and CB3 at different preparation steps (the last digit of the sample name indicates the impregnation step).

Samples	BET Surface Area (m^2/g)	Samples	BET Surface Area (m^2/g)
CB1P3	579	**CB3P1**	740
CB2P3	212	**CB3P2**	624
CB4P3	446	**CB3P3**	594

2.3.1.3 SEM

Scanning electron microscopy (SEM) was utilized to monitor probable variations in the morphology of the zeolite matrix rendered by the synthesis of the various photocatalysts. The images clearly pose agglomeration more or less; however, the basic structure of the different zeolite matrices was essentially preserved after three rounds of impregnation and the implemented thermal operations. Thus, it can be inferred that the presence of various species on the support's matrix does not have any substantial morphological impact on the zeolite matrix. The representative SEM photographs of the different synthesized photocatalysts are provided in Figure 2-4.

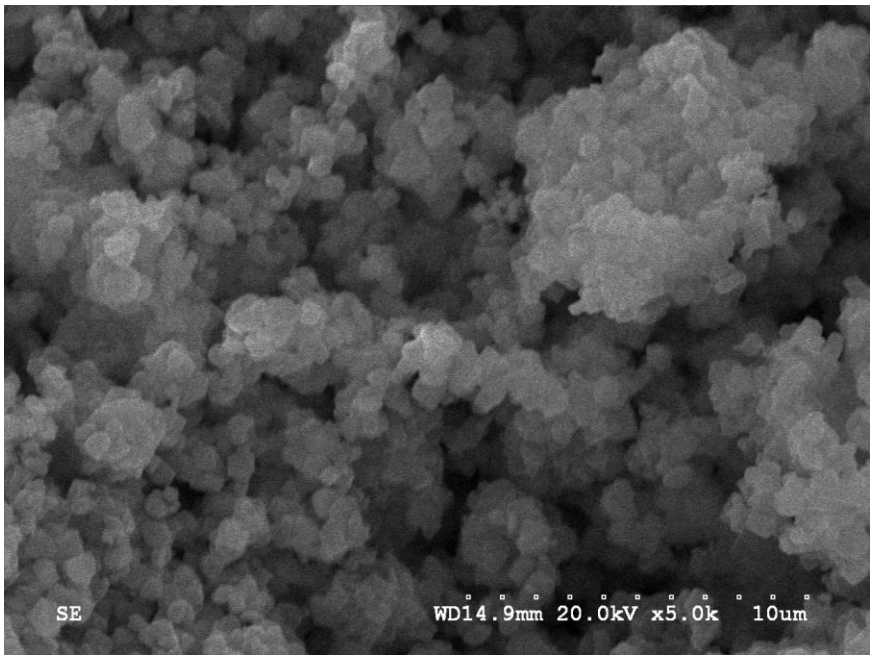

(a)

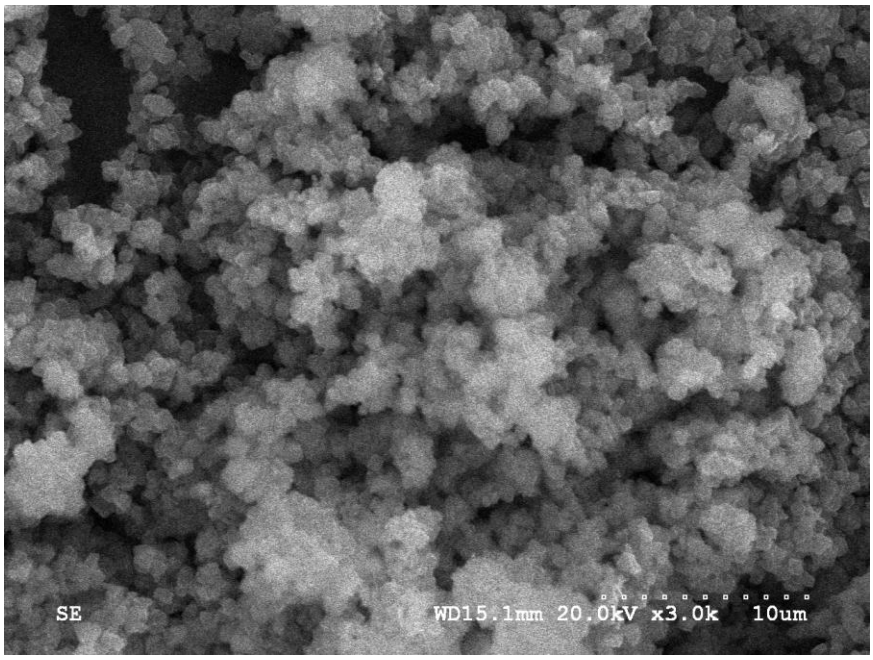

(b)

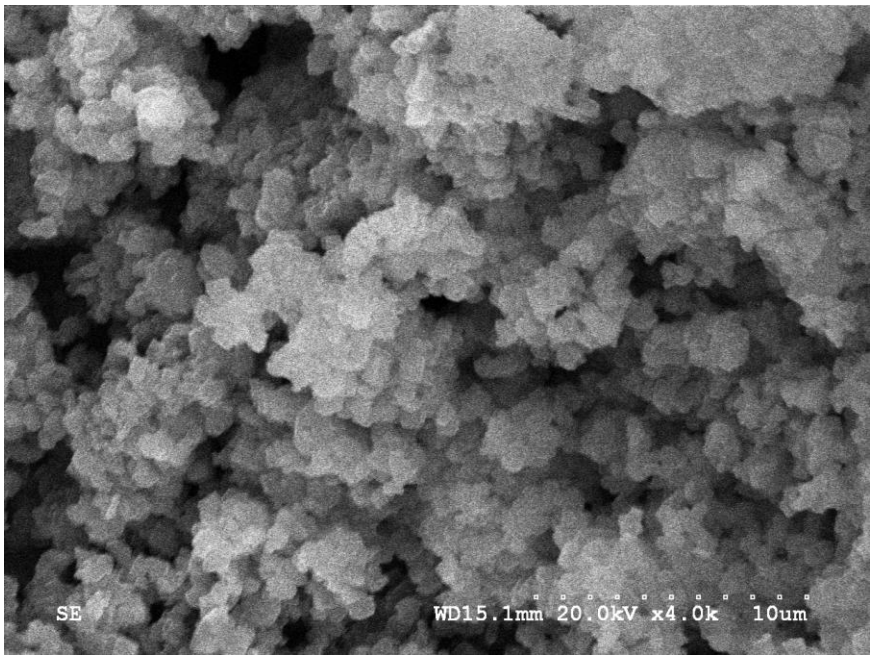

(c)

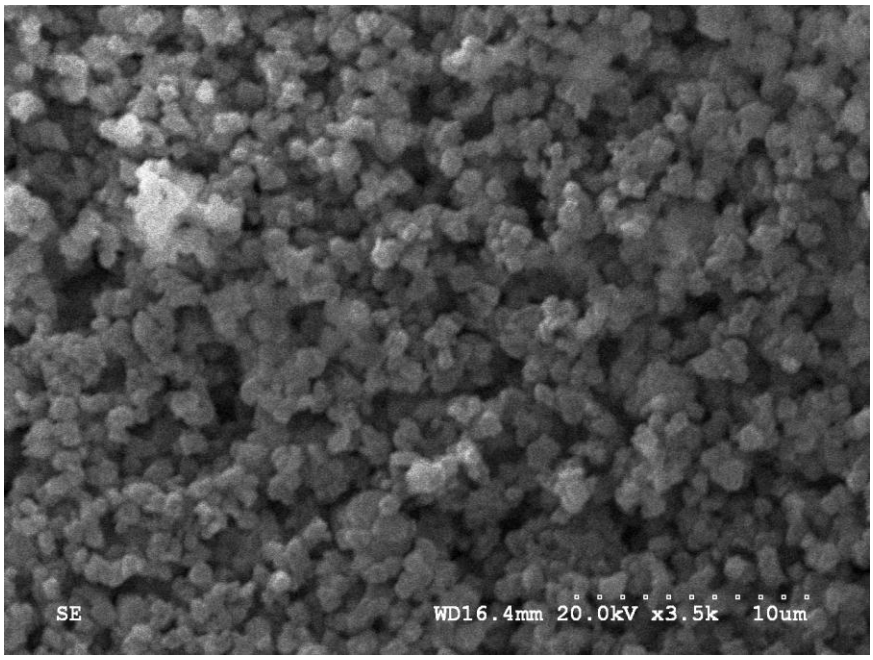

(d)

Figure 2-4: SEM topography of a) CB1P3, b) CB2P3, c) CB3P3, and d) CB4P3.

The micrometer-sized advantage of the supported TiO_2 nanoparticles is also noticeable as it facilitates filtration procedures and increases the reusability of the samples,

while still allowing taking the advantage of the nanometer-sized titania particles. This is an important improvement over the nanometric unsupported photocatalysts for which recuperation is very difficult.

2.3.1.4 UV-VIS DR

UV-VIS diffused reflectance (DR) spectra of the synthesized photocatalysts are presented in Figure 2-5 (the tests were repeated 3-5 times for each sample, showing reproducible results). The photocatalytic activity of various materials can be understood with this important spectroscopic tool. In this application, studying the band gap and its possible changes under various compositions is in the center of attention.

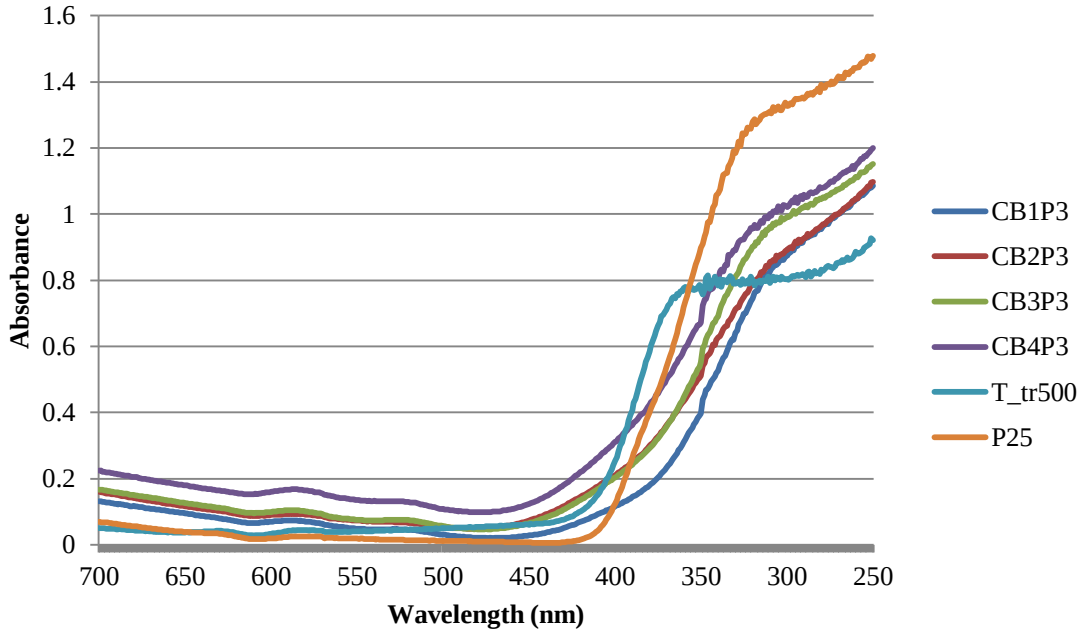

Figure 2-5: UV-VIS DR analysis for the four batches comparing with two standards of P25 and T_tr500.

As presented in Figure 2-5, in comparison to P25 and T_tr500 standard samples, not only there was no gradual shift towards the visible region in the spectra of the synthesized materials but the band gap widening phenomena was obviously dominant through the UV region. Figure 2-6 confirms this, showing a shift toward the UV region for the samples with

various percentages of titania on the zeolite support in comparison to T_tr500 and P25 (without support). This band gap widening is a significant disadvantage of the zeolite-supported TiO_2 and surely affects the photocatalytic activity of the synthesized photocatlysts. Recently, some precise studies using FTIR technique have proven that the band gap widening is the result of Ti-O-Si bond formation during the preparation [135]. Even an anodic shift of both the valence and the conduction band is inferable besides band gap widening which is consistent with the XPS narrow scan results in the next section.

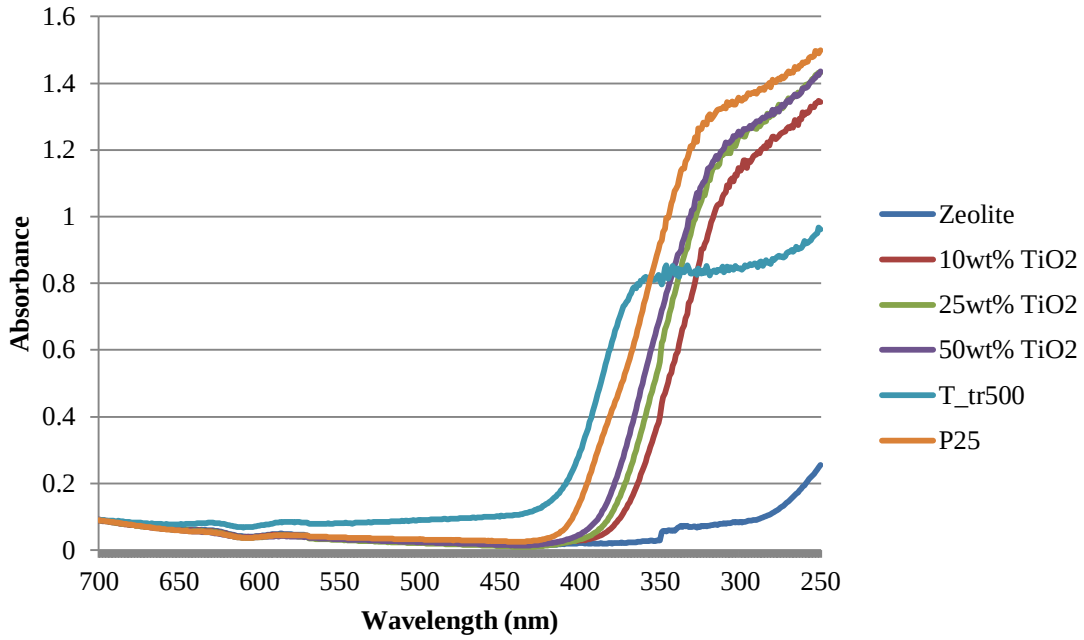

Figure 2-6: UV-VIS DR of various TiO_2 loads of 10, 25 and 50 wt% on the CBV100 comparing with P25 and T_tr500.

Despite the unfavorable shift in the band gap of the synthesized photocatalysts, they showed significantly higher photocatalytic activity in visible region as reported in the upcoming sections (Sections 2.3.2 and 2.3.3). These activities are attributed to the role of the utilized heteropolyacid (PMA) as explained below. The complementary role of the chemical

properties of the zeolite structure to achieve this superior activity is explained in Section 2.3.3.

Figure 2-7 represents the effect of the PMA as the multifunctional solid acid on the absorption spectra of the synthesized photocatalyst comparing to those of the similar samples without PMA and with pure PMA solely. This figure clearly shows that the visible region tail of the final photocatalyst sample originates directly from the successful combination of the TiO_2, PMA and the zeolite support. However, this is not the only effect of PMA. It's proved by detailed studies [110] that under reaction condition and irradiation, HPA is excitable to heteropolyblue (HPB) which is highly active in the visible light and dramatically increases the photocatalytic activity of the samples all along the solar spectrum. This was consistent with the observations around color monitoring in the course of time inside the reaction vessel and the initial increase in the rate of the gas evolutions.

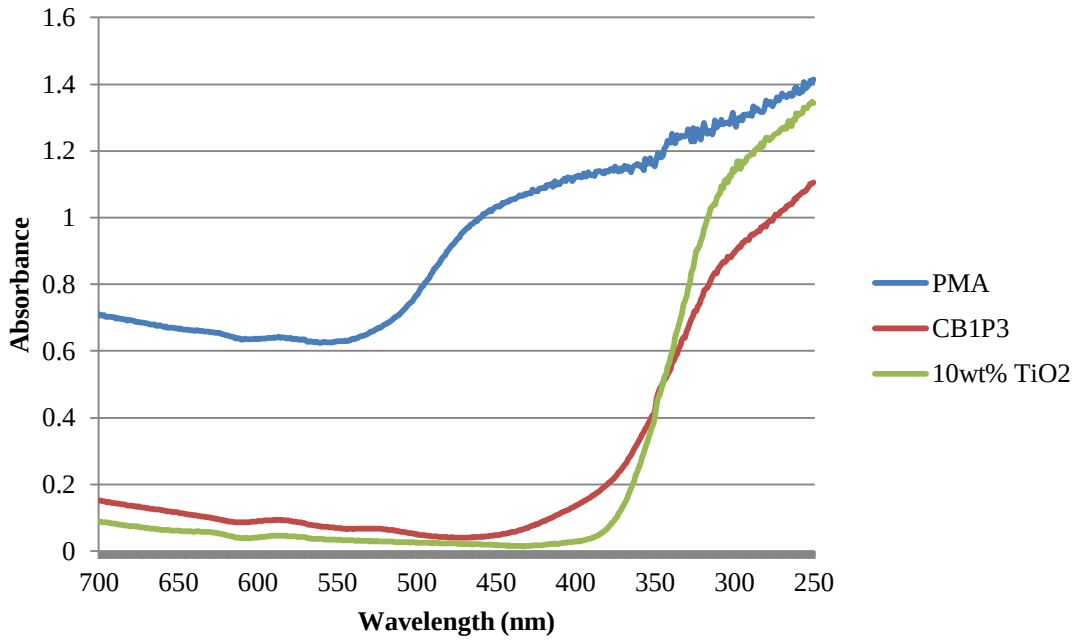

Figure 2-7: UV-VIS DR for the effect of PMA on the photocatalytic activity of the synthesized photocatalysts.

With isolation of the chemical species in UV-VIS DR, the pros and cons of the synthesized photocatalysts were explained in terms of absorption behaviour. However, there are subtle differences in comparison to the previous literature [95, 96, 127, 132, 133, 136, 137] in terms of interpretation especially in addressing the band gap widening phenomena. In fact, most of the aforementioned studies have not focused on the detailed comparison between supported and unsupported photocatalyst to recognize the possible negative impacts originated from the undesirable shift toward UV region as the result semiconductor-support interactions.

2.3.1.5 XPS

Figure 2-8a shows the CB1P3 XPS survey scan of the elements present on the surface of the photocatalyst while the values are tabulated in Table 2-4. The primary results lead to the conclusion consistent with what is presented in the previous sections that Ti and Mo elements are readily exposed on the surface while cobalt is mainly deposited in the pores and is not identified on the surface.

Table 2-4: Si based relative atomic ratio of surface metal elements for the first two batches.

Samples	Al	Na	Ti	Mo
CB1P3	0.44	0.62	1.32	0.72
CB2P3	0.26	0.30	0.62	0.37

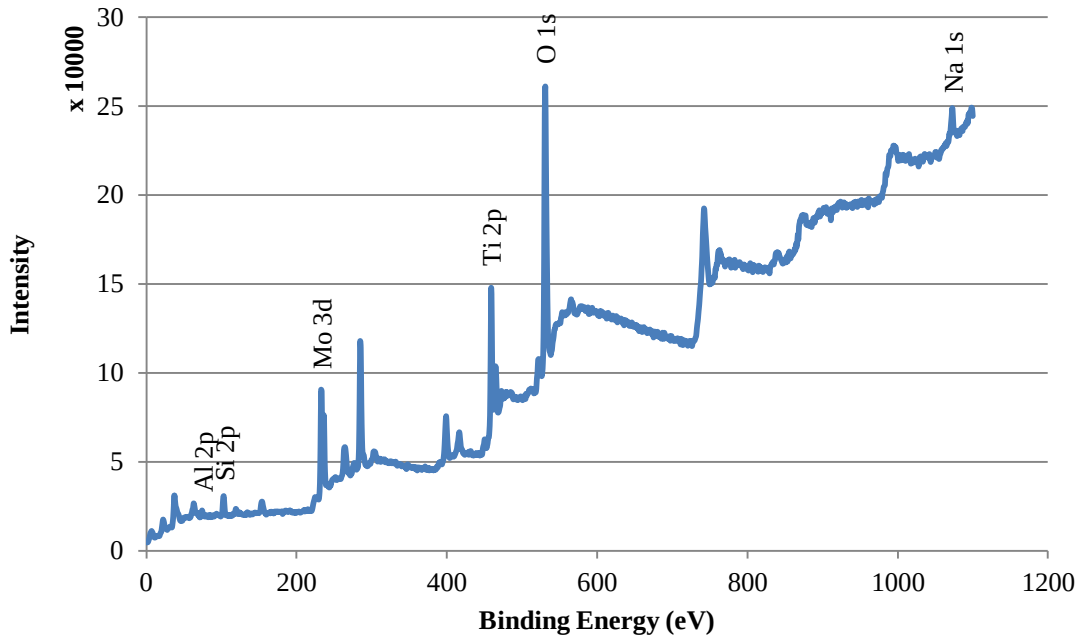

(a)

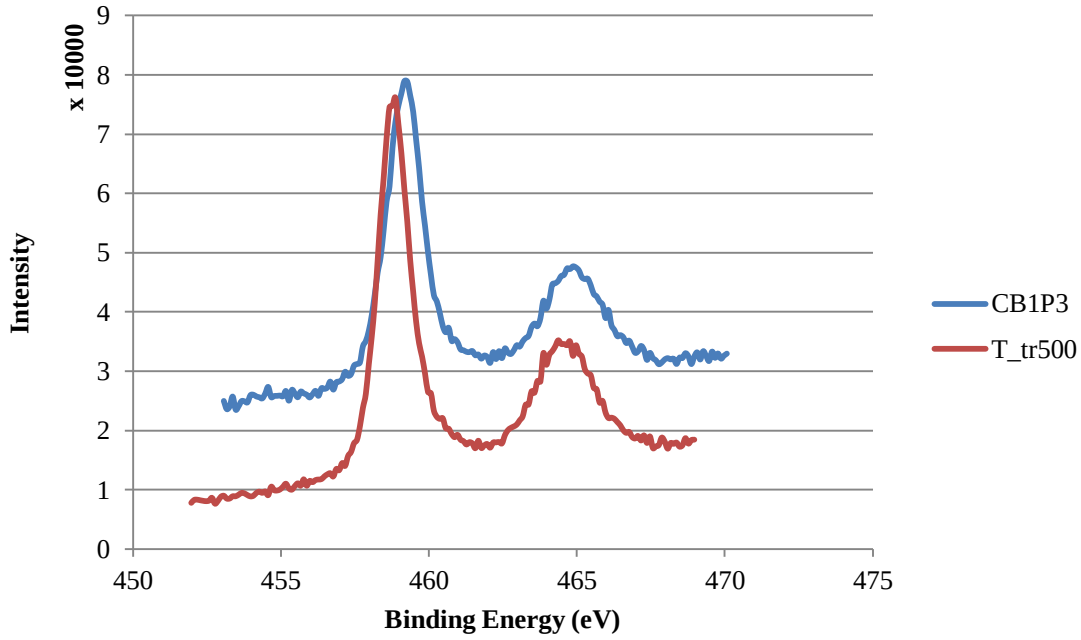

(b)

Figure 2-8: CB1P3 sample XPS analysis: a) survey scan, and b) narrow scan of Ti 2p.

Figure 2-8b shows strong evidence of the anodic shift of the band edges by comparing the narrow scan of Ti 2p energy levels in the final sample (CB1P3) with treated unsupported TiO_2 standard (T_tr500). Since the conduction band of TiO_2 has a prevalently titanium feature, any shift should influence the binding energies of the titanium 2p electrons. As expected for the anodic shift, the 2p3/2 energies increased from 458.8eV for T_tr500 to 459.3eV for CB1P3 with similar trend for CB2P3. This is another demerit of this structured support to decrease the oxidation ability of TiO_2 on the surface. However, in the following sections, it will be illustrated how other factors such as chemical features of the zeolite are involved and outweigh the mentioned disadvantages.

2.3.2 Photocatalyst performance: 2,4-D degradation and hydrogen production

Table 2-5 features the most critical point of the results of this study, wherein the photocatalytic activity, in terms of 2,4-D degradation and hydrogen evolution, are presented. It should be noted that the experiments were repeated up to three to four times for various cases showing reproducibility of the data reported in Table 2-5 with related confidence interval domains. Overall, the domains exhibit reasonable reliability in order to differentiate between the performances of the synthesized photocatalysts without suffering from significant uncertainty. Further data are provided in Appendix C.

The degradation rates of 2,4-D using the four prepared samples are in the same order as that of their standard titania in T_tr500. Although the total TiO_2 loaded on the support is 10 wt%, the same degradation rate is achieved. This is mainly due to nano size effect of titania particles on the support and the presence of PMA as reactivity promoter under visible irradiation. The TiO_2 particle size effectiveness has been investigated in some related studies showing improvement in photocatalytic activity [135]. However, based on analyzing the

experimental data, this parameter, by itself, could not have been the cause of the significant activity improvement of the synthesized samples. The additional photocatalytic activity enhancement is due to the effect of HPA addition and its convertibility to HPB as explained in Section 2.3.1.4, Figure 2-7.

The trend of the concentration changes after applying the background experiments (dark absorption and direct photolysis) is shown in Figure 2-9. There are some fundamental differences of the photo-degradation conditions of this study in comparison to the originally designed environmental photoreactors. Hence, the behaviour of the concentration changes (almost linear) does not follow the first order kinetics model commonly proposed in literature for the photocatalytic decontamination processes [136, 138]. This could be mainly due to the differences in the utilized light source (high-pressure UV lamp), and higher initial concentration of the 2,4-D (100 ppm) in comparison to the typical cases (5 to 10 ppm). The described behaviour was observed for all the synthesized samples.

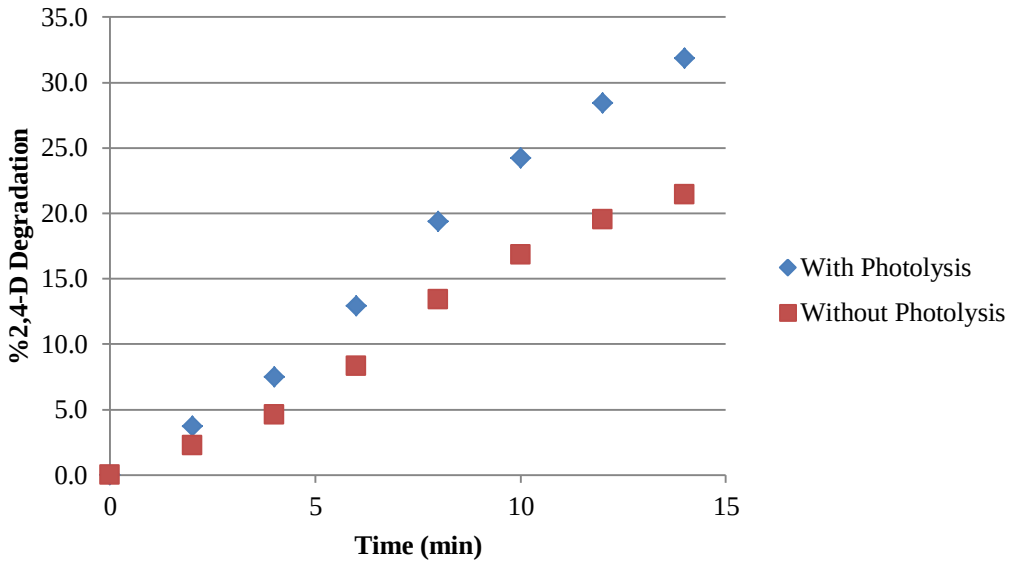

Figure 2-9: Sample degradation percentage of 2,4-D in the course of time for the prepared photocatalysts (15.6 ppm for dark absorption already deduced for the first batch of photocatalyst, CB1P3).

Table 2-5: Photocatalytic activity and hydrogen evolution rates of the experiments (the ± shows 95% confidence interval from 3 experiments).

Samples	%2,4-D Degradation (15min)	Hydrogen Evolution (µmol/g.h)
CB1P3	20.1±1.1	250.8±12.3
CB2P3	21.9	187.2
CB3P3	22.3	96.8
CB4P3	19.6	100.1
P25	13.4	84.2
T_tr500	22.4	93.9

Another observation is that the overall performance of the synthesized photocatalysts had two advantages over Degussa P25 in terms of activity and quality of degradation. First of all, their average degradation rates were about 50% higher than that of P25. In addition, unlike P25, the synthesized batches were able to mineralize 2,4-Dichlorophenol (2,4-DCP), which is the main and the most important by-product of the 2,4-D degradation [139, 140] (observed via HPLC analysis qualitatively). This can be attributed to the structure of the synthesized TiO_2 rather than the utilized support; considering 2,4-DCP mineralization was also observed for unsupported (T_tr500) sample.

An example of hydrogen and oxygen evolution rates by water splitting for one of the synthesized photocatalysts (CB1P3) is presented in Figure 2-10. The rates are increasing significantly during the first 90 minutes of the experiment until they almost reach the plateau of the steady state gas evolution. The first section of the rate increase was observed for all the main synthesized samples. This can be attributed to the formation of the HPB (described in Section 2.3.1.4) and intermediate species, improving the evolution rates in the course of time.

In terms of hydrogen production, there is a significant difference in the rates using different photocatalysts (Table 2-5) which should be further investigated to provide better insight about these results. Hydrogen evolution rates for the CB1P3 and CB2P3 are greater in comparison to those of the standards (T_tr500 and Degussa P25); whereas the rates of H_2 production for CB3P3 and CB4P3 are similar to that of the defined standards. The following section will explain these observations.

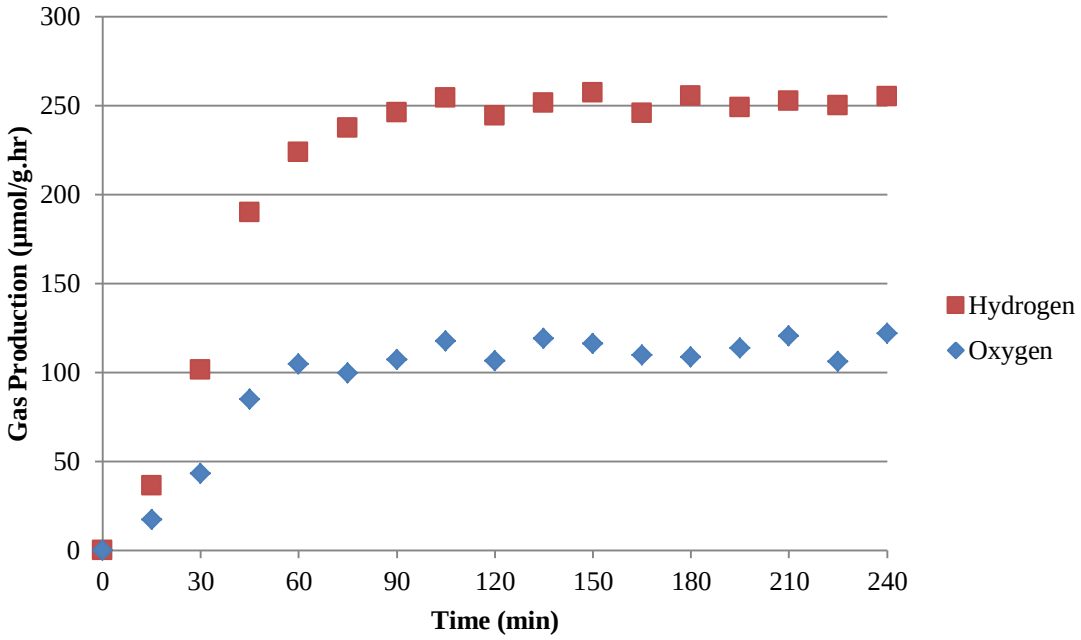

Figure 2-10: Sample water splitting online production rates for the synthesized photocatalysts (CB1P3).

2.3.3 Role of zeolite's chemical characteristics

The UV-VIS and XPS results revealed two important changes in the band gap characteristics of the TiO_2 after being impregnated on the surface of the zeolite; band gap widening and anodic shift in the band edges, both mainly due to the formation of Ti-O-Si bonds on the surface rather than quantum size effect. It has been observed repeatedly in literature using atomic force microscopy (AFM) that the agglomerated titania even in 10% loading has the size of at least 15 to 20 nm which is far from quantum size effect [135-137]. On the other

hand, there are two important competing advantages in the presented composition that possibly can overcome these negative effects to some extent. The first factor is utilizing HPA as a solid acid that can be excited under visible light, thereby enhancing the photocatalytic activity at higher wavelengths as its impact was observed in 2,4-D degradation rates. The other factor that is critical for the hydrogen evolution process is pH dependency of the band edges of TiO_2 with respect to the normal hydrogen electrode (NHE) in aqueous solutions [111, 141].

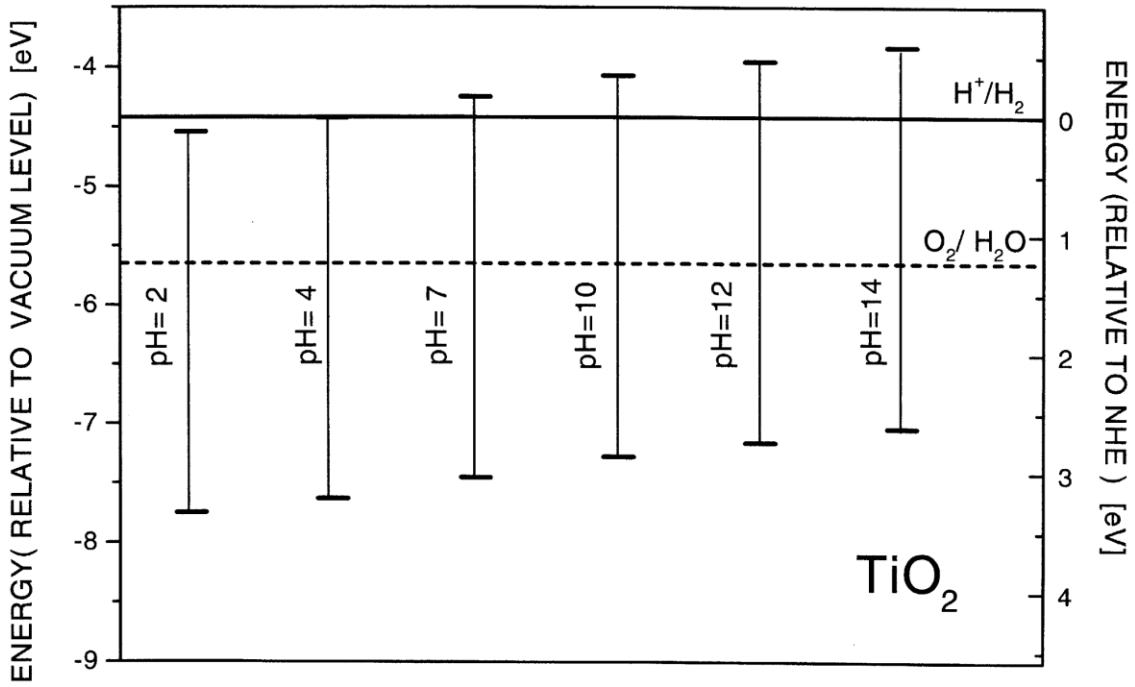

Figure 2-11: Effect of pH on energy of TiO_2 in terms of vacuum level and normal hydrogen electrode level in electrolyte (reprinted with permission of [111]).

Figure 2-11 represents the TiO_2 band edges, indicating the high effectiveness of the basicity on the nanoscale driving forces for the photoelectrochemical decomposition of water. This explains the low hydrogen production rate of the pure TiO_2 based photocatalysts at pH ranges lower than 10, as reported in the literature [142-145]. The considerable rates of hydrogen production in the samples with high basicity i.e. lower Si/Al ratio with high sodium

content (CB1P3 and CB2P3) can be explained as follow. The solid basic pH of the zeolites can possibly compensate for the anodic shift of the band edges presented in Figure 2-12. The lack of this basicity could be the cause of other samples' inability to provide enough energy and driving force to generate hydrogen, resulting in lower evolution rates. Monitoring the pH during the course of reaction showed slight increases in the basicity of the solution; however, to be impartial, this cannot be a robust indication of what is happening near the surface of the photocatalyst. Hence, the lack of in-situ characterization techniques in photocatalytic processes is still the bottleneck of the further online reaction and kinetic analysis. In this way, only the theoretical line of reasoning as discussed in this section is applicable for explanation of the experimental data.

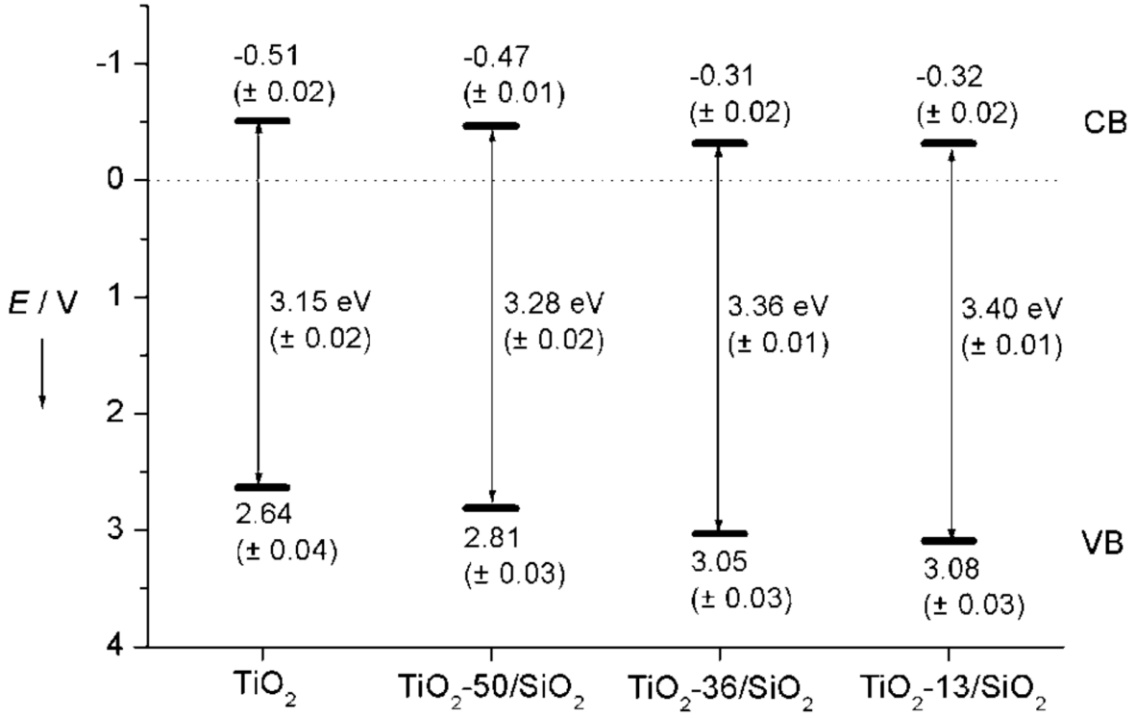

Figure 2-12: Band gap energies and band-edge positions (pH=7) for different materials. The values for valence band (VB) and conduction band edges (CB) are given in volts (vs. NHE) (reprinted with permission from [135]).

Based on our experimental results, the structure impact is not as determining as the chemical properties of the support in hydrogen evolution for the following reasons. According to EDX, XPS and BET analysis, it was proved that the TiO_2 and HPA are mostly on the surface of the support and only cobalt ions are present in the pores. However, the utilized wet impregnation technique in the catalysis realm probably causes an egg shell distribution of the cobalt ions almost near the surface; according to the low concentration of the impregnated cobalt and mass transfer limitations. So, during the reaction, all the phenomena happen on and near the surface, undermining the significant role of the zeolite structure. It should be noted that the ultrafine porosity of the zeolite has an undeniable influence on the performance of this class of the photocatalysts which is better explained in the next chapter. Hence, the discussions regarding the insignificance of the structure role is just applied locally in this section in order to make its chemical role clearer. On the other hand, when the basicity of the structure converted to the acidity through proton exchange via sulfuric acid, as the final qualitative examination of this idea, the rate of hydrogen evolution dramatically decreased which clearly strengthens the chemical impact of the material rather than its structure.

2.4 Conclusion

In the realm of photocatalytic water splitting under visible light, careful interpretation of various observations is crucial, due to the multidisciplinary nature of this phenomenon. In this study, application of the zeolites as the support for the titania-based photocatalysts was achieved successfully under visible light. It was concluded that the promising H_2 evolution rates were mainly dependent on the chemical characteristics of the support, specifically the basicity properties which bring more affinity for hydrogen production. This effect can even

overcome the negative impacts of the dispersion and interactions of the semiconductor with the zeolite as the support. Two factors essentially play the negative role in this combination; band gap widening and anodic shift of the TiO_2 band edges, which are the results of Ti-O-Si bond formation rather than quantum size effect. Presence of the HPA as the multifunctional solid acid with the high activity under visible light and its potential of conversion to HPB under reaction condition are among the complementary elements to add more visible light activity to the synthesized photocatalysts.

Chapter 3: Cobalt precursor role in the photocatalytic activity of the zeolite-supported TiO_2-based photocatalysts[2]

3.1 Introduction

Photocatalytic water splitting using various semiconductors has been studied extensively as a promising technique for green hydrogen production under solar irradiation [13]. Development of visible-light-activated photocatalysts based on earth-abundant materials is highly appreciated; considering the currently used materials some even pricier than gold [146]. Therefore, utilizing nonprecious titanium-dioxide-based materials for water cleavage is still in the center of attention. This is mainly due to the great capability of titania to serve water dissociation reaction with suitable corrosion and photo-corrosion resistivity in aqueous mediums [16]. However, there are some challenges associated with their band gap modification, which is in UV region [16]. In addition, for traditional TiO_2 usage, it has been observed that the rate of hydrogen generation is dependent on the pH of the system with the best performance obtained in the pH range of 11 to 14 [143]. Addition of platinum (Pt) deposits to titanium dioxide as cocatalyst is another way to facilitate the hydrogen evolving reaction. However, to prevent the back reaction between H_2 and O_2 on the Pt surface, some chemical additives, such as Na_2CO_3 in an amount of 2.2 mol/l are also needed to increase the hydrogen evolution rates [147]. This leads to the almost unsuitability of the optimum reaction solution of the conventional TiO_2 for being environmentally benign. Therefore, during recent years, numerous studies have been performed based on the impregnation of titania on support

[2] A version of this chapter has been submitted for publication.
Amin Taheri Najafabadi, Fariborz Taghipour, Cobalt precursor role in the photocatalytic activity of the zeolite-supported TiO_2 based photocatalysts under visible light: A promising tool toward zeolite-based core-shell photocatalysis.

materials [93, 148] to overcome the aforementioned issues for water cleavage application. Some of the major incentives of implementing supported photocatalyst idea are providing more flexibility in surface engineering, inhibition of the electron-hole recombination as limiting parameter in photocatalytic redox systems, taking the advantage of the nano-sized titanium dioxide while using that in easily-separable micro-sized level, utilizing the support to add more solid promoters, and structural and chemical characteristics of the support by itself.

A combination of the zeolite-supported TiO_2 with the cobalt-based cocatalysts (i.e. made of earth-abundant material) has been observed with promising hydrogen evolution rates in the presence of heteropolyacids under visible light [96]. The related synthesis process consists of three steps of impregnation as follows: (i) TiO_2 deposition on the zeolite surface, (ii) cobalt incorporation via ion exchange process through the zeolite pores, and (iii) heteropolyacid addition to the particles. Each step follows with a thermal treatment that varies from calcination at 500°C to hot plate drying at 80±5°C and 65±5°C, respectively. The focus of this study is on the second step. The objective is to investigate the impact of using two commercially available types of cobalt precursor namely cobalt chloride and cobalt nitrate on the photocatalytic activity of the synthesized photocatalysts, especially hydrogen evolution performance. Nitrate and chloride compounds of cobalt were examined on two classes of the zeolites namely Na-Y and Na-Mordenite which have emerged as suitable supports for hydrogen evolution application in our previous studies presented in Chapter 2.

From the catalysis preparation point of view, nitrate precursors are preferred in comparison to the chlorides which might have poisoning effect on the electric double layer and absorption [149]. However, based on some fundamental differences of photocatalysis, a

different behaviour was observed, articulated in this work. The synthesized supported photocatalysts are evaluated for both H_2 evolution potential and photocatalytic degradation of organic compounds, specifically, 2,4-Dichlorophenoxyacetic acid (2,4-D) with the related characterizations. Various important aspects of chemical contribution of the cobalt precursor are investigated simultaneously to make the interpretation of the results clearer.

3.2 Experimental approach

3.2.1 Materials

Synthesis of the photocatalysts was performed using Na-Y zeolite (SiO_2/Al_2O_3 =5.1, ID: CBV100), and Na-Mordenite Zeolite (SiO_2/Al_2O_3 =13, ID: CBV10A) all from Zeolyst International Company US branch. The other materials used in the preparation of photocatalysts were cobalt chloride hexahydrate 98%, cobalt nitrate hexahydrate 98%, phosphomolybdic acid (PMA) 78% as the utilized HPA, and titanium isopropoxide 97% all from Sigma-Aldrich Canada, as well as isopropanol from Fisher Scientific of Canada. All the chemicals were of analytical grade, using double-distilled water (DDW) in all the synthesis steps.

3.2.2 Photocatalyst preparation

The framework of the preparation follows the procedure described in Section 2.2.2. As depicted in Figure 3-1, the materials are added to the zeolite matrix consecutively in three steps of titania impregnation via sol-gel technique, cobalt addition via ion exchange and PMA adding as the heteropolyacid. As mentioned earlier, the focus of this part is on the impregnation process and the suitability of the available precursors. CB5P3 and CB6P3 are almost identical with their companions, CB1P3 and CB2P3, respectively and the only difference is the cobalt precursor used during the synthesis. Table 3-1 represents the specific

amount of ingredients for the preparation of each of the four specific batches. For the names, the number in front of "CB" is the sample number and the number in front of "P" is the impregnation step. The same standards of Degussa P25 and T_tr500 were prepared for the sake of performance comparison.

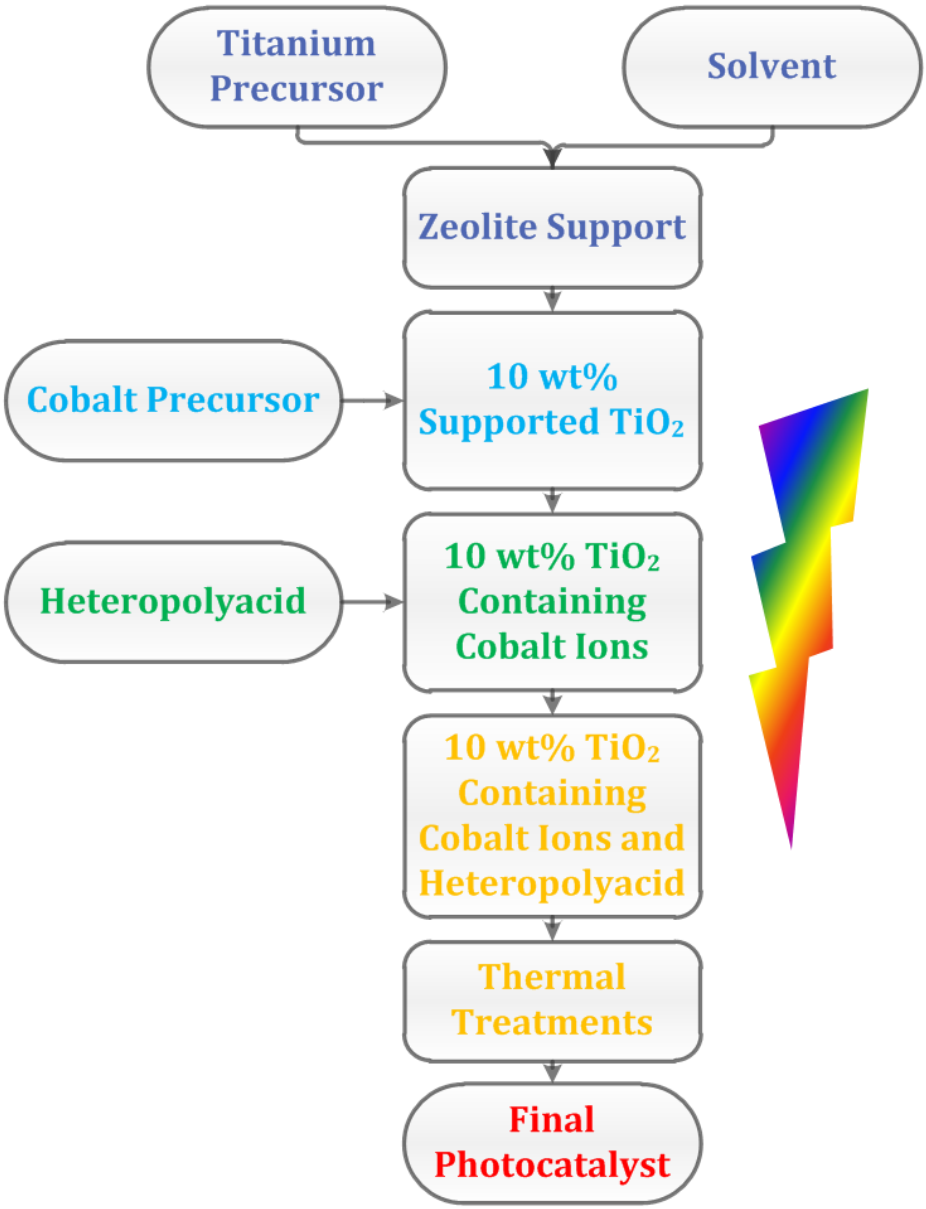

Figure 3-1: General preparation steps for the synthesized photocatalysts.

Table 3-1: Summary of the four synthesized photocatalyst information (units of chemical usage are in grams).

Name	Zeolite	Si/Al	Raw Surface Area(m^2/g)	Type	Na_2O wt%	Titanium Precursor	*Cobalt Precursor	PMA
CB1P3	5.000	5.1	900	Y	13	1.850	0.127	0.500
CB2P3	5.000	13	425	Mordenite	6.5	1.850	0.064	0.500
CB5P3	5.000	5.1	900	Y	13	1.850	0.156	0.500
CB6P3	5.000	13	425	Mordenite	6.5	1.850	0.078	0.500

*** CB1P3 and CB2P3 were prepared by chloride precursor while CB5P3 and CB6P3 were prepared by nitrate precursor.**

3.2.3 Characterization

A Micromeritics surface area analyzer (ASAP2020) was utilized to determine the BET surface area of the synthesized photocatalysts. Elemental analysis and the surface morphology of the samples were studied by energy-dispersive x-ray (EDX) spectroscopy and scanning electron microscope (SEM), respectively using Hitachi Model S3000N VPSEM. UV-VIS diffuse reflectance (DR) spectra were obtained using an Agilent Cary 5000 spectrophotometer. Barium sulfate was used as the white reference material with utilizing Praying Mantis™ diffuse reflection accessory for powder analysis.

3.2.4 Photocatalytic activity analysis

The photocatalytic performance evaluation procedure including 2,4-D photo-degradation and hydrogen evolution is described in Sections 2.2.4 and 2.2.5, respectively. Figure 3-2 shows the general schematic of the experimental setup for hydrogen evolution as well as 2,4-D degradation analysis. Background experiments were performed based on the descriptions of Sections 2.2.4 and 2.2.5 as well as the detailed explanations of Appendix B.

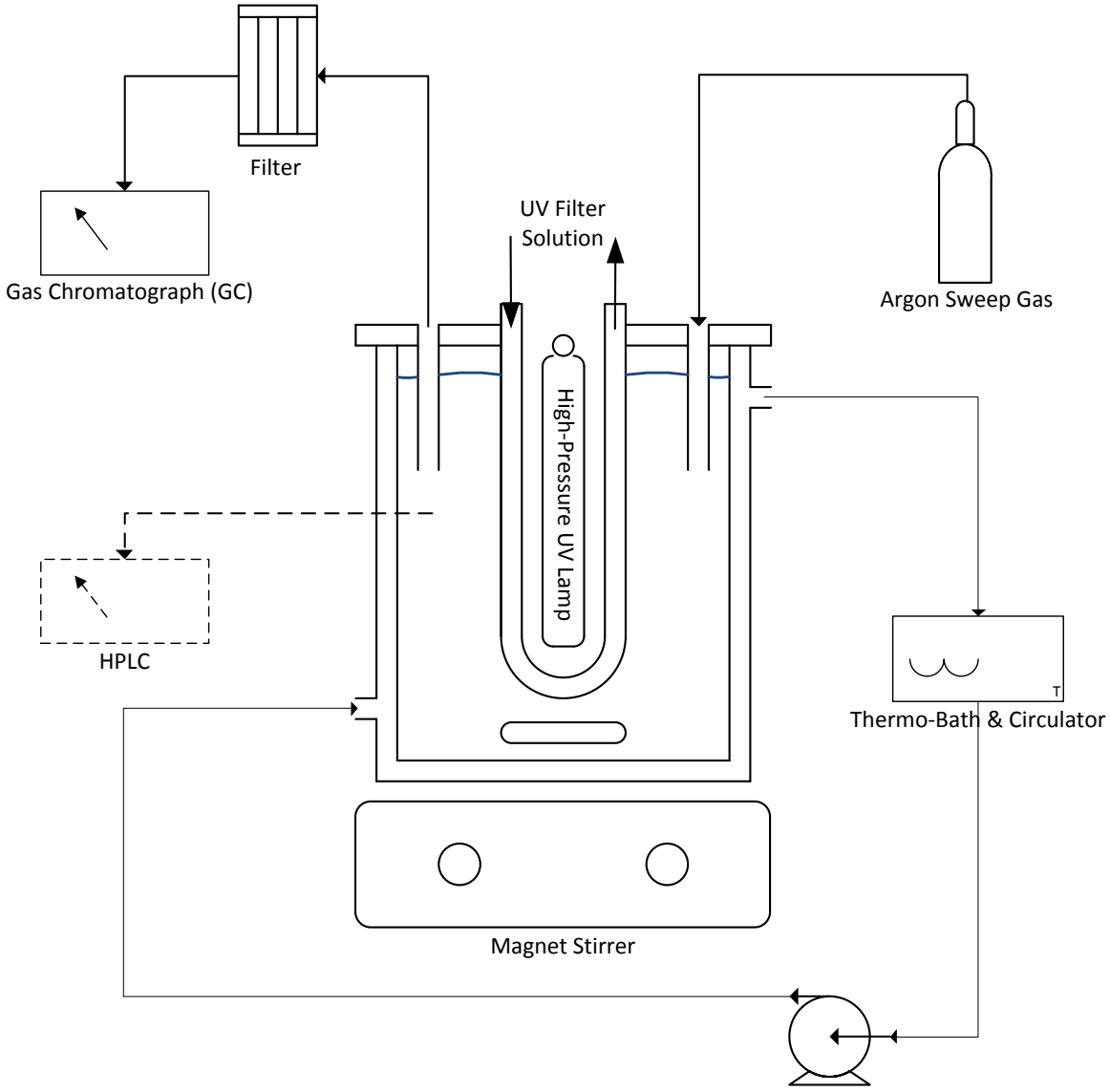

Figure 3-2: Experimental setup for hydrogen evolution (gas sampling by GC) and 2,4-D photo-degradation (liquid sampling by HPLC).

3.3 Results and discussion

3.3.1 Characterization

3.3.1.1 EDX

The elemental analysis results of the synthesized photocatalysts are given in Table 3-2.The important point is that although it was tried to wash the samples thoroughly after cobalt ion

exchange process in the preparation stage, Cl and N compounds are still present in the composition, showing their affinity to strongly interact with the zeolite structure. This commonly happens in the preparation processes, as the precursor's undesired chemicals cannot be removed entirely from the support [150]. From this analysis, the probability of witnessing related consequences in the photocatalytic activity of the samples with different precursor compounds increases as the result of nitrate and chloride remnants.

Table 3-2: Elemental analysis for photocatalysts (numbers are in weight percent).

Sample	Si	Al	Na	Ti	Mo	Co	Cl	N
CB1P3	18.20	6.74	5.38	5.56	2.00	0.30	0.10	-
CB2P3	24.91	3.54	2.72	5.71	2.25	0.28	0.09	-
CB5P3	18.22	6.31	4.56	4.64	2.7	0.55	-	0.53
CB6P3	26.16	3.8	2.71	4.32	3.74	0.28	-	0.49

Overall, the percentages of various elements are consistent with the theoretical values. The homogeneity of the prepared batches was also validated in this study using sample analysis from various regions of each batch, showing significantly uniform distribution.

3.3.1.2 BET

Table 3-3 shows the BET surface area for various prepared samples. In a separate study, the surface area and average pore diameter for various percentages of TiO_2 on the zeolite was monitored (Figure 3-3). No considerable variation was observed, confirming the inference of titania's position on the surface, drawing the same conclusion for the PMA as well. On the other hand, a considerable drop in the surface area and average pore diameter was observed

following the cobalt ion exchange step, demonstrating the presence of cobalt compounds inside the pores (see Section 2.3.1.2, Figure 2-3).

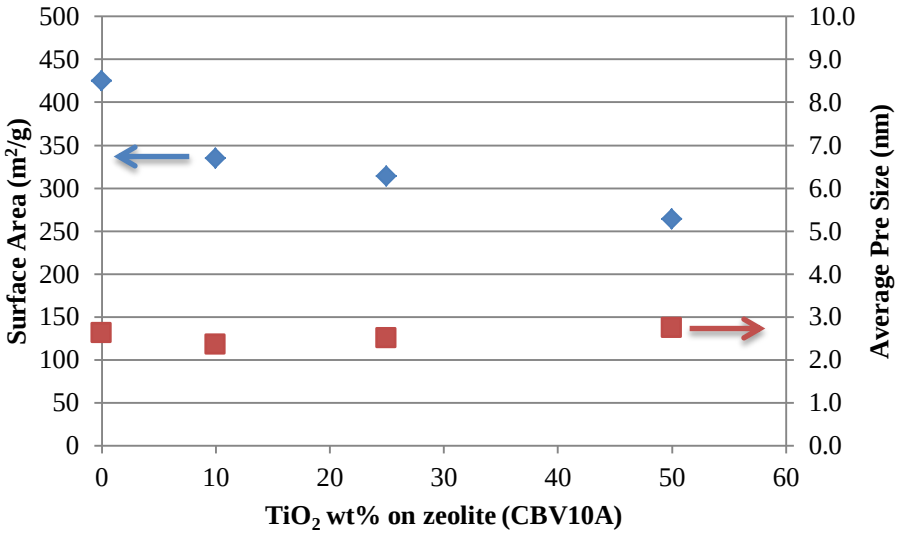

Figure 3-3: Surface area and average pore size variations of various percentages of TiO_2 on the zeolite type CBV10A.

Consequently, the larger the precursor, the more significant drop in surface area in comparison to the related parent zeolite matrix. As the nitrates have larger size and higher molar weight in comparison to the chlorides [151], it is observed that the surface areas of their related photocatalysts are lesser than their chlorides' companions.

Table 3-3: BET surface area results for various prepared samples.

Samples	BET Surface Area (m^2/g)	Samples	BET Surface Area (m^2/g)
CB1P3	579	**CB5P3**	520
CB2P3	212	**CB6P3**	162

3.3.1.3 SEM

Scanning electron microscopy was utilized to inspect probable variations in the morphology of the zeolite matrix caused by the synthesis of the various photocatalysts, incorporating different cobalt precursors during the preparation process. The images suggest agglomeration more or less; however, the basic structure of the zeolite matrices was essentially preserved after three rounds of impregnation and the related treatments, independently from cobalt precursor's type. Thus, it can be concluded that the presence of species on the support's matrix, and utilizing cobalt precursors do not have any notable morphological impact on the zeolite structure. The representative SEM photographs of the extra synthesized photocatalysts (CB5P3 and CB6P3) are provided in Figure 3-4.

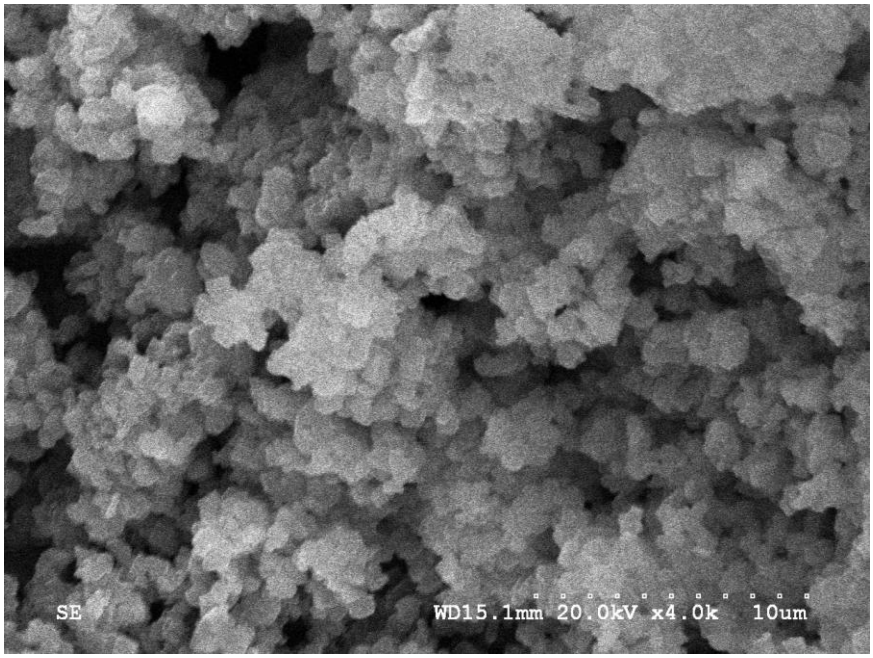

(a)

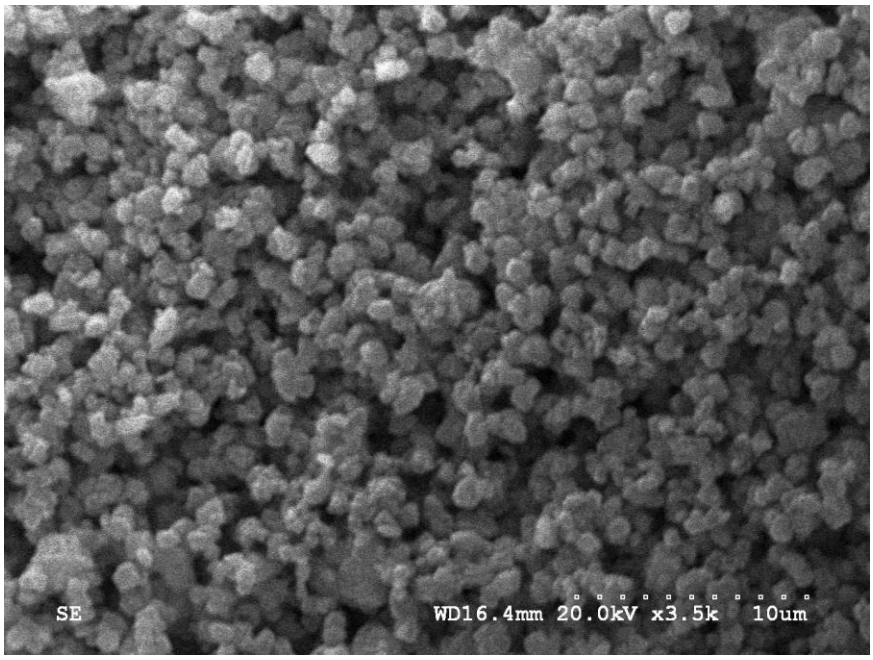

(b)

Figure 3-4: SEM images of the prepared photocatalysts: a) CB5P3, and b) CB6P3.

3.3.1.4 UV-VIS DR

UV-VIS DR spectra of the synthesized photocatalysts are presented in Figure 3-5, focusing on the band gap analysis and its possible changes under various preparations. The analysis was repeated 3-5 times for each sample, showing reproducibility of the data.

Setting aside the standards, it is inferable that for each class of the zeolite when the applied precursor is cobalt nitrate (CB5P3 and CB6P3), a shift toward visible region is happening. This observation was unexpected but verified after repeating, showing the validity of the experiments. Hence, it seems that it emulates the phenomenon of nitrogen doping, which is reported to shift TiO_2 band gap toward visible light [152]. In fact, if the whole photocatalyst composition is considered as an interconnected system, incorporation of nitrogen compounds can potentially affect the overall absorbance spectra, introducing another advantage of the zeolite-supported photocatalysts. This becomes more intriguing

when this technique is compared with the traditional doping procedures which are generally energy-consumptive and in some cases complex [152].

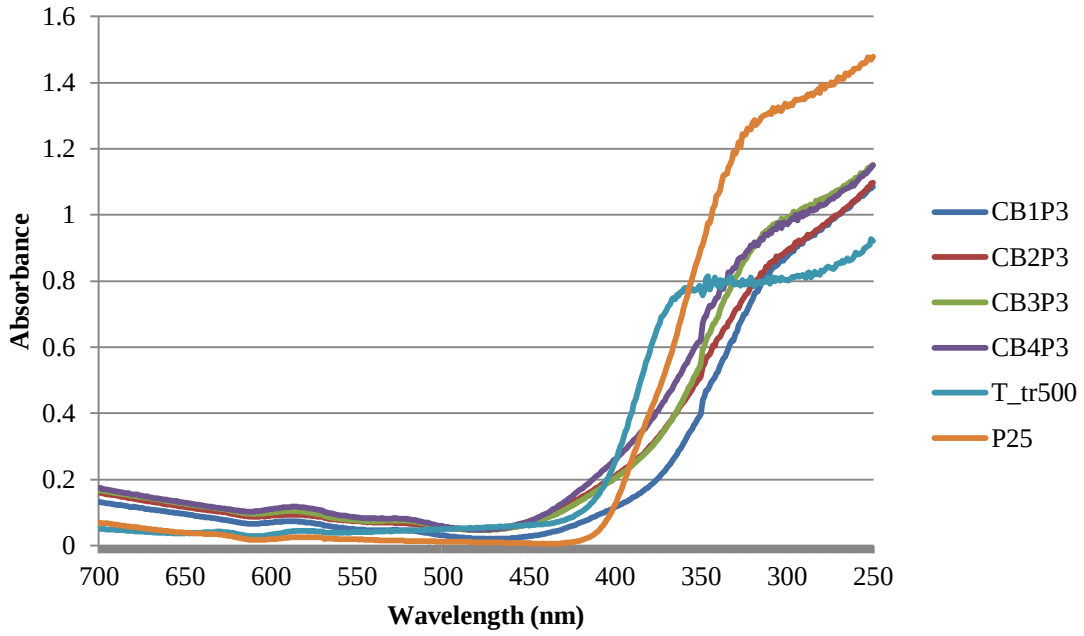

Figure 3-5: UV-VIS DR analysis for the four synthesized photocatalysts comparing with the two standards of P25 and T_tr500.

Furthermore, Mordenite-supported samples exhibited better absorption in comparison to Y-supported versions, demonstrating how interaction of various zeolite types affects the absorption spectra (i.e. band gap) of the impregnated TiO_2. However, Mordenite-based photocatalysts showed relatively lower hydrogen evolution rates (see Section 3.3.2), confirming inadequacy of UV-VIS analysis to provide compelling explanations for the photocatalytic behaviour.

3.3.2 Photocatalyst performance: 2,4-D degradation and hydrogen production

Table 3-4 presents the photocatalytic activities of the prepared batches in terms of 2,4-D degradation and hydrogen evolution. The degradation rates of 2,4-D using the four prepared samples are in the same order as that of their parent standard unsupported titania in T_tr500

(averagely 50% higher than P25), even though the total TiO_2 loaded on the support of the synthesized samples is 10 wt% of that in the standards. This is basically due to the nano-size effect of titania particles on the zeolite and visible light activity of HPA as a promoter.

Table 3-4: Photocatalytic activity and hydrogen evolution rates of the experiments (the ± shows 95% confidence interval from 3 experiments).

Samples	%2,4-D Degradation (15min)	Hydrogen Evolution (µmol/g.h)
CB1P3	20.1±1.1	250.8±12.3
CB2P3	21.9	187.2
CB5P3	21.3	181.6
CB6P3	20.4	123.1
P25	13.4	84.2
T_tr500	22.4	93.9

There are some studies reporting the negative effect of Cl^- on photocatalytic oxidation of organic compounds, proposing chlorides' interference with active sites on the photocatalyst surface by their absorption [153, 154]. However, in our experiments, this so-called poisoning effect was not observed for the samples prepared with chloride precursor. This is potentially another advantage of this composition to remove the poisoning effect of chloride ions on the photo-oxidation active sites, which is discussed in detail in the upcoming section.

In terms of hydrogen production, there is a significant difference in the rates using different cobalt precursors (Table 3-4) which should be further investigated to provide better insight about these results. All the hydrogen evolution rates are greater in comparison to those of the standards (T_tr500 and Degussa P25); whereas the rates of H_2 production for

chloride precursor versions (CB1P3 and CB2P3) are about 30% higher than those of nitrate compounds (CB5P3 and CB6P3). It is worthy to note that the relatively higher hydrogen production rates of the Y-supported photocatalysts in comparison to those of the Mordenite-supported ones is mainly attributed to the higher basicity of their parent zeolite matrices rather than the structure. This is in contrast with the unfavorable difference of their corresponding UV-VIS absorbance spectra discussed in Section 3.3.1.4.

An example of hydrogen and oxygen evolution rates by water splitting for two of the synthesized photocatalysts (CB1P3 and CB5P3) is presented in Figure 3-6. The only difference of the samples is in the cobalt precursor used during the preparation (chlorides for CB1P3 whereas nitrates for CB5P3). The rates are increasing significantly during the first 90 minutes of the starting the experiment until they reach an almost constant rate of gas evolution. While the CB5P3 exhibits about 30% lower hydrogen production rates due to the usage of nitrates as the cobalt precursor, both samples have almost similar rates of oxygen evolution. Further discussion on reasoning of this behavior is made in the next section, explaining the impact of cobalt precursor on the photocatalytic performance of the synthesized photocatalysts.

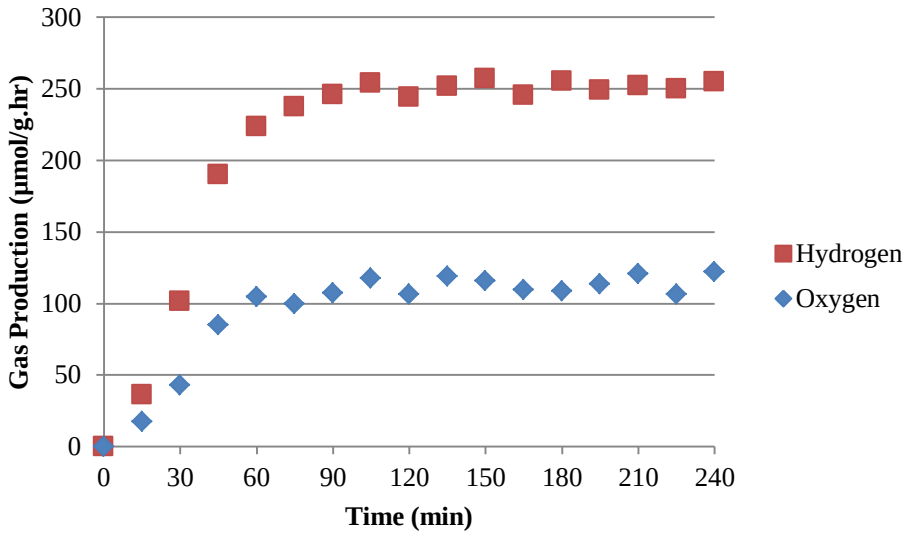

(a)

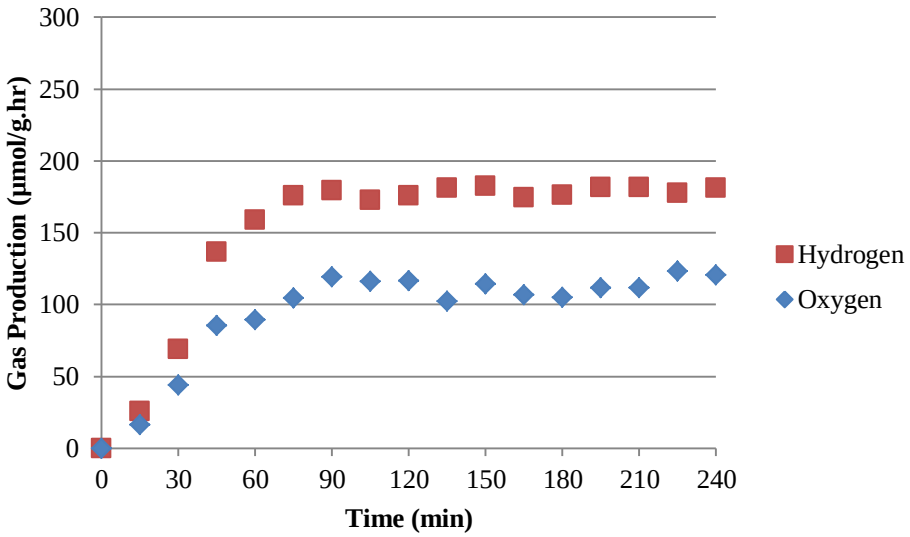

(b)

Figure 3-6: Sample water splitting online production rates for the two synthesized photocatalysts: a) CB1P3, and b) CB5P3.

3.3.3 The role of cobalt precursor

Based on the experimental data, it was concluded that cobalt precursor remnants have multiple impacts on the photocatalytic performance of the synthesized photocatalysts. One of

these effects was reported in Section 3.3.1.4 which is a positive shift toward visible light region for the nitrate-based samples. This looks promising; however, a more suitable absorbance spectrum is necessary but insufficient for photocatalytic activity. Considering the whole photocatalyst composition as an interactive system, incorporation of N compounds has had a notable impact on the overall absorbance, to some degree emulating the nitrogen doping effect.

The most determining effect of the precursor can be the electrochemical impact of the residues on the surface of the zeolite. Table 3-5 presents redox reaction possibilities with their thermodynamically priorities considering various cobalt precursors. According to the data, NO_3^- is more vulnerable to reduction than H^+, competing with the proton reduction via excited conduction band electrons, therefore decreasing the H_2 production rate. Photocatalytic reduction of the nitrates during the water cleavage process is addressed using semiconductor photocatalyst [155].

Analysis of the reactant solution by ion chromatography (IC) is a trusted way in the cases where the photo-reduction happens in the HNO_3 solution, detecting NO_2^- as the reaction product. Analyzing the solutions following the reaction with Metrohm IC device did not show any ionic release inside the solution. In addition, the online hydrogen evolution rate versus time was quite stable at the suppressed level after almost the first 90 minutes. Considering the catalytic functionality of the zeolite, this suggests participation of the nitrates in the regenerative cycles rather than their complete consumption, allowing them to keep their parasitic role stable. The similar interpretation has been proposed for the suppressing role of other ions [131], clearly posing that all the phenomena are happening near the surface without influencing the reaction solution composition. Besides, robustness of the preparation

was confirmed using this analysis, detecting no released ion from the surface of the photocatalyst even at very low content.

Table 3-5: Redox reaction possibilities with their thermodynamically priorities considering various cobalt precursors (numbers from [151]).

Cathodic Reaction Candidates	$E_c^0(V)$	**Priority**
$NO_3^- + 3H^+ + 2e^- \leftrightarrow HNO_2 + H_2O$	0.940	1
$2H^+ + 2e^- \leftrightarrow H_2$	0.000	2
$Co^{2+} + 2e^- \leftrightarrow Co$	-0.277	3
Anodic Reaction Candidates	$E_c^0(V)$	**Priority**
$O_2 + 4H^+ + 4e^- \leftrightarrow 2H_2O$	1.229	1
$Cl_2 + 2e^- \leftrightarrow 2Cl^-$	1.396	2

On the other hand, based on Table 3-5, oxidation of Cl^- is thermodynamically more difficult than the oxidation of H_2O. However, considering 2-electron redox process of Cl^- oxidation in comparison with 4-electron oxidation process of H_2O, it is likely to observe Cl_2 production during the water splitting reaction. In our experiments, no Cl_2 evolution was observed unlike previous studies which have reported Cl_2 formation using HCl solutions [131]. Therefore, it is deducible that chlorides are not involved in such oxidation competition. The possible explanation would be the different position of chloride ions in comparison to the oxidations sites. Figure 3-7 depicts cobalt precursor position in the zeolite pore with reasonable distance from photo-oxidation active sites on the surface. As it is concluded in Section 3.3.1.2, TiO_2 nanoparticles and HPA are located on the surface whereas the cobalt precursor is positioned in the pores. Similar oxygen evolution rates were observed for the two identical compositions with chloride and nitrate precursors of cobalt (Figure 3-6).

This could be interpreted as another indication that the chlorides are placed in the pores, reasonably far from photo-oxidation sites to compete with oxygen evolution reaction. This can be another advantage of the zeolite-supported photocatalysts, providing a reasonable separation space in the gas evolution sites. It can be also a possible explanation for resolving the hindrance of oxidation active sites by Cl^- anions in the photo-degradation of 2,4-D. To some degree, our experiments emulate the new concept of core-shell photocatalysis for the separation of reduction and oxidation active sites, lowering the back reaction rates.

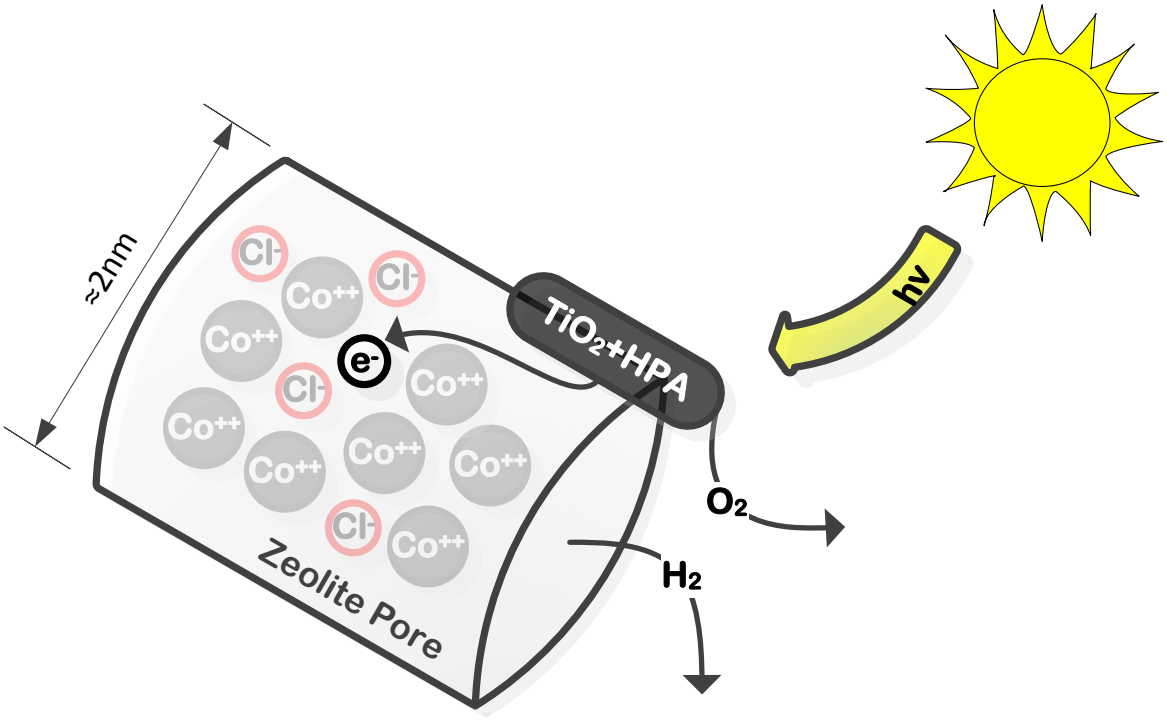

(a)

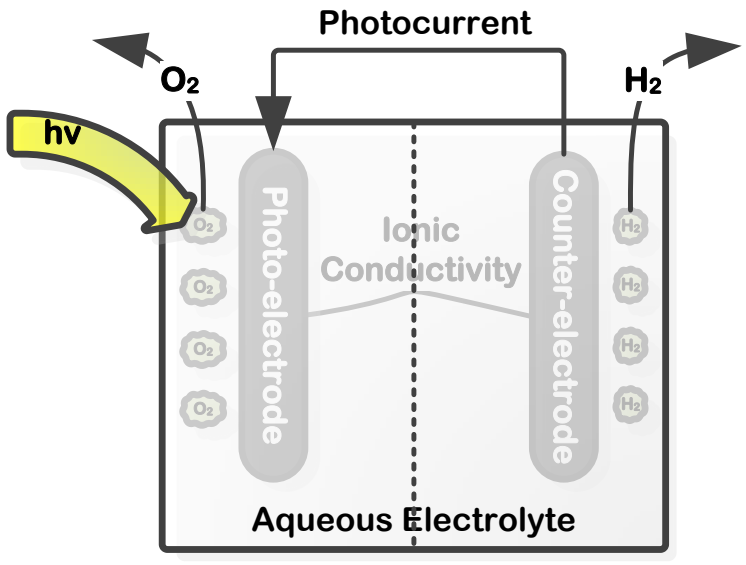

(b)

Figure 3-7: a) Cobalt precursor position in the zeolite pore with reasonable distance from photo-oxidation active sites on the surface. b) Separate evolution analogy shown in the photo-anode configuration.

It is important to note that for titania the electron diffusion length is ≈10μm [156], while the hole diffusion length is ≈10nm [157], implying a great opportunity for having separate redox sites. Thus, if the photocatalyst size is assumed as few microns, although only a limited surface is exposed to the irradiation, almost the whole core of the samples (i.e. zeolite matrix) can potentially be involved in the reduction process (i.e. hydrogen evolution). This becomes more viable when the interconnected structure of the zeolite and hopping mechanism for local electron transfer are taken into account [105]. Thus, zeolites can bring more feasibility comparing with some of the other complex and expensive structured materials for the core-shell photocatalysis approach in water splitting application [158].

3.4 Conclusion

Although using nitrate compounds are preferred to the chlorides because of the catalyst poisoning effect of Cl^-, they did not emerge as promising precursor materials for photocatalytic water dissociation using zeolite-supported TiO_2-based photocatalysts. It was observed that nitrate precursor can improve the absorbance of the photocatalyst through visible light similar to nitrogen doping in some degree. However, for hydrogen evolution, they caused almost 30% lower activities in comparison to the chloride compounds. It was inferred that this might be due to the photo-reduction competition of the nitrate compounds with respect to proton reduction potential. However, no considerable change in the reaction solution composition was observed, suggesting the stable solid state parasitic reactivity of nitrate anions with regenerative cycles. On the other hand, the expected poisoning and parasitic effects of chlorides were not occurred for 2,4-D degradation and hydrogen evolution, respectively. This can be rendered by the reasonable space between the chloride ions' position in the pores and the photo-oxidation active sites on the surface.

In fact, this research beyond its specific case studies, to some extent showed a promising feasibility of using the zeolite-supported semiconductors in the cutting-edge field of core-shell photocatalysis. It is important to address that zeolites are the only class of structured materials which are now mass produced, available in a wide range of structure, pore size, and chemical properties at a relatively low price. Hence, potentially they can be more applicable for this purpose in comparison to some of the other complex and expensive structured materials.

Chapter 4: Conclusions, highlights and recommendations for future work

4.1 Overall conclusions

In Chapter 2, the chemical point of view of the successful combination of zeolite, titania, HPA, and cobalt for photocatalytic water splitting under visible light was studied. In this regard, four classes of zeolites were evaluated: Na-Y, Na-Mordenite, H-Y and H-Beta with various Si/Al ratios and sodium content. Among the synthesized photocatalysts, Na-Y and Na-Mordenite containing 10 wt% titania emerged as the potential photocatalysts for the hydrogen evolution reaction under visible light with hydrogen generation rates of 250.8 and 187.2 μmol/g.h, respectively in comparison to 84.2 μmol/g.h for Degussa P25; while for H-Y and H-Beta these values were 96.8 and 100.1 μmol/g.h, respectively. Simultaneously deeper characterization techniques were employed to make the role of HPA and nanometer-sized titania on the support clearer, evaluating their performance for environmental applications as well. The following highlights were concluded as the result of the studies performed in Chapter 2:

- Zeolite chemical properties are crucial in photocatalytic hydrogen production.
- Basic zeolite, TiO_2, heteropolyacid and cobalt together are active under visible light.
- TiO_2 impregnation on zeolite causes band gap widening and band edges' anodic shift.
- Heteropolyacid enhances the visible light activity being convertible to HPB.
- Zeolite's basicity can overshadow the anodic shift advancing hydrogen evolution.

In Chapter 3, the impact of cobalt precursors on the photocatalytic activity of the final synthesized photocatalysts was evaluated. From the preparation point of view, the synthesis of the objective photocatalyst compound consists of three impregnation steps of TiO_2, Co, and HPA, respectively, followed by a specific thermal treatment for each stage. The focus of

this Chapter was on the cobalt impregnation step. The impact of two commercially available cobalt precursors on the photocatalytic activity of the final synthesized photocatalysts, especially hydrogen production rate was investigated. Nitrate and chloride compounds of cobalt were examined on two classes of the zeolites namely Na-Y and Na-Mordenite which had been emerged as suitable supports for hydrogen evolution application. Although nitrate-based photocatalysts exhibited an improvement in the UV-VIS absorbance spectra toward visible light, they caused an almost 30% lower H_2 production rate in comparison to the chloride salts. The favorable shift toward visible light is possibly due to the incorporation of nitrogen (N) anions in the interconnected photocatalyst structure. However, their lower hydrogen production rate is mainly attributed to the competitive photo-reduction reactions of solid remnant nitrate anions, causing this so-called parasitic phenomenon. In addition, overshadowing the poisoning and parasitic effects of Cl^- anions on the photo-oxidation sites in the zeolite-supported composition was another notable outcome of this study. This emulates the core-shell photocatalysis concept insofar with providing a reasonable distance between redox sites. The following highlights were concluded as the result of the studies performed in Chapter 3:

- Cobalt precursor can have a determining role on photocatalytic hydrogen production.
- Nitrate residues suppress the hydrogen production via competitive photo-reduction.
- The composition removes the poisonous and parasitic impact of surface chloride remnants.
- The synthesized photocatalyst emulates core-shell concept for separate evolution.

4.2 Recommendations for future work

There is still a noticeable affinity toward usage of TiO_2 in the world of research based on its superior capabilities for photocatalytic processes. Thus, it is worthy to move forward with

further modifications whether with more enhanced anion doing techniques or dye sensitizing approach. Besides efforts on modification of the titania's visible light response, there have been many studies on finding new materials to satisfy the requirements of photocatalytic water splitting which is always helpful to think out of box and discover new areas. Among those, gallium zinc oxynitrides are mostly in the center of attention due to their high activity under visible irradiation [34, 131, 159]. As a suggestion it would be intriguing to form them in the structured architecture, evaluating the possible performance improvements due to the crystallinity. Especially their interaction with the zeolites as the support, and taking the advantage of a chemically active structured support would be worthy to investigate; considering this point that most of the researches performed on this specific material are just in the order of gram employing unsupported types with fairly conventional preparation techniques [34, 131, 159]. Potentially, this would be a considerable room to make progress, of course requiring the related preparation designs.

As mentioned in Section 1.5.4, structural impact can be significant in the case of employing careful interconnected structures synthesis. In this research, zeolites have been utilized to meet this criterion with providing the nano-sized tetrahedral formation of the titania on the structured support. Further studies can be done on growing nanotubes or nanorods of TiO_2 or any other suitable semiconductor in various environments with the addition of chemical promoters to improve the visible light absorption, achieving three dimensional antenna configurations as explained in Section 1.5.4 [100, 160].

From the technical point of view, based on the operational and safety constraints, the typical running time for the experiments was 4 hours, fortunately having steady rates in that time domain. However, it is important for further studies to go through long-term

performance, and the possible variations of the reactions' performance in the course of time [147]. A comprehensive detection of all the possibly generated species in the system via more robust instrumentation and extra investments is necessary to provide better understanding of the phenomena happening during the photocatalytic processes. Examining various electrolyte solutions observing the released species after the aforementioned improvements would be fairly straightforward and telling. This was achieved in this research via simultaneous GC, IC, and various qualitative analyses.

The final word is based on the fundamental line of reasoning of the obtained results of this thesis. It was proved that impregnation of the titania on the zeolite can have a negative impact on the absorption with band-gap widening phenomenon. However, it was shown that visible light activity of HPA as well as basic chemical structure of the zeolite overshadow this effect, and improve the performance under visible-light. If the same effect is applicable to other semiconductors due to the strong bond formation between the semiconductor and the support, this would be intriguing to turn this disadvantage to the advantage using narrow-band semiconductors which are not primarily suitable for water splitting application such as CdSe. It should be noted that working on more facile techniques in the synthesis of such multicomponent compositions is crucial from the engineering point of view for mass production purposes.

Further fundamental studies on the diffusion length of the photons inside structured materials such as zeolite, activated carbons, etc. are necessary to estimate the effective impregnation depth of the semiconductor on the support. This can be done via much more sophisticated analysis such as femtosecond studies finding the dynamics of charge carriers on the ultra-thin layers of the photocatalyst. As pointed out in Section 1.5.3, the intrinsically fast

occurrence of these processes brings the importance of employing fast kinetic analysis techniques, which in the case of solid semiconductor powders is challenging.

4.3 Safety and apparatus considerations

Process automatic control having careful monitoring over the reactor temperature and related cooling system are the complementary elements of going for longer experiments. It is important to emphasize on the deadly hazards associated with the failure of the apparatus due to the operating weaknesses. This can become extremely serious especially when the lamp is running inside the sleeve of the photoreactor, and the reactor gets pressurized due to the flow blockage. Melting down of the high-pressure UV lamp as the result of the cooling failure is also considered as one of the fatal damage scenarios. Due to the first usage of the high-pressure UV lamp from well-known Japanese Company, USHIO, in Canada, permission from Canadian safety association (CSA) was proceeded, applying significant modifications on the lamp and the related ballast to meet the requirements. Hence, the license was issued conditionally only under the operator presence during the time of the experiment. For longer continuous usage, it's necessary to satisfy the representatives with further negotiations based on the successful running times up to 4 hours, increasing the working hours gradually and cautiously up to 24 hours and higher.

References

1. Lewis, N.S. and D.G. Nocera, *Powering the planet: Chemical challenges in solar energy utilization.* Proceedings of the National Academy of Sciences of the United States of America, 2006. **103**(43): p. 15729-15735.

2. Green, M.A., Solar cells : operating principles, technology, and system applications, Prentice-Hall, Englewood Cliffs, NJ, 1982.

3. Plunkett, J.R. and United States. Energy Information Administration., International energy outlook and projections, Nova Science Publishers, Hauppauge, N.Y., 2011.

4. Rajeshwar, K., R.D. McConnell, and S. Licht, Solar hydrogen generation : toward a renewable energy future, Springer, New York, NY, 2008.

5. Navarro Yerga, R.M., M.C. Álvarez Galván, F. del Valle, J.A. Villoria de la Mano, and J.L.G. Fierro, *Water Splitting on Semiconductor Catalysts under Visible-Light Irradiation.* ChemSusChem, 2009. **2**(6): p. 471-485.

6. Jiang, Z., T. Xiao, V.L. Kuznetsov, and P.P. Edwards, *Turning carbon dioxide into fuel.* Philosophical Transactions of the Royal Society of London, Series A: Mathematical, Physical and Engineering Sciences, 2010. **368**(1923): p. 3343-3364.

7. Service, R.F., *Solar energy - Is it time to shoot for the Sun?* Science, 2005. **309**(5734): p. 548-551.

8. Delasa, H. and B. Serrano-Rosales, Advances in Chemical Engineering, Volume 36: Photocatalytic Technologies, Academic Press, 2009.

9. Vayssieres, L., On solar hydrogen & nanotechnology, John Wiley & Sons (Asia), Singapore ; Hoboken, NJ, 2009.

10. Akkerman, I., M. Janssen, J. Rocha, and R.H. Wijffels, *Photobiological hydrogen production: photochemical efficiency and bioreactor design.* International Journal of Hydrogen Energy, 2002. **27**(11–12): p. 1195-1208.

11. Funk, J.E. and R.M. Reinstrom, *Energy Requirements in Production of Hydrogen from Water.* Industrial & Engineering Chemistry Process Design and Development, 1966. **5**(3): p. 336-342.

12. Vayssieres, L., On Solar Hydrogen & Nanotechnology, John Wiley & Sons, 2010.

13. Kudo, A. and Y. Miseki, *Heterogeneous photocatalyst materials for water splitting.* Chem. Soc. Rev., 2009. **38**(1): p. 253-278.

14. Fujishima, A. and K. Honda, *Electrochemical Photolysis of Water at a Semiconductor Electrode.* Nature, 1972. **238**(5358): p. 37-+.

15. Ni, M., M.K.H. Leung, D.Y.C. Leung, and K. Sumathy, *A review and recent developments in photocatalytic water-splitting using TiO2 for hydrogen production.* Renewable and Sustainable Energy Reviews, 2007. **11**(3): p. 401-425.

16. Matsuoka, M., M. Kitano, M. Takeuchi, K. Tsujimaru, M. Anpo, and J.M. Thomas, *Photocatalysis for new energy production: Recent advances in photocatalytic water splitting reactions for hydrogen production.* Catalysis Today, 2007. **122**(1-2): p. 51-61.

17. Nowotny, J., C.C. Sorrell, T. Bak, and L.R. Sheppard, *Solar-hydrogen: Unresolved problems in solid-state science.* Solar Energy, 2005. **78**(5): p. 593-602.

18. Maruska, H.P. and A.K. Ghosh, *Photocatalytic Decomposition of Water at Semiconductor Electrodes.* Solar Energy, 1978. **20**(6): p. 443-458.

19. Bard, A.J. and M.A. Fox, *Artificial Photosynthesis: Solar Splitting of Water to Hydrogen and Oxygen.* Accounts of Chemical Research, 1995. **28**(3): p. 141-145.

20. Holman, J., Heat Transfer, 10th edition, McGraw-Hill Science, 2009.

21. Archer, M.D. and J.R. Bolton, *Requirements for Ideal Performance of Photochemical and Photovoltaic Solar-Energy Converters.* Journal of Physical Chemistry, 1990. **94**(21): p. 8028-8036.

22. Hulstrom, R., R. Bird, and C. Riordan, *Spectral solar irradiance data sets for selected terrestrial conditions.* Solar Cells, 1985. **15**(4): p. 365-391.

23. Ikeda, S., A. Tanaka, K. Shinohara, M. Hara, J.N. Kondo, K.I. Maruya, and K. Domen, *Effect of the particle size for photocatalytic decomposition of water on Ni-loaded K4Nb6O17.* Microporous Materials, 1997. **9**(5-6): p. 253-258.

24. Ellis, A.B., S.W. Kaiser, J.M. Bolts, and M.S. Wrighton, *Study of N-Type Semiconducting Cadmium Chalcogenide-Based Photoelectrochemical Cells Employing Polychalcogenide Electrolytes.* Journal of the American Chemical Society, 1977. **99**(9): p. 2839-2848.

25. Williams, R. and R.H. Bube, *Photoemission in the Photovoltaic Effect in Cadmium Sulfide Crystals.* Journal of Applied Physics, 1960. **31**(6): p. 968-978.

26. Philip Colombo Jr, D., K.A. Roussel, J. Saeh, D.E. Skinner, J.J. Cavaleri, and R.M. Bowman, *Femtosecond study of the intensity dependence of electron-hole dynamics in TiO2 nanoclusters.* Chemical Physics Letters, 1995. **232**(3): p. 207-214.

27. Ohno, T., F. Tanigawa, K. Fujihara, S. Izumi, and M. Matsumura, *Photocatalytic oxidation of water by visible light using ruthenium-doped titanium dioxide powder.* Journal of Photochemistry and Photobiology A: Chemistry, 1999. **127**(1-3): p. 107-110.

28. Sinha, A.S.K., N. Sahu, M.K. Arora, and S.N. Upadhyay, *Preparation of egg-shell type Al2O3-supported CdS photocatalysts for reduction of H2O to H2.* Catalysis Today, 2001. **69**(1-4): p. 297-305.

29. Anpo, M. and M. Takeuchi, *The design and development of highly reactive titanium oxide photocatalysts operating under visible light irradiation.* Journal of Catalysis, 2003. **216**(1-2): p. 505-516.

30. Ishii, T., H. Kato, and A. Kudo, *H2 evolution from an aqueous methanol solution on SrTiO3 photocatalysts codoped with chromium and tantalum ions under visible light irradiation.* Journal of Photochemistry and Photobiology A: Chemistry, 2004. **163**(1-2): p. 181-186.

31. Zalas, M. and M. Laniecki, *Photocatalytic hydrogen generation over lanthanides-doped titania.* Solar Energy Materials and Solar Cells, 2005. **89**(2-3): p. 287-296.

32. Aroutiounian, V.M., V.M. Arakelyan, and G.E. Shahnazaryan, *Metal oxide photoelectrodes for hydrogen generation using solar radiation-driven water splitting.* Solar Energy, 2005. **78**(5): p. 581-592.

33. Galińska, A. and J. Walendziewski, *Photocatalytic Water Splitting over Pt−TiO2 in the Presence of Sacrificial Reagents.* Energy and Fuels, 2005. **19**(3): p. 1143-1147.

34. Maeda, K., T. Takata, M. Hara, N. Saito, Y. Inoue, H. Kobayashi, and K. Domen, *GaN:ZnO Solid Solution as a Photocatalyst for Visible-Light-Driven Overall Water Splitting.* Journal of the American Chemical Society, 2005. **127**(23): p. 8286-8287.

35. Wang, D., Z. Zou, and J. Ye, *Photocatalytic Water Splitting with the Cr-Doped Ba2In2O5/In2O3 Composite Oxide Semiconductors.* Chemistry of Materials, 2005. **17**(12): p. 3255-3261.

36. Kato, H. and A. Kudo, *Visible-Light-Response and Photocatalytic Activities of TiO2 and SrTiO3 Photocatalysts Codoped with Antimony and Chromium.* The Journal of Physical Chemistry B, 2002. **106**(19): p. 5029-5034.

37. Ishii, T., H. Kato, and A. Kudo, *H2 evolution from an aqueous methanol solution on SrTiO3 photocatalysts codoped with chromium and tantalum ions under visible light irradiation.* Journal of Photochemistry and Photobiology A: Chemistry, 2004. **163**(1–2): p. 181-186.

38. Kudo, A. and M. Sekizawa, *Photocatalytic H2 evolution under visible light irradiation on Zn1-xCuxS solid solution.* Catalysis Letters, 1999. **58**(4): p. 241-243.

39. Kudo, A. and M. Sekizawa, *Photocatalytic H2 evolution under visible light irradiation on Ni-doped ZnS photocatalyst.* Chemical Communications, 2000(15): p. 1371-1372.

40. Khan, S.U.M., M. Al-Shahry, and W.B. Ingler, *Efficient photochemical water splitting by a chemically modified n-TiO2.* Science, 2002. **297**(5590): p. 2243-2245.

41. Choi, W.Y., A. Termin, and M.R. Hoffmann, *The Role of Metal-Ion Dopants in Quantum-Sized Tio2 - Correlation between Photoreactivity and Charge-Carrier Recombination Dynamics.* Journal of Physical Chemistry, 1994. **98**(51): p. 13669-13679.

42. Blasse, G., G.J. Dirksen, and P.H.M. de Korte, *Materials with cationic valence and conduction bands for photoelectrolysis of water.* Materials Research Bulletin, 1981. **16**(8): p. 991-998.

43. Asahi, R., T. Morikawa, T. Ohwaki, K. Aoki, and Y. Taga, *Visible-light photocatalysis in nitrogen-doped titanium oxides.* Science, 2001. **293**(5528): p. 269-271.

44. Hitoki, G., T. Takata, J.N. Kondo, M. Hara, H. Kobayashi, and K. Domen, *An oxynitride, TaON, as an efficient water oxidation photocatalyst under visible light irradiation (lambda <= 500 nm).* Chemical Communications, 2002(16): p. 1698-1699.

45. Umebayashi, T., T. Yamaki, H. Itoh, and K. Asai, *Band gap narrowing of titanium dioxide by sulfur doping.* Applied Physics Letters, 2002. **81**(3): p. 454-456.

46. Serpone, N., E. Borgarello, and M. Gratzel, *Visible-Light Induced Generation of Hydrogen from H2s in Mixed Semiconductor Dispersions - Improved Efficiency through Inter-Particle Electron-Transfer.* Journal of the Chemical Society-Chemical Communications, 1984(6): p. 342-344.

47. Lee, J.S., *Photocatalytic water splitting under visible light with particulate semiconductor catalysts.* Catalysis Surveys from Asia, 2005. **9**(4): p. 217-227.

48. Yoshimura, J., A. Kudo, A. Tanaka, K. Domen, K.-i. Maruya, and T. Onishi, *H2 evolution caused by electron transfer between different semiconductors under visible light irradiation.* Chemical Physics Letters, 1988. **147**(4): p. 401-404.

49. Tsuji, I., H. Kato, and A. Kudo, *Visible-Light-Induced H2 Evolution from an Aqueous Solution Containing Sulfide and Sulfite over a ZnS–CuInS2–AgInS2 Solid-Solution Photocatalyst.* Angewandte Chemie, 2005. **117**(23): p. 3631-3634.

50. Inoue, Y., Y. Asai, and K. Sato, *Photocatalysts with Tunnel Structures for Decomposition of Water .1. Bati4o9, a Pentagonal Prism Tunnel Structure, and Its Combination with Various Promoters.* Journal of the Chemical Society-Faraday Transactions, 1994. **90**(5): p. 797-802.

51. Kambe, S., M. Fujii, T. Kawai, S. Kawai, and F. Nakahara, *Photocatalytic hydrogen production with Cd(S, Se) solid solution particles: Determining factors for the highly efficient photocatalyst.* Chemical Physics Letters, 1984. **109**(1): p. 105-109.

52. Sayama, K., R. Yoshida, H. Kusama, K. Okabe, Y. Abe, and H. Arakawa, *Photocatalytic decomposition of water into H-2 and O-2 by a two-step photoexcitation reaction using a WO3 suspension catalyst and an Fe3+/Fe2+ redox system.* Chemical Physics Letters, 1997. **277**(4): p. 387-391.

53. Ohno, T., F. Tanigawa, K. Fujihara, S. Izumi, and M. Matsumura, *Photocatalytic oxidation of water on TiO2-coated WO3 particles by visible light using Iron(III) ions as electron acceptor.* Journal of Photochemistry and Photobiology a-Chemistry, 1998. **118**(1): p. 41-44.

54. Abe, R., K. Sayama, and H. Sugihara, *Development of new photocatalytic water splitting into H(2) and O(2) using two different semiconductor photocatalysts and a shuttle redox mediator IO(3) (-)/I(-).* Journal of Physical Chemistry B, 2005. **109**(33): p. 16052-16061.

55. Tennakone, K. and S. Wickramanayake, *Cyclic Photocleavage of Water with the Intermediate Redox Couple Hg2o/Hg.* Journal of Physical Chemistry, 1986. **90**(7): p. 1219-1222.

56. Abe, R., K. Sayama, K. Domen, and H. Arakawa, *A new type of water splitting system composed of two different TiO2 photocatalysts (anatase, rutile) and a IO3-/I- shuttle redox mediator.* Chemical Physics Letters, 2001. **344**(3-4): p. 339-344.

57. Sayama, K., K. Mukasa, R. Abe, Y. Abe, and H. Arakawa, *A new photocatalytic water splitting system under visible light irradiation mimicking a Z-scheme mechanism in photosynthesis.* Journal of Photochemistry and Photobiology a-Chemistry, 2002. **148**(1-3): p. 71-77.

58. Maruthamuthu, P., M. Ashokkumar, K. Gurunathan, E. Subramanian, and M.V.C. Sastri, *Hydrogen Evolution from Water with Visible Radiation in Presence of Cu(Ii)/Wo3 and Electron Relay.* International Journal of Hydrogen Energy, 1989. **14**(8): p. 525-528.

59. Kalyanasundaram, K. and M. Gratzel, *Applications of functionalized transition metal complexes in photonic and optoelectronic devices.* Coordination Chemistry Reviews, 1998. **177**: p. 347-414.

60. Balzani, V., Electron transfer in chemistry, Wiley-VCH, Weinheim ; New York, 2001.

61. Youngblood, W.J., S.-H.A. Lee, K. Maeda, and T.E. Mallouk, *Visible Light Water Splitting Using Dye-Sensitized Oxide Semiconductors.* Accounts of Chemical Research, 2009. **42**(12): p. 1966-1973.

62. Saehana, S., R. Prasetyowati, M.I. Hidayat, P. Arifin, Khairurrijal, and M. Abdullah, *Performance Improvement of TiO[sub 2] Based Solar Cells by Coating Cu Nanoparticles into the Space between TiO[sub 2].* AIP Conference Proceedings, 2011. **1415**(1): p. 163-166.

63. Hagfeldt, A. and M. Graetzel, *Light-Induced Redox Reactions in Nanocrystalline Systems.* Chemical Reviews, 1995. **95**(1): p. 49-68.

64. GUST, D. and T.A. MOORE, *Mimicking Photosynthesis.* Science, 1989. **244**(4900): p. 35-41.

65. Scholes, G.D., G.R. Fleming, A. Olaya-Castro, and R. van Grondelle, *Lessons from nature about solar light harvesting.* Nat Chem, 2011. **3**(10): p. 763-774.

66. Walter, M.G., A.B. Rudine, and C.C. Wamser, *Porphyrins and phthalocyanines in solar photovoltaic cells.* Journal of Porphyrins and Phthalocyanines, 2010. **14**(9): p. 759-792.

67. Campagna, S., G. Denti, S. Serroni, A. Juris, M. Venturi, V. Ricevuto, and V. Balzani, *Dendrimers of Nanometer-Size Based on Metal-Complexes - Luminescent and Redox-Active Polynuclear Metal-Complexes Containing up to 22 Metal Centers.* Chemistry-a European Journal, 1995. **1**(4): p. 211-221.

68. Juris, A., V. Balzani, S. Campagna, G. Denti, S. Serroni, G. Frei, and H.U. Guedel, *Near-Infrared Luminescence of Supramolecular Species Consisting of Osmium(II)- and/or Ruthenium(II)-Polypyridine Components.* Inorganic Chemistry, 1994. **33**(7): p. 1491-1496.

69. Bignozzi, C.A., R. Argazzi, C. Chiorboli, F. Scandola, R.B. Dyer, J.R. Schoonover, and T.J. Meyer, *Vibrational and Electronic Spectroscopy of Electronically Excited Polychromophoric Ruthenium(II) Complexes.* Inorganic Chemistry, 1994. **33**(8): p. 1652-1659.

70. Ashokkumar, M., *An overview on semiconductor particulate systems for photoproduction of hydrogen.* International Journal of Hydrogen Energy, 1998. **23**(6): p. 427-438.

71. Reber, J.F. and K. Meier, *Photochemical Production of Hydrogen with Zinc-Sulfide Suspensions.* Journal of Physical Chemistry, 1984. **88**(24): p. 5903-5913.

72. Kominami, H., T. Matsuura, K. Iwai, B. Ohtani, S. Nishimoto, and Y. Kera, *Ultra-Highly Active Titanium(Iv) Oxide Photocatalyst Prepared by Hydrothermal Crystallization from Titanium(Iv) Alkoxide in Organic-Solvents.* Chemistry Letters, 1995(8): p. 693-694.

73. Brus, L.E., *Electron--electron and electron-hole interactions in small semiconductor crystallites: The size dependence of the lowest excited electronic state.* The Journal of Chemical Physics, 1984. **80**(9): p. 4403-4409.

74. Rossetti, R. and L.E. Brus, *Picosecond Resonance Raman-Scattering Study of Methylviologen Reduction on the Surface of Photoexcited Colloidal Cds Crystallites.* Journal of Physical Chemistry, 1986. **90**(4): p. 558-560.

75. Rino, J.P. and N. Studart, *Structural correlations in titanium dioxide.* Physical Review B, 1999. **59**(10): p. 6643-6649.

76. Chestnoy, N., T.D. Harris, R. Hull, and L.E. Brus, *Luminescence and Photophysics of Cds Semiconductor Clusters - the Nature of the Emitting Electronic State.* Journal of Physical Chemistry, 1986. **90**(15): p. 3393-3399.

77. Hoffmann, M.R., S.T. Martin, W.Y. Choi, and D.W. Bahnemann, *Environmental Applications of Semiconductor Photocatalysis.* Chemical Reviews, 1995. **95**(1): p. 69-96.

78. Haase, M., H. Weller, and A. Henglein, *Photochemistry of Colloidal Semiconductors .26. Photoelectron Emission from Cds Particles and Related Chemical Effects.* Journal of Physical Chemistry, 1988. **92**(16): p. 4706-4712.

79. Nedeljkovic, J.M., M.T. Nenadovic, O.I. Micic, and A.J. Nozik, *Enhanced Photoredox Chemistry in Quantized Semiconductor Colloids.* Journal of Physical Chemistry, 1986. **90**(1): p. 12-13.

80. Koch, U., A. Fojtik, H. Weller, and A. Henglein, *Photochemistry of semiconductor colloids. Preparation of extremely small ZnO particles, fluorescence phenomena and size quantization effects.* Chemical Physics Letters, 1985. **122**(5): p. 507-510.

81. Anpo, M., T. Shima, S. Kodama, and Y. Kubokawa, *Photocatalytic Hydrogenation of Ch3cch with H2o on Small-Particle Tio2 - Size Quantization Effects and Reaction Intermediates.* Journal of Physical Chemistry, 1987. **91**(16): p. 4305-4310.

82. Kormann, C., D.W. Bahnemann, and M.R. Hoffmann, *Preparation and Characterization of Quantum-Size Titanium-Dioxide.* Journal of Physical Chemistry, 1988. **92**(18): p. 5196-5201.

83. Kim, K.D., H.J. Bae, and H.T. Kim, *Synthesis and characterization of titania-coated silica fine particles by semi-batch process.* Colloids and Surfaces A: Physicochemical and Engineering Aspects, 2003. **224**(1–3): p. 119-126.

84. Kuznetsova, I.N., V. Blaskov, I. Stambolova, L. Znaidi, and A. Kanaev, *TiO2 pure phase brookite with preferred orientation, synthesized as a spin-coated film.* Materials Letters, 2005. **59**(29–30): p. 3820-3823.

85. Lee, J.H. and Y.S. Yang, *Effect of hydrolysis conditions on morphology and phase content in the crystalline TiO2 nanoparticles synthesized from aqueous TiCl4 solution by precipitation.* Materials Chemistry and Physics, 2005. **93**(1): p. 237-242.

86. Lin, J., Y. Lin, P. Liu, M.J. Meziani, L.F. Allard, and Y.-P. Sun, *Hot-Fluid Annealing for Crystalline Titanium Dioxide Nanoparticles in Stable Suspension.* Journal of the American Chemical Society, 2002. **124**(38): p. 11514-11518.

87. Yu, J.C., J.G. Yu, W.K. Ho, and L.Z. Zhang, *Preparation of highly photocatalytic active nano-sized TiO2 particles via ultrasonic irradiation.* Chemical Communications, 2001(19): p. 1942-1943.

88. Chae, S.Y., M.K. Park, S.K. Lee, T.Y. Kim, S.K. Kim, and W.I. Lee, *Preparation of Size-Controlled TiO2 Nanoparticles and Derivation of Optically Transparent Photocatalytic Films.* Chemistry of Materials, 2003. **15**(17): p. 3326-3331.

89. Cot, F., A. Larbot, G. Nabias, and L. Cot, *Preparation and characterization of colloidal solution derived crystallized titania powder.* Journal of the European Ceramic Society, 1998. **18**(14): p. 2175-2181.

90. Seifried, S., M. Winterer, and H. Hahn, *Nanocrystalline Titania Films and Particles by Chemical Vapor Synthesis.* Chemical Vapor Deposition, 2000. **6**(5): p. 239-244.

91. Ayllon, J.A., A. Figueras, S. Garelik, L. Spirkova, J. Durand, and L. Cot, *Preparation of TiO2 powder using titanium tetraisopropoxide decomposition in a plasma enhanced chemical vapor deposition (PECVD) reactor.* Journal of Materials Science Letters, 1999. **18**(16): p. 1319-1321.

92. Ho, W. and J.C. Yu, *Sonochemical synthesis and visible light photocatalytic behavior of CdSe and CdSe/TiO2 nanoparticles.* Journal of Molecular Catalysis A: Chemical, 2006. **247**(1–2): p. 268-274.

93. Shen, S. and L. Guo, *Hydrothermal synthesis, characterization, and photocatalytic performances of Cr incorporated, and Cr and Ti co-incorporated MCM-41 as visible light photocatalysts for water splitting.* Catalysis Today, 2007. **129**(3-4): p. 414-420.

94. Zhao, D., S. Budhi, A. Rodriguez, and R.T. Koodali, *Rapid and facile synthesis of Ti-MCM-48 mesoporous material and the photocatalytic performance for hydrogen evolution.* International Journal of Hydrogen Energy, 2010. **35**(11): p. 5276-5283.

95. Chatti, R.V., N. Dubey, M.V. Joshi, N.K. Labhsetwar, P.N. Joshi, and S.S. Rayalu, *Influence of zeolitic structure on photoreduction property and hydrogen evolution reaction.* International Journal of Hydrogen Energy, 2010. **35**(5): p. 1911-1920.

96. Dubey, N., N.K. Labhsetwar, S. Devotta, and S.S. Rayalu, *Hydrogen evolution by water splitting using novel composite zeolite-based photocatalyst.* Catalysis Today, 2007. **129**(3-4): p. 428-434.

97. Nada, A.A., M.H. Barakat, H.A. Hamed, N.R. Mohamed, and T.N. Veziroglu, *Studies on the photocatalytic hydrogen production using suspended modified photocatalysts.* International Journal of Hydrogen Energy, 2005. **30**(7): p. 687-691.

98. Mahmoodi, N.M., M. Arami, and J. Zhang, *Preparation and photocatalytic activity of immobilized composite photocatalyst (titania nanoparticle/activated carbon).* Journal of Alloys and Compounds, 2011. **509**(14): p. 4754-4764.

99. Wang, C.Y., C. Bottcher, D.W. Bahnemann, and J.K. Dohrmann, *A comparative study of nanometer sized Fe(III)-doped TiO2 photocatalysts: synthesis, characterization and activity.* Journal of Materials Chemistry, 2003. **13**(9): p. 2322-2329.

100. Kamat, P.V., K. Tvrdy, D.R. Baker, and J.G. Radich, *Beyond Photovoltaics: Semiconductor Nanoarchitectures for Liquid-Junction Solar Cells.* Chemical Reviews, 2010. **110**(11): p. 6664-6688.

101. Ichikawa, S. and R. Doi, *Photoelectrocatalytic hydrogen production from wateron transparent thin film titania of different crystal structures and quantum efficiency characteristics.* Thin Solid Films, 1997. **292**(1-2): p. 130-134.

102. Diebold, U., *The surface science of titanium dioxide.* Surface Science Reports, 2003. **48**(5-8): p. 53-229.

103. Baerlocher, C., W.M. Meier, and D. Olson, Atlas of zeolite framework types, 5th rev. ed., Elsevier, Amsterdam ; New York, 2001.

104. Jens, W., *Zeolites and catalysis.* Solid State Ionics, 2000. **131**(1–2): p. 175-188.

105. Jansen, J.C., Advanced zeolite science and applications, Elsevier, Amsterdam ; New York, 1994.

106. Kozhevnikov, I.V., *Catalysis by heteropoly acids and multicomponent polyoxometalates in liquid-phase reactions.* Chemical Reviews, 1998. **98**(1): p. 171-198.

107. Misono, M., I. Ono, G. Koyano, and A. Aoshima, *Heteropolyacids. Versatile green catalysts usable in a variety of reaction media.* Pure and Applied Chemistry, 2000. **72**(7): p. 1305-1311.

108. Izumi, Y., K. Iida, K. Usami, and T. Nagata, *An efficient method for acetolysis of cyclic ethers catalyzed by heteropolyacid.* Applied Catalysis a-General, 2003. **256**(1-2): p. 199-202.

109. Cotton, F.A., Advanced inorganic chemistry, 6th ed., Wiley, New York, 1999.

110. Anandan, S. and M. Yoon, *Heteropolyacid-encapsulated TiHY zeolite as an inorganic photosynthetic reaction center mimicking the plant systems.* Journal of Photochemistry and Photobiology A: Chemistry, 2003. **160**(3): p. 181-184.

111. Bak, T., J. Nowotny, M. Rekas, and C.C. Sorrell, *Photo-electrochemical hydrogen generation from water using solar energy. Materials-related aspects.* International Journal of Hydrogen Energy, 2002. **27**(10): p. 991-1022.

112. Shaban, Y.A. and S.U.M. Khan, *Visible light active carbon modified n-TiO2 for efficient hydrogen production by photoelectrochemical splitting of water.* International Journal of Hydrogen Energy, 2008. **33**(4): p. 1118-1126.

113. Lin, H.Y., T.H. Lee, and C.Y. Sie, *Photocatalytic hydrogen production with nickel oxide intercalated K4Nb6O17 under visible light irradiation.* International Journal of Hydrogen Energy, 2008. **33**(15): p. 4055-4063.

114. Lin, H.Y., Y.F. Chen, and Y.W. Chen, *Water splitting reaction on NiO/InVO4 under visible light irradiation.* International Journal of Hydrogen Energy, 2007. **32**(1): p. 86-92.

115. Lunawat, P.S., S. Senapati, R. Kumar, and N.M. Gupta, *Visible light-induced splitting of water using CdS nanocrystallites immobilized over water-repellant polymeric surface.* International Journal of Hydrogen Energy, 2007. **32**(14): p. 2784-2790.

116. Sathish, M., B. Viswanathan, and R.P. Viswanath, *Alternate synthetic strategy for the preparation of CdS nanoparticles and its exploitation for water splitting.* International Journal of Hydrogen Energy, 2006. **31**(7): p. 891-898.

117. Koriche, N., A. Bouguelia, A. Aider, and M. Trari, *Photocatalytic hydrogen evolution over delafossite.* International Journal of Hydrogen Energy, 2005. **30**(7): p. 693-699.

118. Ye, J., Z. Zou, and A. Matsushita, *A novel series of water splitting photocatalysts NiM2O6 (M=Nb,Ta) active under visible light.* International Journal of Hydrogen Energy, 2003. **28**(6): p. 651-655.

119. Bessekhouad, Y. and M. Trari, *Photocatalytic hydrogen production from suspension of spinel powders AMn2O4(A=Cu and Zn).* International Journal of Hydrogen Energy, 2002. **27**(4): p. 357-362.

120. Sabate, J., M.A. Anderson, H. Kikkawa, M. Edwards, and C.G. Hill Jr, *A kinetic study of the photocatalytic degradation of 3-chlorosalicylic acid over TiO2 membranes supported on glass.* Journal of Catalysis, 1991. **127**(1): p. 167-177.

121. Matthews, R.W., *Response to the comment. "Photocatalytic reactor design: an example of mass-transfer limitations with an immobilized catalyst".* Journal of Physical Chemistry, 1988. **92**(23): p. 6853-6854.

122. Xu, Y.M. and X.L. Chen, *Photocatalytic Reduction of Dichromate over Semiconductor Catalysts.* Chemistry and Industry, 1990(15): p. 497-498.

123. Xu, Y.M., P.E. Ménassa, and C.H. Langford, *Photodecomposition of several chloroaromatics using a commercial prototype reactor.* Chemosphere, 1988. **17**(10): p. 1971-1976.

124. Matthews, R.W., *Solar-Electric Water-Purification Using Photocatalytic Oxidation with Tio2 as a Stationary Phase.* Solar Energy, 1987. **38**(6): p. 405-413.

125. Anpo, M., H. Nakaya, S. Kodama, Y. Kubokawa, K. Domen, and T. Onishi, *Photocatalysis over Binary Metal-Oxides - Enhancement of the Photocatalytic Activity of Tio2 in Titanium Silicon-Oxides.* Journal of Physical Chemistry, 1986. **90**(8): p. 1633-1636.

126. Sato, S., *Effects of surface modification with silicon oxides on the photochemical properties of powdered titania.* Langmuir, 1988. **4**(5): p. 1156-1159.

127. Rayalu, S.S., N. Dubey, N.K. Labhsetwar, S. Kagne, and S. Devotta, *UV and visibly active photocatalysts for water splitting reaction.* International Journal of Hydrogen Energy, 2007. **32**(14): p. 2776-2783.

128. Ha, P.S., H.J. Youn, H.S. Jung, K.S. Hong, Y.H. Park, and K.H. Ko, *Anatase–Rutile Transition of Precipitated Titanium Oxide with Alcohol Rinsing.* Journal of Colloid and Interface Science, 2000. **223**(1): p. 16-20.

129. Dabler, A., A. Feltz, J. Jung, W. Ludwig, and E. Kaisersberger, *Characterization of rutile and anatase powders by thermal analysis.* Journal of Thermal Analysis and Calorimetry, 1988. **33**(3): p. 803-809.

130. Ohtani, B., *Preparing articles on photocatalysis - Beyond the illusions, misconceptions, and speculation.* Chemistry Letters, 2008. **37**(3): p. 217-229.

131. Maeda, K., H. Masuda, and K. Domen, *Effect of electrolyte addition on activity of (Ga1-xZnx)(N1-xOx) photocatalyst for overall water splitting under visible light.* Catalysis Today, 2009. **147**(3-4): p. 173-178.

132. Chatti, R., S.S. Rayalu, N. Dubey, N. Labhsetwar, and S. Devotta, *Solar-based photoreduction of methyl orange using zeolite supported photocatalytic materials.* Solar Energy Materials and Solar Cells, 2007. **91**(2-3): p. 180-190.

133. Dubey, N., S.S. Rayalu, N.K. Labhsetwar, R.R. Naidu, R.V. Chatti, and S. Devotta, *Photocatalytic properties of zeolite-based materials for the photoreduction of methyl orange.* Applied Catalysis A: General, 2006. **303**(2): p. 152-157.

134. Yan, X.L., T. Ohno, K. Nishijima, R. Abe, and B. Ohtani, *Is methylene blue an appropriate substrate for a photocatalytic activity test? A study with visible-light responsive titania.* Chemical Physics Letters, 2006. **429**(4-6): p. 606-610.

135. Gärtner, M., V. Dremov, P. Müller, and H. Kisch, *Bandgap Widening of Titania through Semiconductor Support Interactions.* ChemPhysChem, 2005. **6**(4): p. 714-718.

136. Petkowicz, D.I., R. Brambilla, C. Radtke, C.D.S. da Silva, Z.N. da Rocha, S.B.C. Pergher, and J.H.Z. dos Santos, *Photodegradation of methylene blue by in situ generated titania supported on a NaA zeolite.* Applied Catalysis A: General, 2009. **357**(2): p. 125-134.

137. Petkowicz, D.I., S.B.C. Pergher, C.D.S. da Silva, Z.N. da Rocha, and J.H.Z. dos Santos, *Catalytic photodegradation of dyes by in situ zeolite-supported titania.* Chemical Engineering Journal, 2010. **158**(3): p. 505-512.

138. Herrmann, J.M., *Photocatalysis fundamentals revisited to avoid several misconceptions.* Applied Catalysis B: Environmental, 2010. **99**(3-4): p. 461-468.

139. Boval, B. and J.M. Smith, *Photodecomposition of 2,4-dichlorophenoxyacetic acid.* Chemical Engineering Science, 1973. **28**(9): p. 1661-1675.

140. Burrows, H.D., M. Canle L, J.A. Santaballa, and S. Steenken, *Reaction pathways and mechanisms of photodegradation of pesticides.* Journal of Photochemistry and Photobiology B: Biology, 2002. **67**(2): p. 71-108.

141. Linsebigler, A.L., G.Q. Lu, and J.T. Yates, *Photocatalysis on Tio2 Surfaces - Principles, Mechanisms, and Selected Results.* Chemical Reviews, 1995. **95**(3): p. 735-758.

142. Karakitsou, K.E. and X.E. Verykios, *Influence of Catalyst Parameters and Operational Variables on the Photocatalytic Cleavage of Water.* Journal of Catalysis, 1992. **134**(2): p. 629-643.

143. Kiwi, J. and M. Gratzel, *Optimization of Conditions for Photochemical Water Cleavage - Aqueous Pt/TiO2 (Anatase) Dispersions under Ultraviolet-Light.* Journal of Physical Chemistry, 1984. **88**(7): p. 1302-1307.

144. Karakitsou, K. and X.E. Verykios, *Definition of the Intrinsic Rate of Photocatalytic Cleavage of Water over Pt-Ruo2/TiO2 Catalysts.* Journal of Catalysis, 1995. **152**(2): p. 360-367.

145. Lee, K., W.S. Nam, and G.Y. Han, *Photocatalytic water-splitting in alkaline solution using redox mediator. 1: Parameter study.* International Journal of Hydrogen Energy, 2004. **29**(13): p. 1343-1347.

146. Hisatomi, T., K. Maeda, K. Takanabe, J. Kubota, and K. Domen, *Aspects of the Water Splitting Mechanism on (Ga1-xZnx)(N1-xOx) Photocatalyst Modified with Rh2-yCryO3 Cocatalyst.* Journal of Physical Chemistry C, 2009. **113**(51): p. 21458-21466.

147. Sayama, K. and H. Arakawa, *Effect of carbonate salt addition on the photocatalytic decomposition of liquid water over Pt-TiO2 catalyst.* Journal of the Chemical Society, Faraday Transactions, 1997. **93**(8): p. 1647-1654.

148. Sato, S., *Effects of Surface Modification with Silicon-Oxides on the Photochemical Properties of Powdered TiO2.* Langmuir, 1988. **4**(5): p. 1156-1159.

149. Arrua, L.A., B.J. McCoy, and J.M. Smith, *Effect of catalyst poisoning on adsorption and surface reaction rates in liquid-phase hydrogenation.* Industrial & Engineering Chemistry Research, 1990. **29**(6): p. 1050-1057.

150. Regalbuto, J.R., Catalyst preparation : science and engineering, CRC Press/Taylor & Francis, Boca Raton, Fla. ; London, 2007.

151. Lange, N.A. and J.G. Speight, Lange's handbook of chemistry, 16th ed., McGraw-Hill, New York ; London, 2005.

152. Zaleska, A., *Doped-TiO2: A Review.* Recent Patents on Engineering, 2008. **2**(3): p. 157-164.

153. Chen, D. and A.K. Ray, *Photodegradation kinetics of 4-nitrophenol in TiO2 suspension.* Water Research, 1998. **32**(11): p. 3223-3234.

154. Abdullah, M., G.K.C. Low, and R.W. Matthews, *Effects of common inorganic anions on rates of photocatalytic oxidation of organic carbon over illuminated titanium dioxide.* Journal of Physical Chemistry, 1990. **94**(17): p. 6820-6825.

155. Kato, H. and A. Kudo, *Photocatalytic reduction of nitrate ions over tantalate photocatalysts.* Physical Chemistry Chemical Physics, 2002. **4**(12): p. 2833-2838.

156. Dloczik, L., O. Ileperuma, I. Lauermann, L.M. Peter, E.A. Ponomarev, G. Redmond, N.J. Shaw, and I. Uhlendorf, *Dynamic Response of Dye-Sensitized Nanocrystalline Solar Cells: Characterization by Intensity-Modulated Photocurrent Spectroscopy.* Journal of Physical Chemistry B, 1997. **101**(49): p. 10281-10289.

157. Salvador, P., *Hole diffusion length in n-TiO2 single crystals and sintered electrodes: Photoelectrochemical determination and comparative analysis.* Journal of Applied Physics, 1984. **55**(8): p. 2977-2985.

158. Maeda, K. and K. Domen, *Photocatalytic Water Splitting: Recent Progress and Future Challenges.* Journal of Physical Chemistry Letters, 2010. **1**(18): p. 2655-2661.

159. Hisatomi, T., K. Miyazaki, K. Takanabe, K. Maeda, J. Kubota, Y. Sakata, and K. Domen, *Isotopic and kinetic assessment of photocatalytic water splitting on Zn-added Ga2O3 photocatalyst loaded with Rh2-yCryO3 cocatalyst.* Chemical Physics Letters, 2010. **486**(4-6): p. 144-146.

160. Kubacka, A., M. Fernández-García, and G. Colón, *Advanced Nanoarchitectures for Solar Photocatalytic Applications.* Chemical Reviews, 2011.

161. Takata, T., S. Ikeda, A. Tanaka, M. Hara, J.N. Kondo, and K. Domen, *Mechano-catalytic overall water splitting on some oxides (II).* Applied Catalysis A: General, 2000. **200**(1–2): p. 255-262.

162. Hara, M., M. Komoda, H. Hasei, M. Yashima, S. Ikeda, T. Takata, J.N. Kondo, and K. Domen, *A Study of Mechano-Catalysts for Overall Water Splitting.* The Journal of Physical Chemistry B, 2000. **104**(4): p. 780-785.

Appendices

Appendix A Details of the experimental setup

This appendix aims to describe various sections of the experimental setup built for the photocatalytic activity measurements under visible light in the course of this research. Figure A-1 shows the entire experimental setup by assembling more than 100 items. It is consisted of a photoreactor mounted on a magnet stirrer, high-pressure UV lamp and its ballast, UV filtration-cooling system, analytical grade filters, and the controller board. The aforementioned parts are described in the upcoming sections.

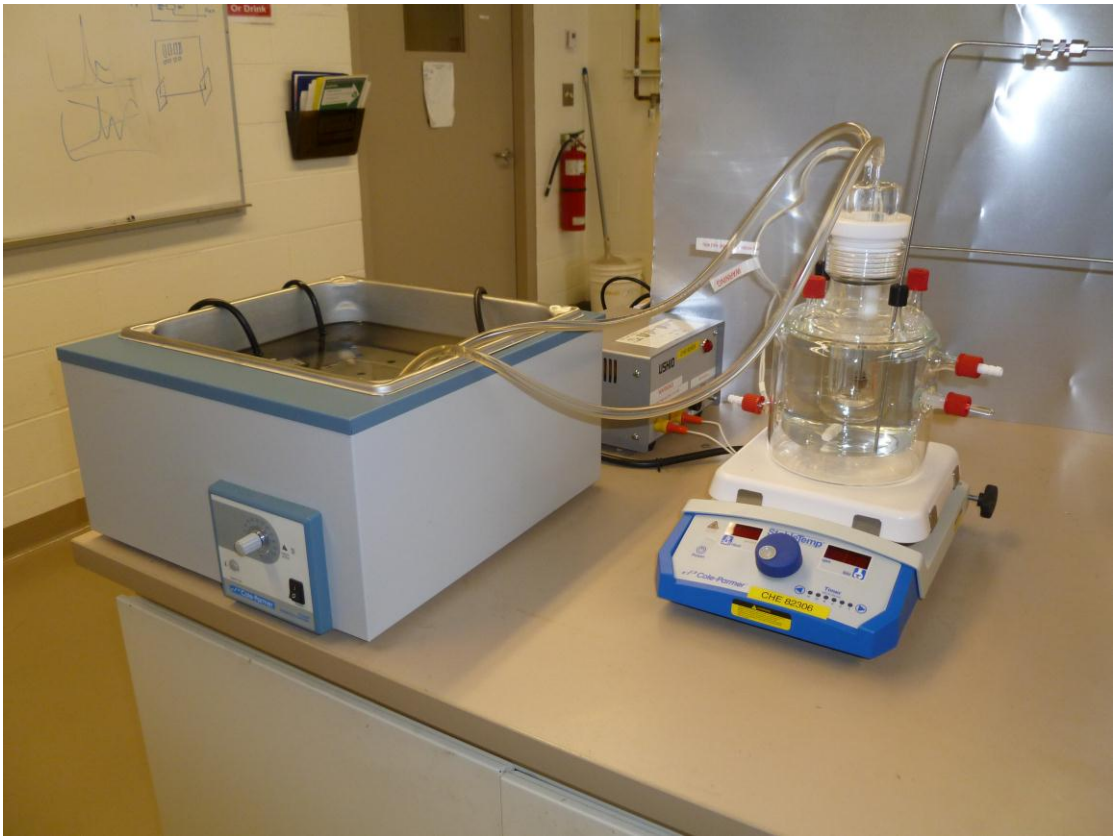

Figure A-1: Pictures for the entire experimental setup designed and manufactured during the course of this research.

A.1 Photoreactor

Figure A-2 demonstrates two dimensional design of the photoreactor with rough dimensions in millimeters excluding wall thicknesses. After preliminary sketch and exchanging the opinions with the manufacturer (CanSci Glass), the vessel was finalized and prepared for different purposes from gas evolution reactions to soluble organic contaminant photo-degradation, having one liter effective volume for the solution. Figure A-3 shows the picture of the manufactured photoreactor model with an extra body port on the right, for continuous liquid sampling or placing the photo-sensor sporadically, checking lamp output. The body material is borosilicate glass whereas the jacket of the lamp is made of quartz glass having almost 100% irradiation transition for facile future modifications of the lamp source. Two

extra ports considered at the top are used for placing pressure gauge and pressure relief valve having more control over vessel pressurizing.

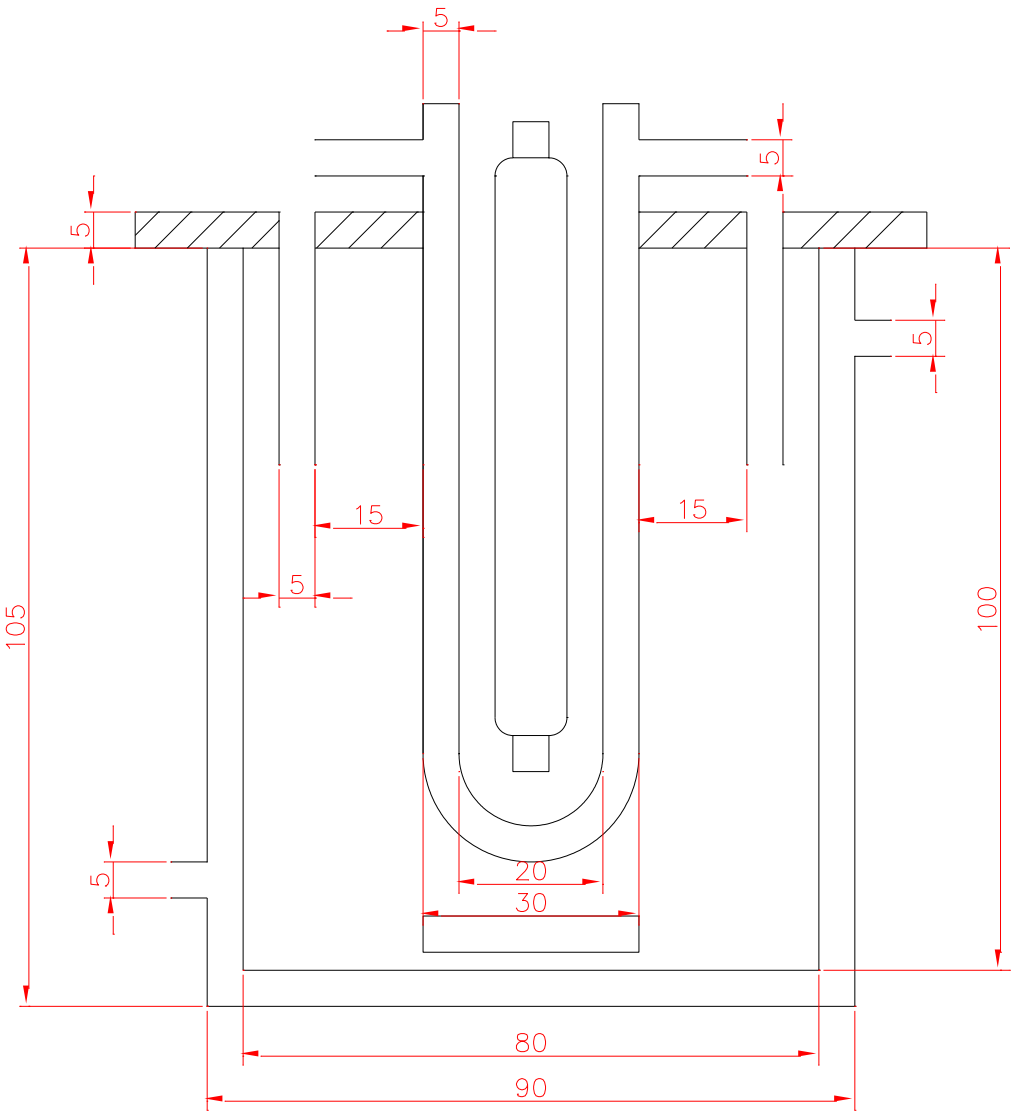

Figure A-2: Two dimensional design of the photoreactor with rough dimensions in millimeters excluding wall thicknesses.

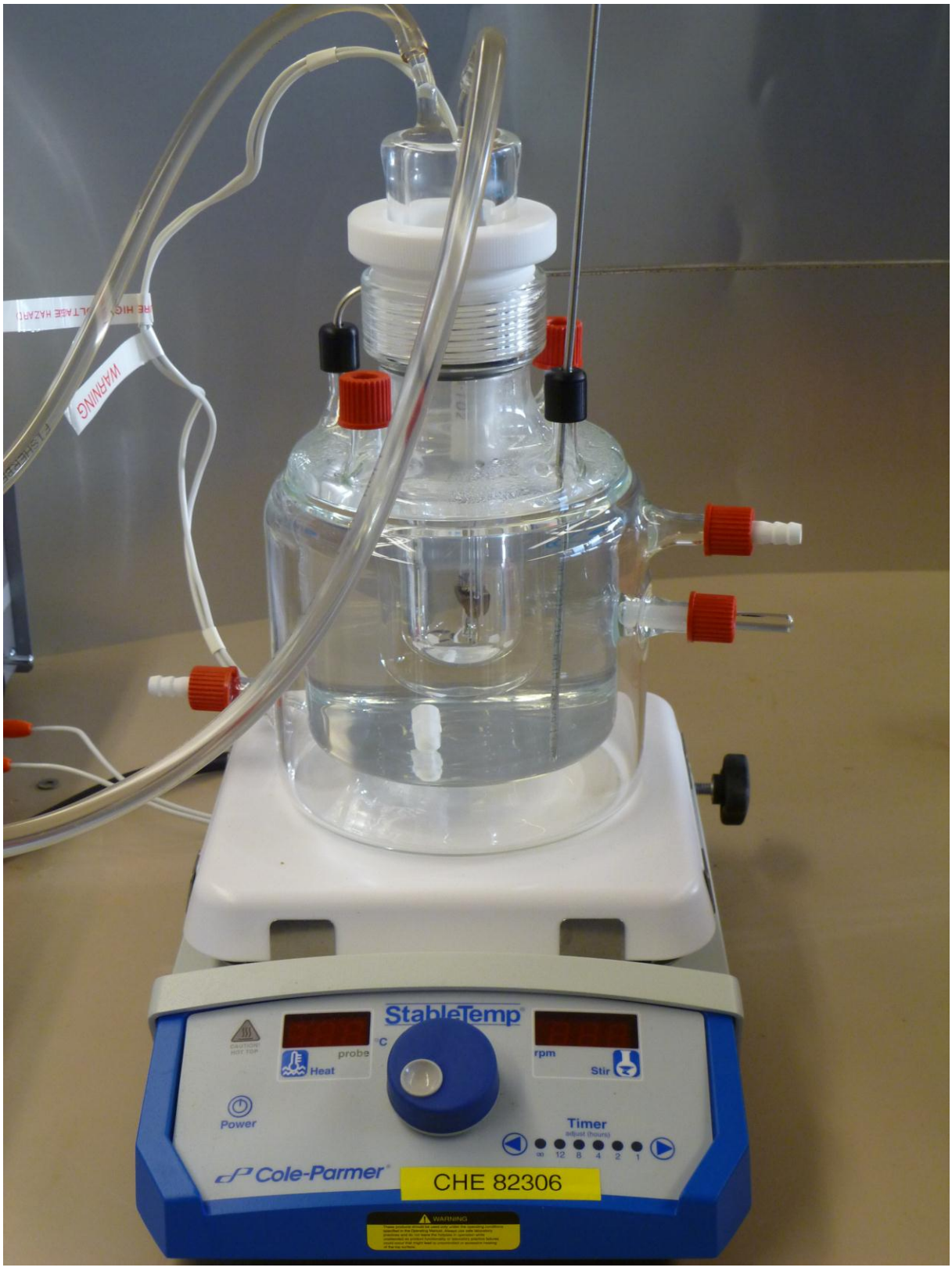

Figure A-3: Picture of the real manufactured photoreactor model with the extra body port in the right.

A.2 Lamp and ballast

The utilized lamp source in this thesis is a high-pressure UV lamp from USHIO Japan. There are some important reasons of high-pressure UV lamp selection in this design. First of all, because of the position of the lamp in the middle of the reactor, utilizing Xenon bulbs would have been almost impossible due to the overwhelming heat generation and insufficiency of the fan-less cooling stream to overcome this issue. Secondly, as the alternative, high-pressure UV lamps are the best candidates due to their much lower heat production as well as minimum UV output ratio and the possibility of selective UV removal using cooling solution. However, the only well-known manufacturer of these types of lamps, USHIO Company, is located in Japan. After the lighting system delivery in the University of British Columbia, the safety certification process was followed with the Canadian safety association (CSA). The technical catalogue of the lamp (UM-102) and the related ballast (UM-103B-B) is provided in Figure A-4. Figure A-5 shows the pictures of the lamp and ballast certified by CSA.

Photochemical reaction light source operation manual

1. General

   This system is suited for photochemical reaction with 100 watts high pressure UV lamp, this system is constructed by lamp and ballast.

2. Product name

   UM-103

3. Composition

   This system is composed of listed items as follows.

1) UM-102	High pressure UV lamp	Drawing number: H-680152	1pc.
2) UM-103B-B	Ballast	Drawing number: 3K3-10830	1pc.

   3) Option cables

4. Ambient condition

   This system is allowed to be operated in ambient temperature -10℃～+60℃ and humidity 30～80%.

5. Structure

   1) High pressure UV lamp

      Constructed by arc tube, protective resistance and arc tube bracket

   2) Ballast

      Constructed by leakage trans and condenser in metal case

      Appearance dimension is stated in attached drawing 3K3-10830.

6. Rating

   1) Ballast rating

Input Voltage	100V±10V
Frequency	50, 60 Hz
Capacity	150VA

Primary Current	1.5A MAX
Primary power factor	80% MIN
Secondary abbreviation current	1.5A MAX
Lamp current	1.1A±0.1A
Lamp voltage	110V±10V
Insulation classification	B dry-type
Operating condition	Continuous operation

2) High pressure UV lamp rating

Lamp input	132VA MAX
Lamp voltage	110V±10V
Lamp current	1.1A±0.1A
Stability time	5 minutes MAX

7. Installation and ignition
   1) Put lamp and ballast in place
   2) Connect cables after installation
   3) Turn over switch to direction, responded to frequency
   4) Turn on the switch, and lamp will be ignited
   5) Lamp will be stable in approximately 5 minutes

8. Caution
   1) Do not touch the lamp with bare hands.
   2) Operate ballast with appropriate frequency.
   3) Lamp can not be ignite soon after turning off, please ignite after enough cooling. (Approximate 3 minutes)

9. Remark

   Please check our catalogue, regarding to parts or handling of photochemical reaction.

高圧UVランプ

HIGH-PRESSURE UV LAMPS

ウシオ 高圧UVランプは、光化学反応プラント用に開発され、点灯中の水銀蒸気圧は1～10気圧で、幅広い紫外線領域の線スペクトルをもっています。これらの線スペクトルエネルギーを利用し、紫外線硬化タイプのインキ、塗料、接着剤を重合反応させるUV照射用光源としてさまざまな分野に活用されています。

■分光分布図　SAMPLE UM-452

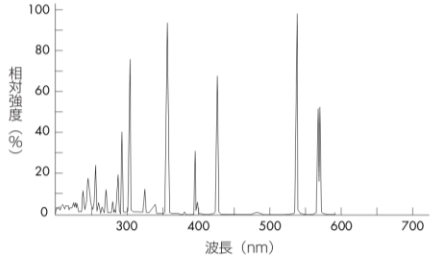

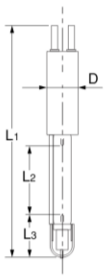

Fig.1

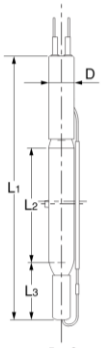

Fig.2

型式	定格			標準寸法				平均寿命	Fig. No.	適合点灯装置	用途
	電力（W）	電圧（V）	電流（A）	L1（mm）	L2（mm）	L3（mm）	φD（mm）	（h）			
UM-102	100	110	1.1	135	40	25	(18)	1,500	1	UM-103B-B	光化学反応
UM-452	450	130	3.8	222	96	36	(20)	1,500	2	UM-453B-A	

※平均寿命：定格電力で連続点灯した場合の寿命時間の平均を表わします。
寿命とは次の①、②いずれかが発生したときをいいます。
①水平放射照度または全光束が初期の70%になったとき
②点灯不能になったとき

※光化学反応実験用部品は9ページをご覧ください。
※紫外線瞬間乾燥照射装置としてユニキュアシステムシリーズがあります。
専用カタログをご覧ください。

高圧UVランプ点灯装置


▲UM-453B-A

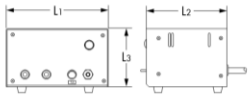

Fig.1

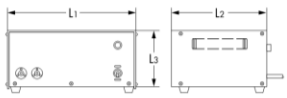

Fig.2

型式	定格				寸法			Fig. No.	連合ランプ
	入力電圧（V）	入力電流（A）	二次開放電圧（V）	周波数（Hz）	L1（mm）	L2（mm）	L3（mm）		
UM-103B-B	100	1.5	195	50／60	210	166	120	1	UM-102（100W）
UM-453B-A	100	5.5	195	50／60	310	209	185	2	UM-452（450W）

Figure A-4: Technical catalogue of the lamp and ballast purchased from USHIO Japan.

(a)

(b)

Figure A-5: Real model pictures of a) lamp, and b) ballast certified by Canadian safety association.

A.3 UV filtration

UV filter solutions are commonly used as an effective way to remove the UV output of the light sources with high accuracy [131]. Figure A-6 shows the typical absorbance spectrum of sodium nitrite ($NaNO_2$) solutions used in this work to filter the UV portion of the lamp output.

Figure A-7 presents the picture of the UV filtration process. There is a quartz jacket designed which circulates the solution all around the lamp to filter UV irradiation selectively while simultaneously cooling the lamp. The solution was analyzed randomly making sure the appropriate UV absorbance.

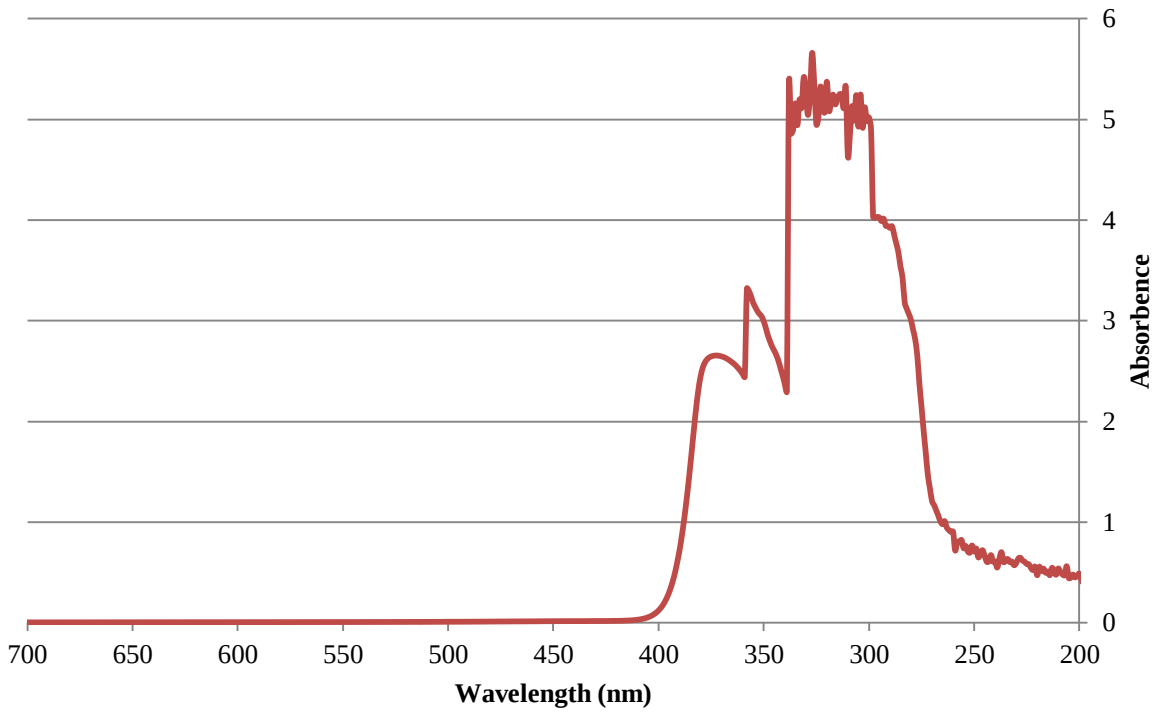

Figure A-6: UV-VIS absorbance spectra of the UV filtering solution ($NaNO_2$ 1 M).

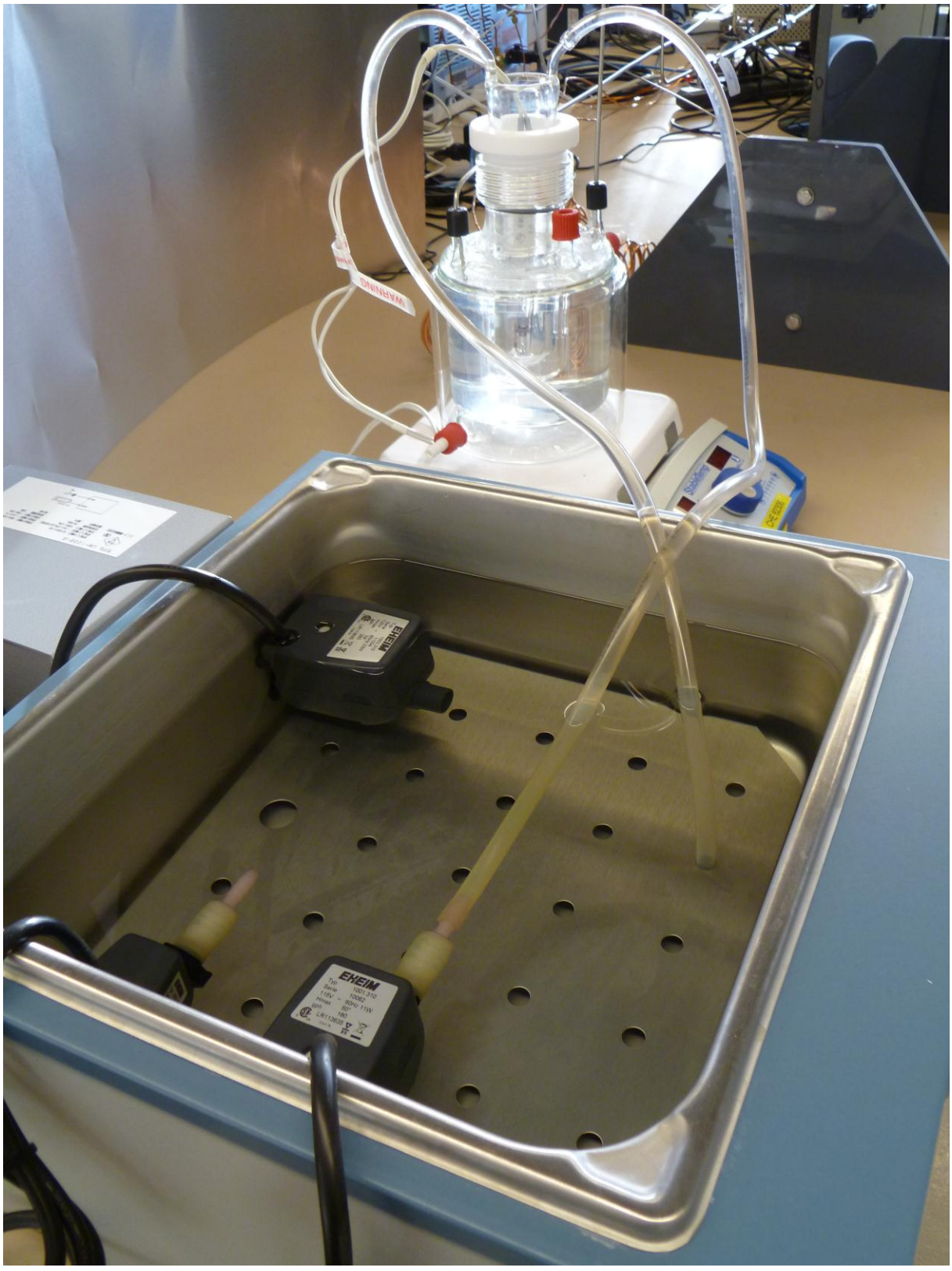

Figure A-7: Image of UV filtration solution circulation having cooling role concurrently.

A.4 Filters

In order to obtain the analytical grade quality of the gaseous products, two consecutive filters, Genie membrane separator and Nafion dryer, were utilized to remove the entrained liquid and the vapor phase of water and other hydrocarbons.

Genie membrane separator, employing zeolite-based separation technologies removes almost 100% of the particulate and liquid entrainments. With the low internal volume (16 cc), simple design, suitable sealing properties, and appropriate liquid draining system, it is among the best candidates for this application. Figure A-8 presents the technical catalogue of the utilized Genie membrane separator for entrainment removal in analytical grade.

Nafion dryer as the complimentary element connected to the Genie membrane, dries the stream continuously from only water, employing a mass exchanger having counter flow of dry gas for moisture removal. The assembly is almost maintenance-free exhibiting excellent corrosion resistance. Having short residence time similar to the connected zeolite-based filter brings the fastest response time to the flow stream. Figure A-9 presents the technical catalogue of the utilized Nafion dryer for gas drying in analytical grade.

GENIE®
membrane separator
Model 170

U.S. Patent 5,476,586

Applications

- Protection against liquids
  - On-line and portable analyzers
  - GC's, Mass Specs, O_2, H_2S, Moisture, and others
- Spot, composite, or continuous gas sampling in any process industry including natural gas, petrochemical, and oil refining

Benefits

- Superior analyzer protection
- Helps preserve sample integrity
- Improves analyzer reliability
- Reduces analyzer maintenance

Features

- Genie® Membrane Technology™
- Low internal volume
- Simple design
- No elastomers required for sealing
- Universal Assembly™ option

Quick Study

The Series 100 Genie® Membrane Separators™ remove 100% of entrained liquid and particulate in gas samples, which allows only gas sample to flow to analyzers. This action protects analyzers and sample system components against liquid damage. The original Genie® Series 100 models are available in several body styles with different membrane types to accommodate a wide variety of applications. The Genie® Supreme Series™ 100 models accommodate the same applications, yet they offer an improved housing design for easy maintenance and the innovative Liquid Block Technology™ that prevents liquid from being forced across the membrane should sample line pressure conditions become upset.

The Model 170 protects gas systems requiring very low sample flow rates on a continuous or intermittent basis. Its small internal volume and low dead volume 1/16" ports allow the Genie® Model 170 to purge quickly, which is ideal for the removing liquid aerosol droplets from gas samples; it is also perfect for protecting components such as laboratory gas chromatographs. Please note that special low volume fittings must be ordered to use a Genie® Model 170 properly.

A Universal Assembly™ preassembled kit is also available which includes all the necessary components required for easy, proper installation into an existing sample system. This model includes a 316 SS Genie® Model 170 equipped with your choice of membrane, rotameter, mounting bracket, and all basic fittings (outlet tubing not included).

Technical Specifications

Maximum pressure rating	170: 500 psig 170UA: 100 psig (due to rotameter limitations)
Maximum recommended supply pressure	Lowest possible pressure consistent with application* *Must not exceed "Pressure rating" listed above
Maximum temperature	185 °F (85 °C) for Type 6/BTU membrane 302 °F (150 °C) for Hi-Flow membrane
Maximum recommended membrane flow rate (For higher flow rates contact the factory)	300 cc/min for Type 6/BTU membrane* 750 cc/min for Hi-Flow membrane* *Maximum flow results in approximately 2 psi membrane differential pressure
Port sizes	Inlet, Outlet, & Bypass: 1/16" low volume fittings
Internal volume	0.16 cc
Wetted materials	Machined parts : 316 stainless steel / NACE compliant All other metal parts: stainless steel / NACE compliant Membrane: Inert

An ISO 9001:2008 certified company

GENIE sampling solutions

Figure A-8: Technical catalogue of the utilized Genie membrane separator for entrainment removal in analytical grade.

MD™-Series Gas Dryers

Protect Moisture-Sensitive Equipment by Selectively Drying Sample or Carrier Gas

- Dries continuously
- Removes only water vapor
- Achieves low dew points
- Requires no electricity
- Maintenance-free operation
- No moving parts
- Excellent corrosion resistance
- Short residence time

Perma Pure MD™-Series gas dryers use exclusive Nafion® selectively permeable membrane tubing to continuously remove only water vapor from gas streams. These dryers operate over a wide range of temperatures, pressures and flow rates while drying to very low dew points.

Principle of Operation

MD-Series gas dryers transfer moisture from one gas stream to a counter-flowing purge gas, much like a shell-and-tube heat exchanger transfers heat. Water molecules permeate through the Nafion tube wall, evaporating into the purge gas stream. The water concentration differential between the two gas streams drives the reaction, quickly drying the air or gas.

Purge gas should be instrument air or other dry gas. If no dry gas is available, a portion of the gas dried by the MD-Series dryer can act as the purge gas in a split-stream or reflux method. For more infromation about the drying process, including the use of the sample gas as the purge gas, please visit our website at www.permapure.com.

Perma Pure offers three MD-Series dryer product lines:

Model Number	MD-050	MD-070	MD-110
Nafion Tube O.D.	0.053"	0.072"	0.108"
Nafion Tube I.D.	0.042"	0.060"	0.086"
Available Lengths[1]	12, 24, 48, 72, 96 or 144 inches		
Housing Materials	Stainless Steel or Fluorocarbon or Polypropylene		
Maximum Flow Rate	200 cc/min.	2 liters/min. [2]	4 liters/min. [2]

[1] MD-050 Series dryers are not offered in 96 and 144-inch lengths.
[2] MD-070 and MD-110 offer approximately the same drying performance. Specify MD-110 when pressure drop is a concern, MD-070 to minimize dead volume. For higher flow rates, please see our PD-Series dryers.

PERMA PURE

Bulletin 103

Figure A-9: Technical catalogue of the utilized Nafion dryer for gas drying in analytical grade.

A.5 Controller board

Figure A-10a shows the front view of the controller board which contains four flow meters and two valves. Three of the four flow meters are already in service and one is considered for the extra development, obtaining more data with respect to various streams of the system. From left to the right, they are used for the flow indication of sweep gas, photoreactor's purified output, and the dryer gas used for main stream vapor drying using Nafion membrane (0-50 CC/min air from Dwyer Company).

Figure A-10b demonstrates the piping of the controller board besides showing the placement of the two consecutive purifiers (Genie membrane separator and Nafion gas dryer). All the piping is stainless steel 1/8"; the 1/16" connections of the Genie separator are immediately converted to 1/8". There is another blocked 1/16" pipeline connected to the Genie separator which is used for draining of the liquid entrainments, and should be checked before and after each experiment making sure it's completely evacuated.

(a)

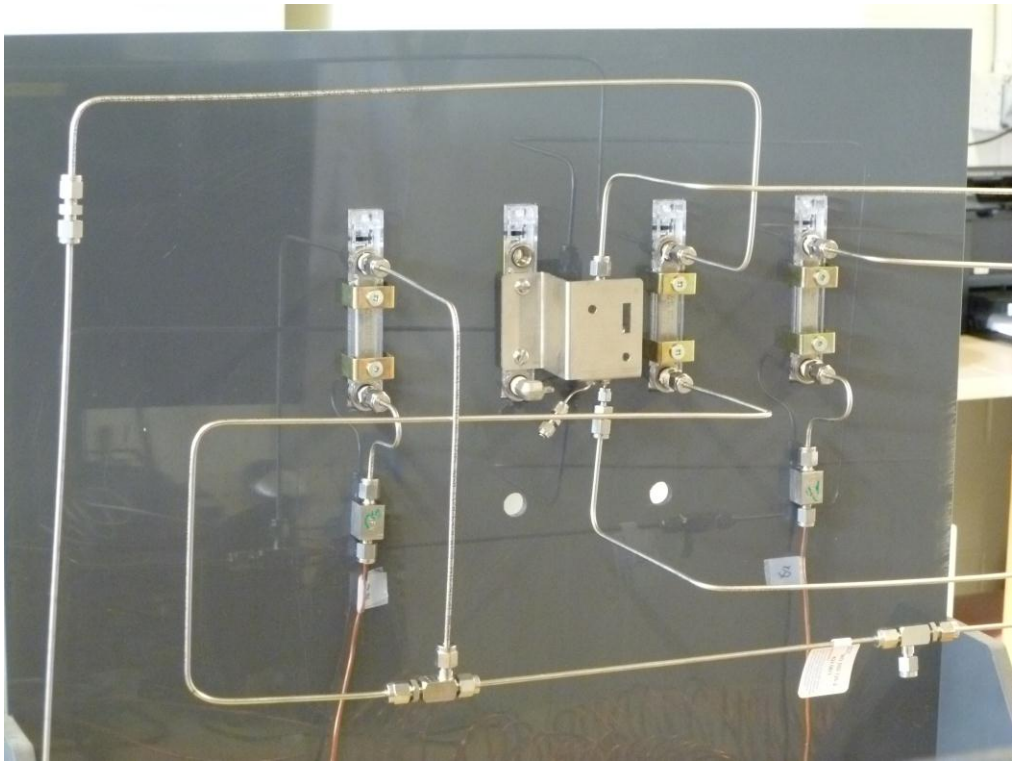

(b)

Figure A-10: Controller board of the experimental setup: a) front view, and b) back view.

Appendix B Background experiments

As the general point, the rational of performing background experiments is to ensure the accurate analysis of the impact of parameters involved in the system's performance. In this regard, as this project was started with photocatalyst preparation and followed by characterization and performance evaluation, each part is potentially prone to various misinterpretations due to the lack of background analysis. The researcher has done his best to consider all the possibilities in the aforementioned stages, achieving reliable conclusions. In this appendix, the most important background experiments are briefly discussed.

Three main studies are targeted for the background experiments: i) photocatalyst preparation and characterization, ii) degradation of the organic compounds, and iii) water splitting investigating related gas evolutions. The upcoming sections aim to explain the major considerations regarding aforementioned modules, and the related background experiments needed to ensure acquiring reliable data for analysis.

B.1 Photocatalyst preparation and characterization

Besides the 6 studied main photocatalysts in the body of the thesis, 14 extra supporting batches were prepared to investigate various other possibilities of photocatalytic performance of the samples. Those include various percentages of titania on the support (10, 25 and 50), isolating consecutive impregnation steps of photocatalyst preparation, usage of activated carbon as the support with various percentages of the impregnated titania (10, 25 and 50), applying phosphotungstic acid (PWA) besides phosphomolybdic acid (PMA) to monitor the impact of various heteropolyacids (HPAs), all on two different types of zeolite to bring the robustness of the conclusions to its highest. Investigating the performance of the selected photocatalysts for the 2,4-D photo-degradation as well as hydrogen evolution test, proved that the effectiveness of the composition under visible light is closely integrated with the

basic zeolite, TiO_2, heteropolyacid and cobalt together. Lack of any of the aforementioned molecules has a significant negative impact on the hydrogen evolution performance, while cobalt did not have a remarkable effect on the 2,4-D degradation rate. In the characterization module, repeating the analysis having different samplings from various portions of the synthesized photocatalysts was necessary and conducted in this research.

B.2 Degradation of organic compounds

In each photocatalytic process study, it's necessary to collect the data in order to identify the reactions proceed only due to the photocatalytic process. Hence, dark absorption and direct photolysis are among the most important background experiments for evaluating the photocatalytic degradation of organic compounds, putting more emphasis on the visible light activity. In dark absorption analysis, after putting the photocatalyst in the vessel starting the stirring process, sampling was performed every five minutes until reaching the absorption saturation point in the absence of the irradiation. The typical waiting time before starting the main experiment for the samples considering the results obtained from this experiment was 1 h, during which between 15 to 20 percent of the 2,4-D was absorbed (sample data reported in Section 2.3.2). As for the direct photolysis, the organic compound solution was studied in the absence of the photocatalyst and presence of the irradiation. Using continuous sampling analysis, the direct photolysis impact was subtracted from the main kinetic analysis. The related data is already addressed in Section 2.3.2. The importance of 2,4-D selection for the organic compound photo-degradation experiment is already addressed in Section 2.2.4.

It should be noted that all the results obtained based on the 100 mg of the synthesized photocatalysts in the 1 liter volume of the photoreactor starting with 100 ppm concentration

of 2,4-D utilizing 100 W high-pressure UV lamp for the experiments. In the case of variation in each of the aforementioned parameters obtaining similar results is not guaranteed.

B.3 Evolution of hydrogen

In the very first thought, the only checking task before starting the experiment, turning the lamp on, is ensuring that the reactor vessel is depleted from air. However, in the last decade, very interesting observation was addressed during the air removal in the dark for hydrogen evolution analysis of certain types of photocatalysts. It was observed that during the solution stirring using magnet, the water is decomposed to hydrogen and oxygen. After detailed studies [161, 162], this phenomenon was attributed to the conversion of the mechanical energy applied to some certain types of the suspended oxide powders rubbed between bottom of the Pyrex glass reactor and the stirring rod. As the result, water dissociation was revealed to occur due to the frictional forces between the oxide powders and the bottom of the reaction vessel so-called mechano-catalytic water splitting. Potentially, this would be the most important background experiment for photocatalytic water splitting under irradiation. However, for the class of the photocatalyst synthesized in this research, mechano-catalytic effect was not observed.

Appendix C Reproducibility of experiments

In this appendix, the reproducibility of the experiments is presented based on three times of experiment repetition for the photocatalyst batch number 1 as the example. Figure C-1 presents the related data for 2,4-D photo-degradation experiments whereas Figure C-2 demonstrates the evolution-time behavior in the case of hydrogen evolutions.

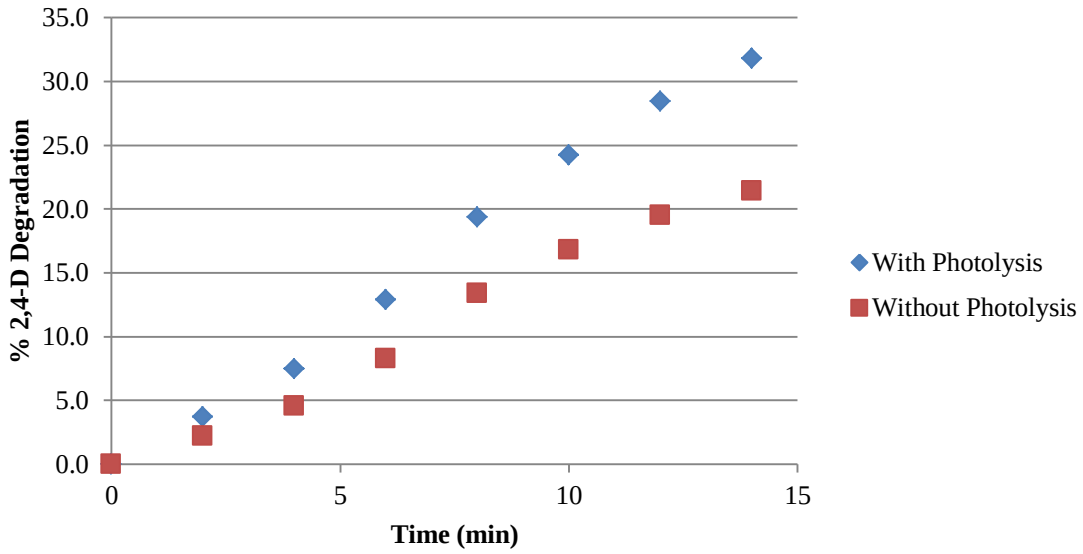

(a)

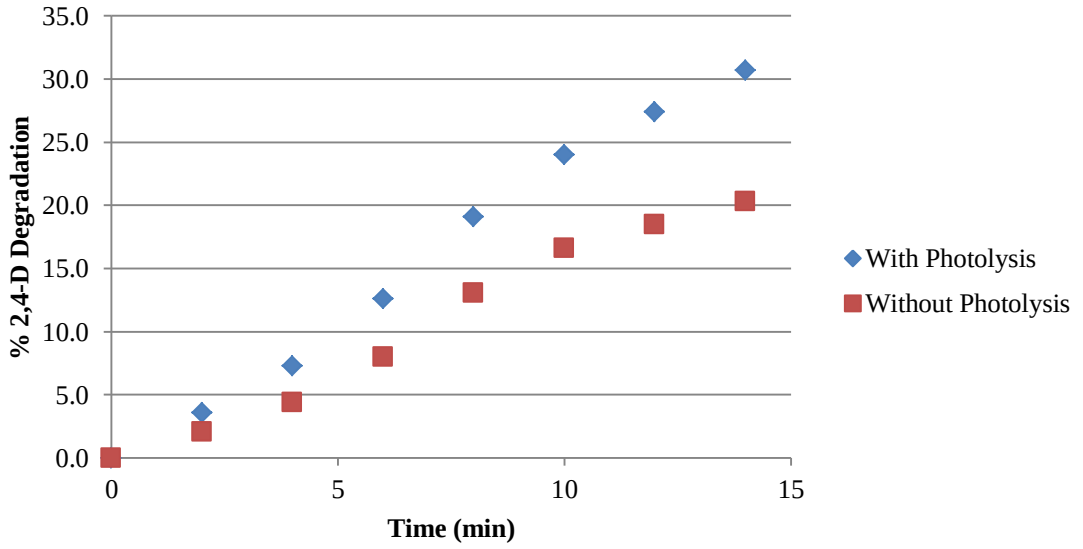

(b)

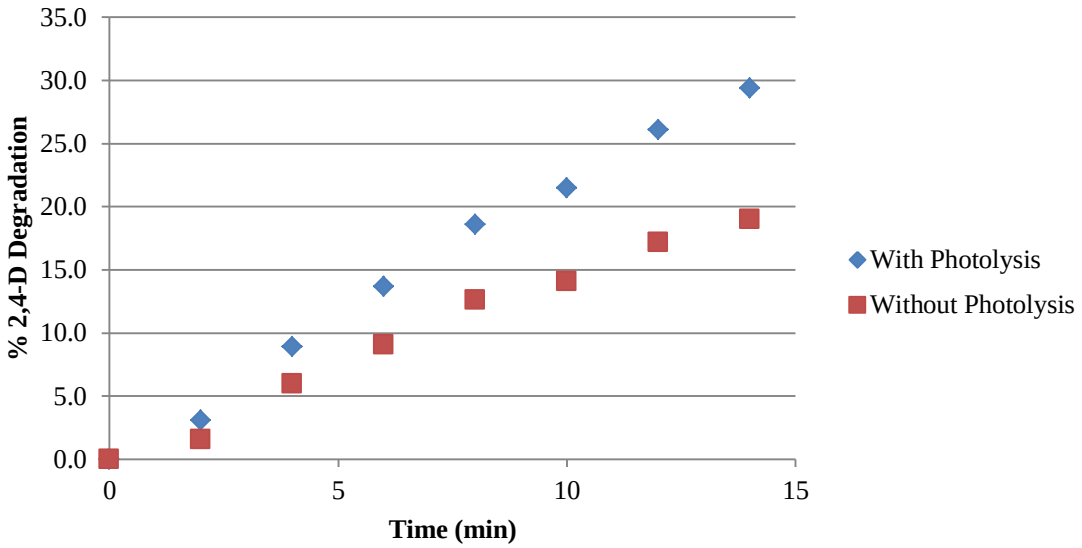

(c)

Figure C-1: Three rounds of 2,4-D degradation analysis for CB1P3 with 20.1±1.1 ppm degradation in 15 minutes which the ± shows 95% confidence interval from 3 experiments.

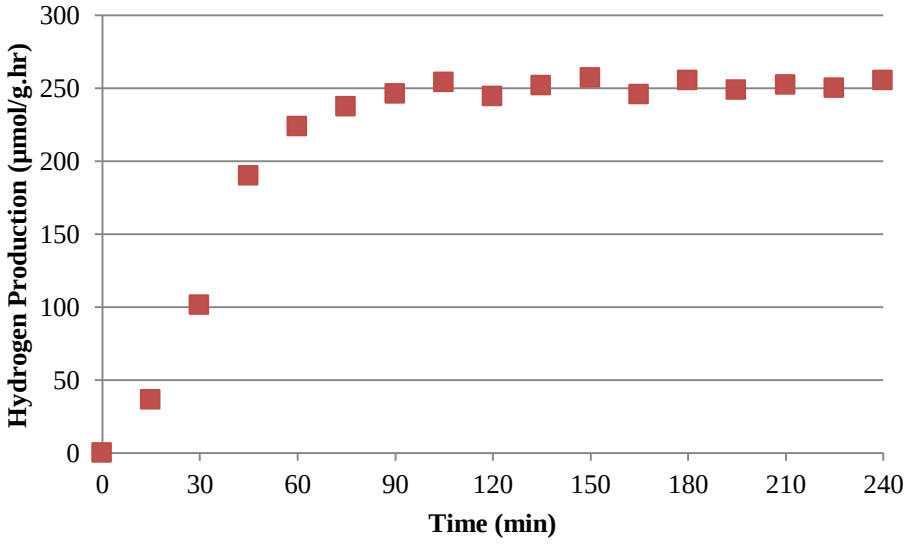

(a)

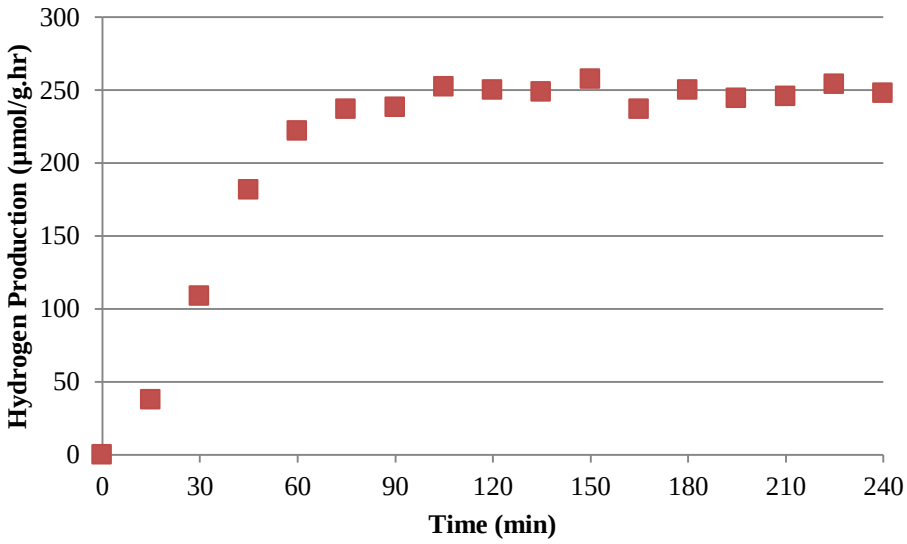

(b)

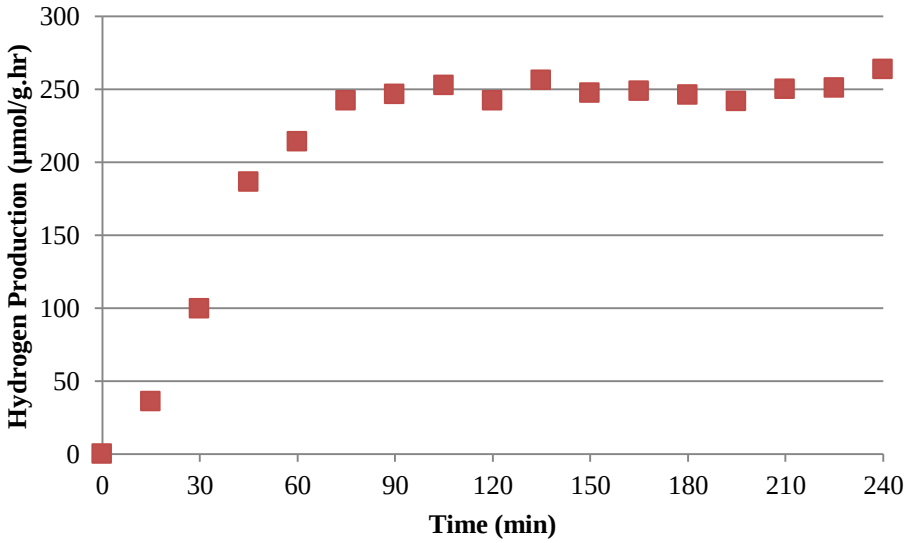

(c)

Figure C-2: Three rounds of hydrogen evolution analysis for CB1P3 with 250.8±12.3 µmol/g.h which the ± shows 95% confidence interval from 3 experiments.